**Terms and Conditions of Use of Digitised Theses from Trinity College Library Dublin**

**Copyright statement**

All material supplied by Trinity College Library is protected by copyright (under the Copyright and Related Rights Act, 2000 as amended) and other relevant Intellectual Property Rights. By accessing and using a Digitised Thesis from Trinity College Library you acknowledge that all Intellectual Property Rights in any Works supplied are the sole and exclusive property of the copyright and/or other IPR holder. Specific copyright holders may not be explicitly identified.  Use of materials from other sources within a thesis should not be construed as a claim over them.

A non-exclusive, non-transferable licence is hereby granted to those using or reproducing, in whole or in part, the material for valid purposes, providing the copyright owners are acknowledged using the normal conventions. Where specific permission to use material is required, this is identified and such permission must be sought from the copyright holder or agency cited.

**Liability statement**

By using a Digitised Thesis, I accept that Trinity College Dublin bears no legal responsibility for the accuracy, legality or comprehensiveness of materials contained within the thesis, and that Trinity College Dublin accepts no liability for indirect, consequential, or incidental, damages or losses arising from use of the thesis for whatever reason. Information located in a thesis may be subject to specific use constraints, details of which may not be explicitly described. It is the responsibility of potential and actual users to be aware of such constraints and to abide by them. By making use of material from a digitised thesis, you accept these copyright and disclaimer provisions. Where it is brought to the attention of Trinity College Library that there may be a breach of copyright or other restraint, it is the policy to withdraw or take down access to a thesis while the issue is being resolved.

**Access Agreement**

By using a Digitised Thesis from Trinity College Library you are bound by the following Terms & Conditions. Please read them carefully.

I have read and I understand the following statement: All material supplied via a Digitised Thesis from Trinity College Library is protected by copyright and other intellectual property rights, and duplication or sale of all or part of any of a thesis is not permitted, except that material may be duplicated by you for your research use or for educational purposes in electronic or print form providing the copyright owners are acknowledged using the normal conventions. You must obtain permission for any other use. Electronic or print copies may not be offered, whether for sale or otherwise to anyone. This copy has been supplied on the understanding that it is copyright material and that no quotation from the thesis may be published without proper acknowledgement.

# Bubble Growth Dynamics in Nucleate Pool Boiling with Liquid Subcooling Effects

Muhad Rozi Mat Nawi

Department of Mechanical and Manufacturing Engineering

Parsons Building

Trinity College
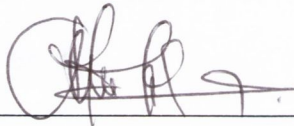
Dublin 2

Ireland

November 2014

A thesis submitted to the University of Dublin in partial fulfilment of the requirements for the degree of Ph.D
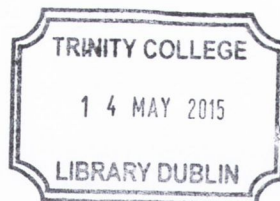
# DECLARATION

I declare that this thesis has not been submitted as an exercise for a degree at this or any other university and it is entirely my own work.

I agree to deposit this thesis in the University's open access institutional repository or allow the library to do so on my behalf, subject to Irish Copyright Legislation and Trinity College Library conditions of use and acknowledgement.

Muhad Rozi Mat Nawi
November 2014

I

# ABSTRACT

Heat transfer in nucleate pool boiling has been characterized by very high dissipated heat fluxes whilst requiring low driving temperature differences. The rate of bubble growth and the subsequent bubble motion has a tremendous influence on the heat transfer. In order to gain a deeper understanding of the mechanisms responsible for this, basic knowledge of bubble growth dynamics is required. To this end, single isolated bubble growth dynamics from an artificial nucleation site in pool boiling has been investigated experimentally in this study. An experimental facility has been developed to perform the study. The experiments have been conducted at atmospheric pressure with an environmental friendly refrigerant HFE-7000 as the working fluid. A high speed video camera with a combination of powerful lens and a tube extension has been used to capture the bubble images during boiling. Image processing in Matlab has been used to process the images and determine relevant parameters which characterize growth and departure.

In the analysis of the bubble growth dynamics, it was found that the bubble's waiting and growth times decrease when the wall superheat is increased, resulting in a significant increase in the bubble frequency. However, bubble growth was determined to be quasi-static such that the bubble size at departure was independent of superheat resulting in an independence of bubble departure size with frequency which contradicts earlier theories. The new growth law was determined which is notably different from the classical growth laws in early classical analytical studies. Bubbles were observed to oscillate at higher wall superheats due to the interaction of the growing bubble with the previous bubble since the waiting time is very short for the high superheats. The measurement of the contact angle is considered to have a non-negligible error due to the mirage effects. A technique has been developed that corrects for the mirage by calculating the contact angle value which satisfies the vertical force balance for the quasi-static bubbles. For this special case, for a given bubble volume all the forces acting on a growing bubble can be considered as independent of wall superheat. The liquid inertia force appears significant at high wall

superheats with an undulating profile due to interaction with the previously departed bubble and the momentum force becomes noticeable for the case of high superheat.

For the experiment with bulk liquid temperatures below the saturation temperature, i.e., subcooled boiling, the shapes of the bubbles at the early growth stage was found less elongated compared to the case of saturated boiling, possibly due to downward force by the fluid moving downward as a result of higher density difference. The bubble size is found to be approximately 29% smaller compared to the bubble volume at departure for the case of saturated boiling due to condensation at the bubble cap. The bubble growth curves show notable differences between the three levels of subcooling, i.e., low, mid and high subcooling with a continuous growth curve closer to the saturated case for low subcooling and an abrupt change for mid and high subcooling. Oscillations were observed for the case of high subcooling due to changes in the net flow of heat and mass into/out-of the bubble. The bubble volumetric growth rate curves depend strongly on the level of subcooling, with them being closer to the saturated growth laws for the lower subcooling though notably different for the higher subcooling cases due to high rates of condensation. The contact angles are found to be independent of subcooling levels with smaller contact angles compared with the saturated case. All the vertical forces acting on a growing bubble can be considered as independent of levels of subcooling and lower magnitudes were measured compared to the saturated boiling measurements.

# ACKNOWLEDGEMENTS

# TABLE OF CONTENT

# LIST OF FIGURES

# LIST OF TABLES

# NOMENCLATURE

## Latin Letters

| Symbol | Name | Units |
|--------|------|-------|
| $\dot{m}$ | Mass flow rate | $kg.s^{-1}$ |
| $A$ | Area | $m^2$ |
| $A$ | A parameter in Eq. (2.6) | - |
| $a$ | A parameter in Eq. (2.49) | - |
| $B$ | A parameter in Eq. (2.10) | - |
| $b$ | A parameter in Eq. (2.49) | - |
| $C$ | A parameter in Eq. (2.13) | - |
| $c$ | A parameter in Eq. (2.49) | - |
| $c_p$ | Specific heat capacity | $J.kg^{-1}.K^{-1}$ |
| $D$ | A parameter in Eq. (2.20) | - |
| $D,d$ | Diameter | m |
| $D_b$ | Bubble's diameter at departure | m |
| $D_0$ | Base diameter | |
| $D_T$ | Tate's diameter | m |
| $F$ | Force | N |
| $f$ | Body force | $N.m^{-3}$ |
| $f_d$ | Bubble departure frequency | $s^{-1}$ |
| $g$ | Gravity acceleration | $m.s^{-2}$ |
| $g_0$ | Conversion constant | |

| Symbol | Description | Units |
|---|---|---|
| $G(\theta)$ | Geometry of bubble neck | |
| $h$ | Heat transfer coefficient | $W.m^{-2}.K^{-1}$ |
| $h$ | Enthalpy | $J.kg^{-1}$ |
| $h_{cg}$ | Height of the center of gravity | m |
| $h_{fg}$ | Latent heat of vaporization | $kJ.kg^{-1}$ |
| $h$ | Height of the bubble | m |
| $I_R$ | Robinson and Judd criterion | - |
| $k$ | Thermal conductivity | $W.m^{-1}.K^{-1}$ |
| $K$ | Empirical constant in Eq. (2.54) | - |
| $L$ | Length | m |
| $L_c$ | Capillary length | m |
| $L_0$ | Characteristics length scale in Eq. (2.57) | |
| $M$ | Molecular weight | $g.mol^{-1}$ |
| $m$ | Mass | kg |
| $n$ | Number of molecules | mol |
| $n$ | Empirical constant in Eq. (2.54) | - |
| $P$ | Pressure | Pa |
| $P$ | Power | W |
| $Q$ | Heat | W |
| $q''$ | Heat flux | $W.m^{-2}$ |
| $R$ | Radius | m |
| $r$ | Length in the radial direction | m |
| $R$ | Thermal resistance | $K.W^{-1}$ |
| $R^*$ | Dimensionless radius | - |

| | | |
|---|---|---|
| $S$ | Entropy | $J.kg^{-1}.K^{-1}$ |
| $S$ | Surface area | $m^2$ |
| $T$ | Temperature | $K$ |
| $t$ | Time | $s$ |
| $t_w$ | Waiting time | $ms$ |
| $t_g$ | Growth time | $ms$ |
| $t*$ | Dimensionless time | - |
| $u$ | Velocity | $m.s^{-1}$ |
| $V$ | Volume | $m^3$ |
| $V*$ | Dimensionless volume | - |
| $x$ | Length in the x-direction | $m$ |
| $y$ | Length in the y-direction | $m$ |
| $z$ | Length in the z-direction | $m$ |

## Greek Letters

| | | |
|---|---|---|
| $\alpha$ | Contact angle | $^\circ$ |
| $\alpha$ | Thermal diffusivity | $m^2.s^{-1}$ |
| $\beta$ | Thermal expansion coefficient | $K^{-1}$ |
| $\beta$ | Bubble growth parameter in Eq. (2.45) | - |
| $\beta$ | Configuration angle in Figure 2.5 | $^\circ$ |
| $\gamma$ | A parameter in Eq. (2.16) | - |
| $\delta$ | Thickness of liquid layer | $m$ |
| $\mu$ | Dynamic viscosity | $kg.m^{-1}.s^{-1}$ |
| $\rho$ | Density | $kg.m^{-3}$ |
| $\sigma$ | Surface tension | $N.m^{-1}$ |

| | | |
|---|---|---|
| $\upsilon$ | Kinematic viscosity | $m^2.s^{-1}$ |
| $\psi$ | A parameter in Eq. (2.63) | - |
| $\emptyset$ | Modified factor of bubble growth [Eq. (2.57)] | - |

## Subscripts and Superscripts

| | |
|---|---|
| $\infty$ | bulk |
| $b$ | related to the bubble |
| $B, buoy$ | buoyancy |
| $base$ | relative to the base of the bubble |
| $C$ | capillary |
| $c$ | cavity, condensation |
| $cg$ | center of gravity |
| $CL$ | contact line |
| $CP$ | contact pressure |
| $C_{tip}$ | tip curvature |
| $Cu$ | copper |
| $d$ | detachment or departure |
| $duy$ | unsteady growth |
| $D$ | drag |
| $e$ | evaporation |
| $eq$ | equivalent |
| $f$ | fluid |
| $g$ | growth |
| $I$ | inertia |
| $\ell$ | liquid phase |
| $LI$ | liquid inertia |
| $mac$ | macrolayer |
| $mic$ | microlayer |
| $mom$ | momentum |
| $o$ | base |

| | |
|---|---|
| r | radial direction |
| sat | saturation |
| sub | subcooling |
| v | vapour phase |
| vf | viscous forces |
| vs | viscous stress |
| w | heated wall or surface |
| x | x-direction |
| y | y-direction |
| z | z-direction |

## Dimensionless Numbers

Bond number, $Bo = \frac{(\rho_l - \rho_v)gr^2}{\sigma}$

Grashof number, $G_r = \frac{g\beta\Delta T_w D^3}{\vartheta^2}$

Jakob number, $Ja = \frac{\rho_l C_{pl}(T_\infty - T_{sat})}{\rho_v h_{fg}}$

Nusselt number, $Nu = \frac{hD}{k}$

Prandtl number, $Pr = \frac{\mu c_p}{k_l}$

Rayleigh number, $Ra = Gr.Pr$

# CHAPTER 1

## INTRODUCTION

In this chapter, the background of the present study is presented. A brief explanation of the basic concepts of boiling are discussed. It is followed by a discussion of the motivation of the present study. This will conclude by presenting research objectives and thesis outlines.

## 1.1    Background

Boiling is a complex process in which mass, momentum, and energy are transferred within and between a solid wall, a liquid phase and vapour phase. When liquid is boiled, a liquid-vapour phase change process occurs such that in some situations/wall superheats, vapour bubbles are formed either on a heated surface or in a superheated liquid layer adjacent to the heated surface. This process is called nucleate boiling and is known to be a highly effective mode of heat transfer and one of the most studied physical phenomena in thermal fluid science and engineering.

The formation of bubbles within superheated liquids is generally observed to occur over a range of temperatures within a metastable range of superheats. Bubble nucleation completely within a superheated liquid is called homogeneous nucleation. Meanwhile, bubble nucleation that occurs at the interface between a metastable phase and another (usually solid) phase that it contacts is called heterogeneous nucleation.

Common example of everyday occurrence of nucleate pool boiling is that of a pot of boiling water on top of the stove. As shown in Figure 1.1, a stagnant pool of liquid is heated by a submerged heating surface and boiling initiates in which bubbles start nucleating, growing and departing from nucleation sites on a heated surface due to an increase in temperature of the heated surface over the saturation temperature of the fluid. According to the Hsu theory [Hsu (1962)], one bubble is assumed to nucleate when the superheated liquid layer above the site grows sufficiently thick to cause the vapour/gas trapped within the cavity to overcome the surface tension force and grow. During boiling, the relative motion of the vapour produced and the surrounding liquid near the heating surface is due primarily to the buoyancy effect on the bubble which lifts it from the surface. Nevertheless, the main body of the liquid as a whole is essentially at rest. This overall process is called nucleate pool boiling.
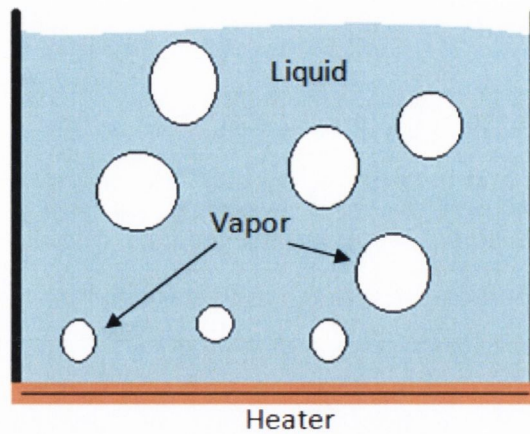
Figure 1.1: Conceptual picture of pool boiling

Heat transfer during nucleate pool boiling has been characterized by very high dissipated heat fluxes whilst requiring low driving temperature differences as indicated in region II in Figure 1.2. The rate of bubble growth has a tremendous influence on the heat transfer. According to the study of Hsu and Graham (1986) at low heat fluxes, where isolated bubble growth occurs, the growth cycle can be qualitatively described as follows. Once the liquid layer above the heater surface reaches the required superheat to activate a given nucleation site, a bubble begins to form and pushes the surrounding liquid outward, except for a thin liquid microlayer that remains in contact with the wall underneath the bubble. Evaporation occurs at the bubble surface and through the microlayer beneath the bubble and the macrolayer surrounding the bubble dome, thus fuelling further bubble growth. When the size of the bubble is sufficiently large, buoyancy causes the bubble to detach from the surface. Subsequent to this, new fresh liquid floods the surface and the cycle restarts. Due to its high heat flux at relatively low levels of excess temperature, the nucleate boiling regime is very desirable for many industrial applications.
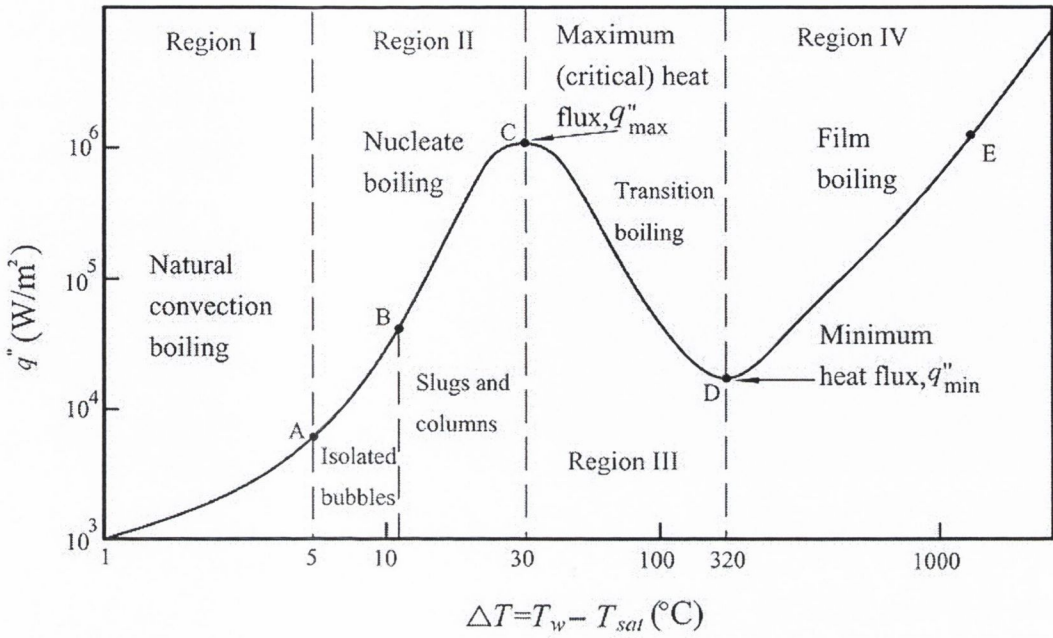
Figure 1.2: Typical boiling curve for water at 1 atm pressure [Faghri and Zhang (2006)]

## 1.2  Motivation

Since the early to mid 1900s, theoretical studies of boiling have been conducted attempting to understand the boiling process and define theories and mathematical models to predict its performance. Even still, global theories and robust empirical formulations seem to be elusive. This is due to a lack of a complete understanding of the fundamental physics of bubble dynamics, flow and heat transfer at these small time and length scales. This is complicated by the fact that bubble dynamics are sensitive to a vast array of interdependent parameters which makes exhaustive experimentation and exact numerical simulations difficult to achieve.

Although this type of heat transfer process has been utilized over the ages, knowledge about the phenomenon and its physical mechanisms of heat transfer is still restricted, mainly because the technology required to measure the time and length scales of the phenomenon has only been developed recently. This being the case, the present study utilizes modern high technology to gain a deeper understanding of the

4

boiling phenomena within the scope of isolated bubble dynamics from an artificial nucleation site.

## 1.3 Objectives

The present study entitled *"Bubble Growth Dynamics in Nucleate Pool Boiling with Liquid Subcooling Effects"*, has the following objectives:

- To design and construct an experimental test facility to allow the visualization of bubble dynamics for pool boiling from a single artificial nucleation site at atmospheric pressure with the option of subcooling.

- To measure the bubble size more precisely using sophisticated modern technique.

- To gain a deeper knowledge and understanding about the bubble dynamics phenomenon in nucleate pool boiling under saturated conditions.

- Evaluate validity of classical theories with simple controlled experiments.

- To provide some initial understanding of the behaviour of single isolated bubble growth during subcooled pool boiling.

## 1.4 Thesis Outlines

This thesis is divided into five chapters. It is organized as follows:

- ✓ **Chapter 1** - Background, motivation, objectives of the present study is presented.

✓ **Chapter 2** - Analytical studies of bubble growth, bubble departure and bubble waiting time are presented. It follows by reviewing some of the experimental studies of single bubble dynamics. The effects of subcooling on bubble growth dynamics in both analytical and experimental earlier studies will be presented in the last part in this chapter.

✓ **Chapter 3** - The experiment designed and built for the present study is presented. It is followed by the experimental procedures, measurement techniques, operating conditions and data analysis.

✓ **Chapter 4** - Results from the experimental work are presented and discussed for saturated conditions and subcooled conditions.

✓ **Chapter 5** - Conclusions.

# CHAPTER 2

## LITERATURE REVIEW

Boiling heat transfer has received much attention for about a century because of the high heat transfer coefficients associated with this mode of heat transfer. Numerous studies have been carried out by many researchers attempting to predict boiling heat transfer rates since the first boiling curves produced by Nukiyama (1934). This chapter is aimed at providing some relevant information regarding the research carried out pertaining to the bubble dynamics and the effects of subcooling in nucleate pool boiling from different researchers across the globe.

This literature review begins by reviewing some of the analytical studies of bubble growth, bubble departure and bubble waiting time. It is then followed by a review of some of the experimental studies of single bubble dynamics. Lastly, the effects of subcooling on bubble growth dynamics for both analytical and experimental studies will be presented.

## 2.1 Analytical Bubble Dynamics

The first important work on bubble dynamics was performed by Rayleigh (1917). He formulated the equation of motion for spherical bubble expansion as a problem of the dynamics of an incompressible and inviscid fluid, which was later to be known as the inertia controlled growth regime. Integration of the momentum equation in the liquid phase, neglecting surface tension influences, results in,

$$\frac{P_v - P_\infty}{\rho_l} = R\frac{d^2R}{dt^2} + \frac{3}{2}\left(\frac{dR}{dt}\right)^2 \tag{2.1}$$

The surface tension term was later added by Plesset and Zwick (1954) by relating the vapor and liquid pressures at the bubble interface through the Young-Laplace pressure drop,

$$\frac{P_v - P_\infty}{\rho_l} = R\frac{d^2R}{dt^2} + \frac{3}{2}\left(\frac{dR}{dt}\right)^2 + \frac{2\sigma}{\rho_l R} \tag{2.2}$$

Eq. (2.2) is known as the extended or modified Rayleigh equation. It relates the pressure difference which drives growth to the inertial forces exerted by the liquid on the bubble and surface tension forces at the interface.

### 2.1.1 Bubble Growth

Bubble growth in infinite superheated liquids was analytically investigated in the 1950s to the 1970s. Generally, the work has been divided into the following two main regions,

(i)     Inertia controlled growth

(ii)    Diffusion controlled growth

The region of bubble growth controlled by inertia forces was famously related to the work of Rayleigh (1917). This region is restricted to the initial stages of rapid growth in which the bubble expansion rate is primarily limited by its ability to 'push' the surrounding liquid. During this stage, the rate of heat transfer to the interface is assumed sufficiently high such that growth is not constrained by the resultant vapour generation into the bubble. For the solution of this growth stage, the vapour pressure is nearly constant and assumed to be near its maximum value of $P_v \approx P_{sat}(T_\infty)$. For bubbles large enough that the surface tension term is negligible [Eq. (2.1)], the interface velocity can be calculated as,

$$\dot{R}^2 = \frac{2}{3}\left(\frac{P_{sat}(T_\infty) - P_\infty}{\rho_l}\right) \tag{2.3}$$

By substituting the Clausius-Clapeyron equation to relate the vapour temperature to the saturation temperature, the solution for inertial controlled growth is obtained [Plesset and Zwick (1954), Mikic et al. (1970)],

$$R(t) = \left(\frac{2}{3}\left[\frac{T_\infty - T_{sat}(P_\infty)}{T_{sat}(P_\infty)}\right]\frac{h_{fg}\rho_v}{\rho_l}\right)^{1/2} t \tag{2.4}$$

From Eq. (2.4), it clearly shows that inertial controlled growth is characterized by a linear relationship between radius and time,

$$R(t) = A.t \tag{2.5}$$

where $A$ is,

$$A = \left(\frac{2}{3}\left[\frac{T_\infty - T_{sat}(P_\infty)}{T_{sat}(P_\infty)}\right]\frac{h_{fg}\rho_v}{\rho_l}\right)^{1/2} \tag{2.6}$$

However, with no experimental data existing at that time, the applicability of Eq. (2.4) was difficult to ascertain as it only becomes significant for very low system pressures. Later, the region of bubble growth controlled by thermal diffusion was introduced , for example in the works of Forster and Zuber (1954) and Plesset and Zwick (1954). In this case, the bubble growth predictions was extended beyond the inertial controlled growth region by taking into account the fact that as the bubble grows, the latent heat requirement of evaporation depletes the energy stored within the superheated layer which has formed at the surface of the bubble [Plesset and Zwick (1954)]. As the bubble grows, its equilibrium vapour temperature decreases from $T_\infty$ to its minimum value of $T_{sat}(P_\infty)$. As the interfacial temperature and corresponding pressure drop, bubble growth becomes limited by the relatively slower diffusion of heat to the vapour-liquid interface, causing the growth rate to continually decrease.

Plesset and Zwick (1954) have obtained a solution for the instantaneous bubble radius prediction for the case of thermal diffusion controlled growth by supplying an approximate expression for the liquid temperature distribution at the interface. This approximate expression was found under the assumption that the drop in temperature from $T_\infty$ to the value of $T$ at the bubble boundary takes place in a layer of liquid adjacent to the bubble which has a small thickness compared with bubble radius. This assumption of a 'thin thermal boundary layer' resulted in an approximate expression for the liquid temperature at the moving interface,

$$T(R,t) = T_\infty - \left(\frac{\alpha}{\pi}\right)^{1/2} \int_0^t \frac{R^2(\partial T/\partial r)_{r=R(t)}}{\left(\int_0^t R^4(y)dy\right)} dx \qquad (2.7)$$

Then, by assuming thermal equilibrium between the liquid at the interface and the vapour and implementing the energy balance at the interface which relates the rate of heat transfer to the bubble to the vapour mass balance, Plesset and Zwick determined that,

$$R(t) \approx 2\sqrt{3}Ja\left(\frac{\alpha t}{\pi}\right)^{1/2} \tag{2.8}$$

Here, $Ja = \frac{\rho_l C_{pl}(T_\infty - T_{sat})}{\rho_v h_{fg}}$ is the dimensionless superheat known as the Jakob number. According to Prosperetti and Plesset (1978), Eq. (2.8) predicts that the radius will increase asymptotically with time if growth is diffusion controlled and is valid only for times large enough that the growth velocity is much smaller than the inertia controlled velocity. From the Eq. (2.8), it clearly shows that the growth is asymptotic;

$$R \approx B.t^{1/2} \tag{2.9}$$

where the Plesset and Zwick solution, $B$ is,

$$B = \left[\frac{12\alpha Ja^2}{\pi}\right]^{1/2} \tag{2.10}$$

Forster and Zuber (1954) performed a similar analysis in which the interface temperature was approximated by integrating the Green's function over the domain of the 'thin thermal boundary layer'. The Clausius-Clapeyron relation was once again used in the relationship between vapour pressure and temperature to give the asymptotic expression,

$$R(t) \approx 2\left(\frac{\pi}{2}\right)Ja\left(\frac{\alpha t}{\pi}\right)^{1/2} \tag{2.11}$$

Eq. (2.11) also clearly shows that the bubble growth relation is asymptotic with the relation,

$$R \approx C.t^{1/2} \tag{2.12}$$

where for the Forster and Zuber solution, $C$ is,

$$C = \sqrt{\pi \alpha J a^2} \tag{2.13}$$

Meanwhile, without the assumption of a 'thin thermal boundary layer' as previously used by Plesset and Zwick (1954) and Forster and Zuber (1954), Scriven (1959) determined the exact solutions of the energy equation including the effects of radial convection resulting from unequal phase densities to obtain an asymptotic relation for thermal diffusion controlled growth,

$$R(t) \approx 2\beta \sqrt{(\alpha t)} \tag{2.14}$$

The constant $\beta$ depends on the system pressure and the degree of superheat. For the case of moderate to high superheats or large Jakob numbers, Eq. (2.14) simplifies to,

$$R(t) \approx 2\sqrt{3} \left( \frac{1}{1+\gamma} \right) Ja \left( \frac{\alpha t}{\pi} \right)^{1/2} \tag{2.15}$$

where,

$$\gamma = \left( \frac{C_{pl} - C_{pv}}{h_{fg}} \right) \Delta T \tag{2.16}$$

When Eq. (2.15) is applied for common fluids and system condition in which $\gamma \ll 1$, it is identical to the solution given by Plesset and Zwick (1954) [Eq. (2.8)]. This implies that for large enough Jakob numbers, the 'thin thermal boundary layer' assumption is

valid [Robinson (2002)]. For the case of small Jakob numbers or low superheats, Scriven (1959) obtained,

$$R(t) \approx \sqrt{2\pi} \left( \frac{1}{1+\gamma} \right) Ja^{1/2} \left( \frac{\alpha t}{\pi} \right)^{1/2} \qquad (2.17)$$

When applied to the common fluids and system conditions ($\gamma \ll 1$), it simplifies to,

$$R(t) \approx \sqrt{2Ja.\, \alpha t} \qquad (2.18)$$

It is also noticed from the Eq. (2.18) that the time taken to diffuse such a distance is itself proportional to $R^2$,

$$R \approx D.\, t^{1/2} \qquad (2.19)$$

where the Scriven solution, $D$ is,

$$D = \sqrt{2Ja.\, \alpha} \qquad (2.20)$$

From the works of Plesset and Zwick (1954), Forster and Zuber (1954) and Scriven (1959) in the case of thermal diffusion controlled bubble expansion, it is noticed that the expressions given have the same asymptotic dependence on time ($\approx t^{1/2}$) but a different dependence on the Jakob number. This implies that for small Jakob numbers, the 'thin thermal boundary layer' assumption may no longer be valid [Robinson (2002)]. It suggests the following dependence on the Jakob number,

$$
\begin{aligned}
R \sim Ja \quad &\text{(large Ja)} \\
&\qquad\qquad\qquad\qquad (2.21) \\
R \sim Ja^{1/2} \quad &\text{(small Ja)}
\end{aligned}
$$

Postulation can be made from the above efforts that the early stage of bubble growth is inertia controlled and the later stage is diffusion controlled. A general relation for bubble growth rates in a uniformly superheated liquid which is applicable for the entire range of the bubble growth, including inertia controlled and diffusion controlled growth, was derived by Mikic et al. (1970). They used the Clausius-Clapeyron equation for the vapour pressure curve, assuming thermal equilibrium in the vapour bubble so that the vapour pressure corresponds to the bubble wall temperature as the bubble grows. The relation was compared with the existing experimental data of Lien and Griffith (1969) for water over a wide range of systems pressures, including low pressure data with a significant inertia controlled region and it was found to be in good agreement. The relation for the variation of bubble radius with time which spans both regions is,

$$R^* = \frac{2}{3}\left[(t^+ + 1)^{3/2} - (t^*)^{3/2} - 1\right] \tag{2.22}$$

where the scaled variables are given by,

$$R^* = \frac{R}{B^2/A}; \quad t^* = \frac{t}{B^2/A^2} \tag{2.23}$$

$$A = \left[b\frac{\Delta T h_{fg}\rho_v}{T_{sat}\rho_l}\right]^{\frac{1}{2}}; \quad B = \left[\frac{12}{\pi}Ja^2\alpha_l\right]^{\frac{1}{2}} \tag{2.24}$$

in which,

$b$ = 2/3 for bubble growth in an infinite medium;

$b$ = $\pi/7$ for bubble growth on a surface

Prosperetti and Plesset (1978) have extended the range of the bubble growth rate relation introduced by Mikic et al. (1970) by introducing scaling variables which

describe growth over the entire range of superheats. By assuming a linear variation of vapour pressure with temperature, they obtained the expression,

$$R^* = \left(\frac{2}{\pi^2}\right)\left(\frac{2}{3}\right)\left[\left(\frac{1}{2}\pi^2 t^* + 1\right)^{3/2} - \left(\frac{1}{2}\pi^2 t^*\right)^{3/2} - 1\right] \tag{2.25}$$

where the scaled variables are expressed as,

$$R^* = \mu^2 \frac{R}{R_c} \qquad t^* = \beta\mu^2 t$$

$$\mu = \frac{1}{3}\left(\frac{2\sigma\alpha}{\pi}\right)^{1/2}\frac{\rho_l h_{fg}}{k(T_\infty - T_{sat})}\left(\rho_l[P_v(T_\infty) - P_\infty]\right)^{-1/4} \tag{2.26}$$

$$\beta = \frac{[P_v(T_\infty) - P_\infty]^{3/2}}{2\sigma\rho_l^{1/2}}$$

Analytical bubble growth studies in the region of thermal diffusion controlled growth were later extended to consider non-uniform temperature fields which approximate the conditions of heterogeneous nucleate boiling at a heating surface; for examples the works of Zuber (1961), Han and Griffith (1965), Cole and Shulman (1966) and Mikic and Rohsenow (1969). Zuber (1961) in his study of non-uniform temperature field effects took into account the heat flux from the heated surface to the liquid. For a spherical bubble, the rate of evaporation was given by:

$$h_{fg}\rho_v\frac{dR}{dt} = b\left[k\frac{T_w - T_{sat}}{\sqrt{\pi\alpha t}} - q_w\right] \tag{2.27}$$

and the bubble growth expression was given by,

$$R = b\frac{2}{\pi}Ja\sqrt{\pi\alpha t}\left[1 - \frac{q_w\sqrt{\pi\alpha t}}{2k(T_w - T_{sat})}\right]$$

(2.28)

with a constant factor, $b$ for the effect of sphericity which lies between 1 and $\sqrt{3}$ with $\pi/2$ as an intermediate value.

Han and Griffith (1965) took into account the thermal boundary layer thickness and a critical wall superheat relation to the cavity to obtain bubble growth rates. The thermal layer thickness was obtained from the consideration of transient conduction into a layer of liquid on the surface. The Han and Griffith bubble growth expression in a non-uniform temperature field is expressed as,

$$R = \frac{\varphi_s\varphi_c}{\varphi_v}\frac{k}{h_{fg}\rho_v}\left\{\frac{2(T_w - T_{sat})}{\sqrt{\pi\alpha}}t^{1/2} - \frac{(T_w - T_\infty)\delta^2}{\delta}\frac{4\alpha t}{4\alpha}\left(\frac{4\alpha t}{\delta^2}erf\frac{\delta}{\sqrt{4\alpha t}}\right)\right.$$
$$\left. + \frac{2}{\sqrt{\pi}}\frac{\sqrt{4\alpha t}}{\delta}exp\left[-\frac{\delta^2}{4\alpha t}\right] - erfc\frac{\delta}{\sqrt{4\alpha t}}\right\}$$

(2.29)

where,

curvature factor, $\varphi_c$ where $1 < \varphi_c < 3^{1/2}$

surface factor, $\varphi_s = \frac{2\pi R^2(1+\cos\theta)}{4\pi R^2} = \frac{1+\cos\theta}{2}$

volume factor, $\varphi_v = \frac{\frac{1}{3}(4\pi R^3) - \frac{1}{3}[2\pi R^3(1-\cos\theta)] + \frac{1}{3}\pi R^3\sin\theta\cos\theta}{\frac{1}{3}(4\pi R^3)} = \frac{2+\cos\theta(2+\sin^2\theta)}{4}$

Mikic and Rohsenow (1969) considered bubble growth in a non-uniform temperature field by using a one-dimensional model corrected for sphericity in order to approach the limit for the bubble growth in a uniformly superheated liquid when the waiting time, $t_w$ approaches infinity. They introduced the assumption that the actual heat flux can be expressed as,

16

$$\frac{q}{A} = Ck\left(\frac{T_w - T_{sat}}{\sqrt{\alpha\pi t}} - \frac{T_w - T_b}{\sqrt{[\pi\alpha(t + t_w)]}}\right) \tag{2.30}$$

where $A$ being area and correction factor $C$ was found to be $\sqrt{3}$. The second term in Eq. (2.30) represents the effects of a non-uniform temperature field. As the growth of the vapour bubble is governed by the heat transfer process, the Eq. (2.30) can be written as,

$$\rho_v h_{fg}\frac{dR}{dt} = k\sqrt{3}\left(\frac{T_w - T_{sat}}{\sqrt{\alpha\pi t}} - \frac{T_w - T_b}{\sqrt{[\pi\alpha(t + t_w)]}}\right) \tag{2.31}$$

By integrating Eq. (2.31) using $R = 0$ at $t = 0$ gives an expression for bubble growth,

$$R = \frac{2}{\pi}\sqrt{3}Ja\sqrt{\pi\alpha t}\left\{1 - \frac{T_w - T_b}{T_w - T_{sat}}\left[\left(1 + \frac{t_w}{t}\right)^{1/2} - \left(\frac{t_w}{t}\right)^{1/2}\right]\right\} \tag{2.32}$$

### 2.1.2  Bubble Departure

Perhaps the first model for predicting bubble departure was introduced by Fritz (1935). The Fritz equation, by utilizing the contact angle, $\alpha$ and the surface tension, $\sigma$ gives the bubble departure diameter as the diameter that satisfies the condition in which the buoyancy force is balanced by the capillary force,

$$\frac{\pi D_{eq}}{6}(\rho_l - \rho_v)g = \pi D_0\sigma\sin\alpha_0 \tag{2.33}$$

where,

$$D_{eq} = \sqrt[3]{\frac{6V_b}{\pi}}$$ (2.34)

Here, it is supposed that the diameter of the bubble base is proportional to the equivalent diameter of the bubble,

$$D_0 = CD_{eq}$$ (2.35)

Then, by substituting Eq. (2.35) into Eq. (2.33) Fritz obtained,

$$\frac{D_{eq}^2}{6}(\rho_l - \rho_v)g = C\sigma \sin \alpha_0$$ (2.36)

which gives the definition of bubble departure diameter as,

$$D_b = \sqrt{6C \sin \alpha_0}\sqrt{\frac{\sigma}{g(\rho_l - \rho_v)}} \cong C\alpha_0\sqrt{\frac{\sigma}{g(\rho_l - \rho_v)}}$$ (2.37)

where $C$ is taken as 0.0208 and $\alpha_0$ is in degrees.

A similar method to predict the bubble departure diameter has been proposed by Chesters (1977). By using the same physical condition as Fritz (1935), he showed that for small values of the shape factor defined as,

$$\beta = \frac{(\rho_l - \rho_v)gR_T^2}{\sigma}$$ (2.38)

where $R_T$ is the bubble radius at the apex, the bubble departure diameter can be predicted as,

18

$$D_b = k \sqrt[3]{\frac{6D_0\sigma}{g(\rho_l - \rho_v)}} \qquad (2.39)$$

The correction factor $k < 1$ was added to account for the over pressure inside the bubble.

Kiper (1971) in his predictive study for determining the minimum bubble departure diameter in saturated nucleate pool boiling, found that the minimum departure size varies with Jakob number only. In his work, the bubble is considered to be of spherical form ending with a small neck which connects the bubble to the heated surface as shown in Figure 2.1. He neglected both the drag force and the vapour inertia force, though he considered the inertia of the fluid. Consistent with the previous models of bubble departure, individual bubbles will depart when the force balance equation is satisfied, with the forces acting on the bubble defined as follows;

(i)     *The buoyancy force*

$$F_B = \frac{\pi}{6} g \frac{\rho_l - \rho_g}{g_0} D^3 \qquad (2.40)$$

where $g_0$ is a conversion constant. The contact area at the base of the bubble is small with respect to the bubble size and the overpressure effect is negligible.

(ii)    *The capillary force*

$$F_C = -\sigma \pi D_0 \cos \alpha \qquad (2.41)$$

Furthermore, if the geometry of the neck is known then the term $D_0\cos\alpha$ can be expressed as;

$$F_C = -\sigma \pi G(\theta) D \tag{2.42}$$

where $G(\theta)$ is related to geometry of the bubble neck.

*(iii)    The liquid inertia force*

The inertial force of the apparent liquid mass surrounding the bubble was initially derived by Keshock and Siegel (1964). They have included the affected mass of the fluid which occupy the bubble volume by $11/16$ as suggested by Han and Griffith (1962). The acceleration of the fluid is approximated by the time rate of change of the bubble growth velocity where the velocity is the change of radius with time as suggested by Clark and Merte (1963) and Adelberg (1963). Then, the inertia force becomes,

$$F_I = \frac{d}{dt} mu = \frac{d}{dt}\left[\left(\frac{11}{16}\frac{\rho_l}{g_0}\frac{\pi D^3}{6}\right)\frac{1}{2}\frac{dD}{dt}\right] \tag{2.43}$$

which can be rewritten in the final form,

$$F_I = \frac{11}{192}\frac{\pi \rho_l}{g_0}\left[D^3 \frac{d^2 D}{dt^2} + 3D^2 \left(\frac{dD}{dt}\right)^2\right] \tag{2.44}$$

By substituting the bubble growth law, i.e., $D = \beta . t^{1/2}$, Kiper (1971) obtained the inertia force as,

$$F_I = \frac{11}{384}\frac{\pi \rho_l}{g_0}\beta^4 \tag{2.45}$$

where $\beta$ is the bubble growth parameter.

*(iv)    The pressure restraining force (form drag)*

This force is due to the specific pressure distribution on the bubble surface which tends to flatten the bubble and hold it against the wall. This force is defined as

$$F_D = -0.0181\pi \frac{\rho_l}{g_0} \beta^4 \tag{2.46}$$

The force balance can be rewritten as;

$$F_B + F_I = F_C + F_D \tag{2.47}$$

By using the foregoing force expressions at the moment of bubble departure, the force balance equation can be written as,

$$aD_b^3 + bD_b + c = 0 \tag{2.48}$$

where;

$$a = \frac{1}{6}g \frac{\rho_l - \rho_g}{g_0}, \quad b = -\sigma G(\theta)_d, \quad c = 0.0105 \frac{\rho_l}{g_0} \beta^4 \tag{2.49}$$

The equation has several solutions though just one was found to predict the experimental result which was;

$$D_b = 2.7Ja \tag{2.50}$$

where $Ja$ is the Jakob number. For otherwise constant fluid properties, this expression predicts that the bubble departure diameter increases linearly with superheat. As such the departure volume will increase as a cubic function of superheat.
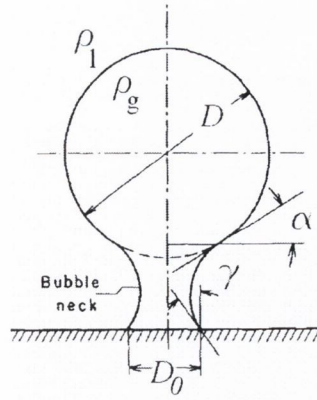
Figure 2.1: Geometry of the growing bubble (Kiper, 1971)

Zeng et al. (1993) proposed a somewhat different model considering that the dominant forces leading to bubble detachment would be the unsteady growth force and the buoyancy force by neglecting the surface tension terms, which were previously considered by many earlier researchers. Under these circumstances the detachment condition occurs when,

$$F_{buoy} + F_{duy} > 0 \qquad (2.51)$$

where the first term is the buoyancy effect which is equal to,

$$F_B = V_b(\rho_l - \rho_v)g \qquad (2.52)$$

The second term is the unsteady growth force in the vertical direction. The author modelled this force by considering a hemispherical bubble expanding in an inviscid liquid. An empirical constant, $C$ was introduced to account for the presence of a wall;

$$F_{duy} = \rho_l \pi r^2 \left(\frac{3}{2}\beta \dot{R}^2 + R\ddot{R}\right) \qquad (2.53)$$

The bubble growth constant $\beta$, was found experimentally as $\beta = 20/3$.

The evaluation of the growth stemmed from knowledge of the bubble growth rate $R(t)$. In general this follows a power law;

$$R(t) = K t_g^n \tag{2.54}$$

where $K$ and $n$ were determined empirically. The unsteady growth force can then be defined as;

$$F_{duy} = -\rho_l \pi K^{2/n} \left[ \frac{3}{2} \beta n^2 + n(n-1) \right] r^{4-(2/n)} \tag{2.55}$$

By balancing of the buoyancy and unsteady growth forces, the value of the detachment diameter was obtained as;

$$D_b = 2 \left\{ \frac{3}{4} \frac{K^{2/n}}{g} \left[ \frac{3}{2} \beta n^2 + n(n-1) \right] \right\}^{n/(2-n)} \tag{2.56}$$

From Eq. (2.56) it is possible to observe that for gravity tending to zero, the vapour bubbles will not depart the heating surface unless there is some external mechanism to induce an inertial force, such as system vibration.

Yang et al. (2000) have predicted the bubble departure diameter by correlating the bubble departure diameter only with the bubble growth time. They determined this after plotting the relationship between dimensionless growth time and departure diameter for the various different liquids and wide range of pressures experimented by Cole (1967), Han and Griffith (1965), Stralen et al. (1975) and Keshock and Siegel (1964) as shown in Figure 2.2. The data was correlated in the form $D_b^+ = \beta_t \left( t_g^+ \right)^{2/3}$. The dimensionless departure diameter and growth time are as follows:

$$D_b^+ = \frac{D_b}{L_0} = \frac{AD_b}{\emptyset B^2} t_g^+ = \frac{1}{\emptyset}\left(\frac{A}{B}\right)^2 t_g \tag{2.57}$$

where

$$A = \sqrt{\frac{2\rho_v(T_w - T_{sat})h_{fg}}{3\rho_l T_s}} \ ; \ B = Ja\sqrt{\frac{12}{\pi}}\alpha_l \ ;$$

$$\emptyset = \left[1 + \frac{1}{2}\left(\frac{\pi}{6Ja}\right)^{2/3} + \frac{\pi}{6Ja}\right] \tag{2.58}$$

By using the correlation proposed by Rohsenow (1951);

$$\frac{Re_b Pr_l}{Nu_b} = C_b Re_b^m Pr_l^n \tag{2.59}$$

where

$$Nu_b = \frac{2f(c)}{3c^2}\frac{D_b A}{\alpha_l Ja} \qquad Re_b = \emptyset\frac{\rho_l B^2}{\mu_l} \tag{2.60}$$

According to Mei et al. (1995),

$$f(c) \approx 1 - \frac{3}{4}\left[1 - \sqrt{1 - c^2}\right]^2 + \frac{1}{4}\left[1 - \sqrt{1 - c^2}\right]^3 \tag{2.61}$$

where the parameters $c = R_b/R_t$, with $R_b$ and $R_t$ defined in Figure 2.3. Combining this Eq. (2.59) then becomes,

$$D_b^* \psi = \frac{3}{2C_b} \left(\frac{\pi}{12}\right)^m Ja^{1-2m} Pr_1^{m-n} \tag{2.62}$$

where

$$\psi = \frac{c^2}{\emptyset^m f(c)} \tag{2.63}$$

Prediction results of Eq. (2.62) were then compared with the measured data of both organics liquids and water for the entire range of experimental conditions and produced exponents of $m$ = 1.4 and $n$ = 0.8. Introducing the values of $m$ and $n$ and Eq. (2.58) into Eq. (2.62) gives;

$$D_b = 8.0351 \times 10^4 \frac{\rho_l}{\rho_v} \frac{\sqrt{c_{pl} T_{sat}}}{h_{fg}} \frac{\alpha Pr_l^{3/5}}{\eta} \tag{2.64}$$

where $\eta = \psi . Ja^{0.3}$
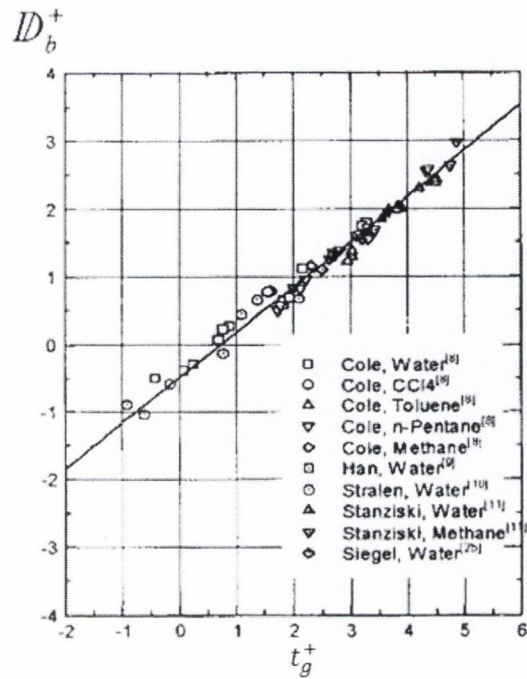
Figure 2.2: Relationship between dimensionless growth time and departure diameter

(Yang et al., 2000)
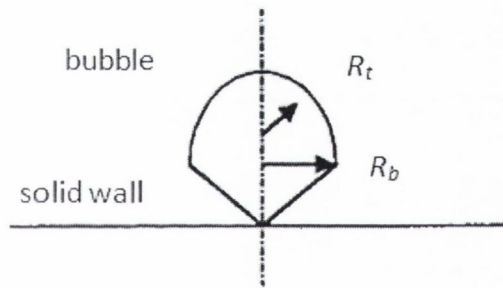


Figure 2.3: Sketch for the growing bubble (Yang et al., 2000)

### 2.1.2.1 Bubble Departure Frequency

Several models and correlations were found from the past analytical studies to predict bubble departure frequency for pool boiling. In addition, bubble departure frequency can be deemed as the reciprocal of the summation of bubble waiting time, $t_w$ and bubble growth time, $t_g$,

26

$$f_d = \frac{1}{t_w + t_g} \tag{2.65}$$

Zuber (1959) proposed an equation describing the product of frequency and departure diameter in terms of fluid properties. He suggested that it is related to the velocity at which bubbles rise in a liquid, expressed as,

$$v_\infty = 1.18 \left[ \frac{\sigma g (\rho_l - \rho_v)}{\rho_l^2} \right]^{1/4} \tag{2.66}$$

He then assumed that,

$$f.D_b \propto v_\infty \tag{2.67}$$

and found an expression of the form,

$$f.D_b = 0.59 \left[ \frac{\sigma g (\rho_l - \rho_v)}{\rho_l^2} \right]^{1/4} \tag{2.68}$$

However, Zuber's expression has been found to fit experimental data for only a limited range of bubble boiling conditions. Importantly, however, the Zuber correlation predicts an inverse relation between bubble frequency and departure diameter.

Later, McFadden and Grassmann (1962) assumed that the frequency-diameter product $f.D_b$ is a function of $D_b, \sigma, \rho_l$ and $\Delta\rho$ shown as follows,

$$\frac{f.D_b^2 \rho_l^{1/2}}{(\sigma D_b)^{1/2}} \propto \left( \frac{g\Delta\rho D_b^2}{\sigma} \right)^n \tag{2.69}$$

Eq. (2.69) describes the bubble frequency and bubble departure diameter in terms of liquid and vapour properties. The left side of Eq. (2.69) represents the square root of inertial force to surface tension force ratio whereas the right side represents the $n^{th}$ power of the ratio of the buoyant force to the surface tension force. They found that $n \approx \frac{1}{2}$ satisfactorily fitted most of the available experimental data at that time. The bubble departure frequency expression by McFadden and Grassmann is thus given as,

$$f.D_b^{1/2} \approx 0.56 \left( \frac{g \Delta \rho}{\rho_l} \right)^{1/2} \qquad (2.70)$$

This correlation predicts that $f \, \alpha \, D_b^{-1/2}$ which is an asymptotic inverse relation of frequency with departure diameter. McFadden and Grassmann also considered the case when bubble departure is acted upon by various other forces, particularly at low heat flux, where the bubble departure frequency can be expressed as,

$$f.D_b^{1/2} \, \alpha \, g^{1/2} \qquad (2.71)$$

Still, the functional relationship between the frequency and departure diameter remains unchanged.

Soon after, Mikic and Rohsenow (1969) predicted a relationship between bubble frequency and departure diameter from their bubble departure expression for saturated boiling as follows,

$$D_b = \frac{4}{\pi} \sqrt{3} Ja \sqrt{\pi \alpha t_c} \left[ 1 + \left( \frac{t_w}{t_g} \right)^{1/2} - \left( 1 + \frac{t_w}{t_g} \right)^{1/2} \right] \qquad (2.72)$$

Rearranging Eq. (2.72) gives,

$$\frac{D_b f^{1/2}}{\frac{4}{\pi}\sqrt{3}Ja\sqrt{\pi\alpha}} = \left(\frac{t_g}{\tau}\right)^{1/2} + \left(1 - \frac{t_g}{\tau}\right)^{1/2} - 1 \tag{2.73}$$

where,

$$f = \frac{1}{t_g + t_w} = \frac{1}{\tau} \tag{2.74}$$

Mikic and Rohsenow stated that the ratio $\left(\frac{t_g}{\tau}\right)$ for a given nucleation site is a function of pressure and would be different at different nucleus sites. From a wide range of $\left(\frac{t_g}{\tau}\right)$, they obtained the simplified expression,

$$D_b.f^{1/2} \cong 0.83 Ja\sqrt{\pi\alpha} \quad (\pm 10\%) \tag{2.75}$$

Interestingly the bubble frequency is predicted to be a function of $[(T_w\text{-}T_{sat})/D_b]^2$ so is a function of both superheat and departure diameter.

### 2.1.3  Bubble Waiting Time

The bubble waiting time is the interval between when the previous bubble departs and the next one nucleates. The waiting time, $t_w$ can be related to the particular cavity size [Mikic and Rohsenow (1969) and Han and Griffith (1965)]. During the waiting time, when the bubble is not growing, the bubble temperature, $T_b$ has been derived from the equation of a vapour bubble in thermodynamic equilibrium,

$$\Delta P = \frac{2\sigma}{R_c} \tag{2.76}$$

which, after applying the Clasius-Clapeyron equation becomes,

$$T_b = T_{sat} + \frac{2\sigma T_{sat}}{R_c \Delta \rho h_{fg}} \tag{2.77}$$

A hemispherical bubble of radius, $R_c$ (located over a cavity of the same radius) will start to grow when the vapour temperature is greater than $T_b$ in Eq. (2.78). The time required to achieve this temperature is the waiting time.

The expression for the temperature distribution in the liquid was given by Mikic and Rohsenow as follows:

$$T(y,t) = T_\infty + (T_w - T_\infty)\text{erfc}\left\{\frac{y}{2\sqrt{[\alpha(t+t_w)]}}\right\}$$
$$- (T_w - T_\infty)\text{erfc}\left\{\frac{y}{2\sqrt{\alpha t}}\right\} \quad \text{for } t > 0 \tag{2.78}$$

By assuming that in a non-uniform temperature field the tip of the considered bubble ($y = R_c$) should be at $T_b$ for the beginning of the bubble growth, Mikic and Rohsenow have an expression from the relations of the Eqs. (2.77) and (2.78) as follows:

$$T_b = T_{sat}\left(1 + \frac{2\sigma T_{sat}}{R_c \Delta \rho h_{fg}}\right) = T_\infty + (T_w - T_\infty)\text{erfc}\frac{R_c}{2\sqrt{\alpha t_w}} \tag{2.79}$$

or:

$$t_w = \frac{1}{4a}\left\{\frac{R_c}{\text{erfc}^{-1}\left[\frac{T_{sat}-T_\infty}{T_w-T_\infty} + \frac{2\sigma T_{sat}}{(T_w-T_\infty)\Delta \rho h_{fg} R_c}\right]}\right\}^2 \tag{2.80}$$

In a similar fashion, the earlier study of Han and Griffith (1965) have equated the bubble temperature to the fluid temperature at the distance of $y = \frac{3}{2} R_c$ from the heating surface, consequently the waiting time is obtained $\frac{9}{4}$ times of the above value in Eq. (2.80) as follows:

$$t_w = \frac{9}{16a} \left\{ \frac{R_c}{\text{erfc}^{-1} \left[ \frac{T_{sat}-T_\infty}{T_w-T_\infty} + \frac{2\sigma T_{sat}}{(T_w-T_\infty)\Delta\rho h_{fg}R_c} \right]} \right\}^2 \qquad (2.81)$$

## 2.2 Experimental Single Bubble Dynamics

Lee et al. (2003) performed an experiment of nucleate pool boiling with constant wall temperatures to investigate single bubbles growing in saturated conditions. They used R11 and R113 as working fluids. A microscale heater array was used to maintain the constant wall temperature. Each heater in the array had dimensions of 0.27 x 0.27 mm, which is comparable with the diameter of a typical single bubble (0.25-0.7 mm). A high-speed CCD camera synchronized with the heat flow rate measurements was used to capture the bubble growth images and the geometry of the bubble was obtained from those images. The captured images showed a spheroidal-shaped bubble during growth. The images also showed an asymptotic bubble radius growth rate proportional to $t^{1/5}$, which was much slower than the previous analytical studies which show a $t^{0.5}$ relationship. To analyse the data, they used dimensionless parameters of time and bubble radius to characterize the asymptotic growth behaviour irrespective of the wall condition. The dimensionless parameters were derived from the ratio of the corresponding latent heat transfer and the conduction heat transfer rate through the bubble interface, $(q_{latent}/\dot{q}_{cond})$.

Quite recently, Siedel et al. (2008) have performed a nucleate pool boiling experiment on an artificial nucleation site to analyse single bubble growth dynamics.

Pentane was used as a working fluid in this work. Bubble growth was recorded by a high speed camera under various wall superheat conditions. They found that the bubble volume at departure was independent of the wall superheat, whereas the growth time was dependant on the superheat. The bubble growth rate was found to follow non-dimensional growth laws; $V^* = t^{*0.6}$ for $t^* > 0.2$ and $V^* = 2 \times t^*$ for $t^* < 0.2$. Furthermore, the bubbles growth times were found to be approximately proportional to the wall superheat. However, the product $(f.D_b)$ was found not to be a constant, in contrast to many earlier models. This was due to the invariant bubble departure diameter with wall superheat.

## 2.3    Subcooling Effects on Bubble Dynamics

### 2.3.1   Analytical Study

Based on the analytical study of waiting time $t_w$ by Han and Griffith (1965) as indicated in Eq. (2.81) for the consideration of $y = \frac{3}{2}R_c$, it clearly predicts that the waiting time increases with the increasing liquid subcooling. In addition, the waiting time also increases with increasing cavity radius, $R_c$. The same trend for the waiting time with changing liquid subcooling can be obtained from the proposed waiting time theory of Mikic and Rohsenow (1969) as shown in Eq. (2.80) for the consideration of $y = R_c$.

Quite recently, relative to the earlier works, Zhao and Tsuruta (2002) presented one of the more comprehensive models for bubble dynamics in subcooled pool boiling. According to this study, one cycle of an individual bubble consists of two parts; one is its lifetime and the other is the waiting time. The lifetime of the individual bubble consists of three periods, i.e., an initial growth period $(0 \leq t \leq t_g)$, a final growth period due to evaporation of a microlayer $(t_g \leq t \leq t_g + t_e)$ and a condensation period $t_c \left(t_g + t_e \leq t \leq t_g + t_e + t_c\right)$ before the individual bubble

collapses as shown in Figure 2.4. Just after the individual bubble collapses and before the next cycle begins, there is a waiting time, $t_w$.



$$0 \le t \le t_g \qquad\qquad t_g \le t \le t_g + \tau_e \qquad t_g + \tau_e \le t \le t_g + \tau_e + \tau_c$$

$$( a ) \qquad\qquad\qquad ( b ) \qquad\qquad\qquad ( c )$$

Waiting time $\tau_w$        Active nuclei

$$( d ) \qquad\qquad\qquad ( e )$$
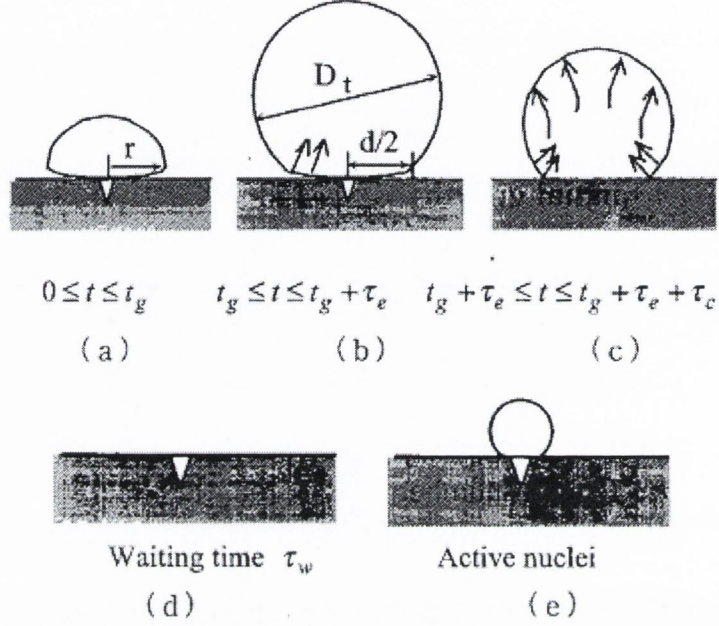
Figure 2.4: One cycle of an individual bubble (Zhao and Tsuruta, 2002)

(i)      *Initial growth period* $\left(0 \le t \le t_g\right)$

During the initial growth of individual bubbles [Figure 2.4 (a)], semi-spherical bubbles grow from an active site and a microlayer is formed under the bubbles, as shown in Figure 2.5 (a). The growth equation of individual bubbles was derived from the heat balance between the latent heat of evaporation of the liquid microlayer and the conduction through the microlayer as follows,

$$\frac{2}{3}\pi R^3 \rho_v h_{fg} = 2\pi k_l \int_0^R \int_{\tau_g}^t \frac{(T_w - T_{sat})}{\delta_{mic}} r \, dt dr, \;\; 0 \le t \le t_g \qquad (2.82)$$

where $\tau_g$ is the time required for formation of the liquid microlayer at the position $r$.

(a) The forming period (b) The evaporation period



(c) Microlayer dryout and macrolayer
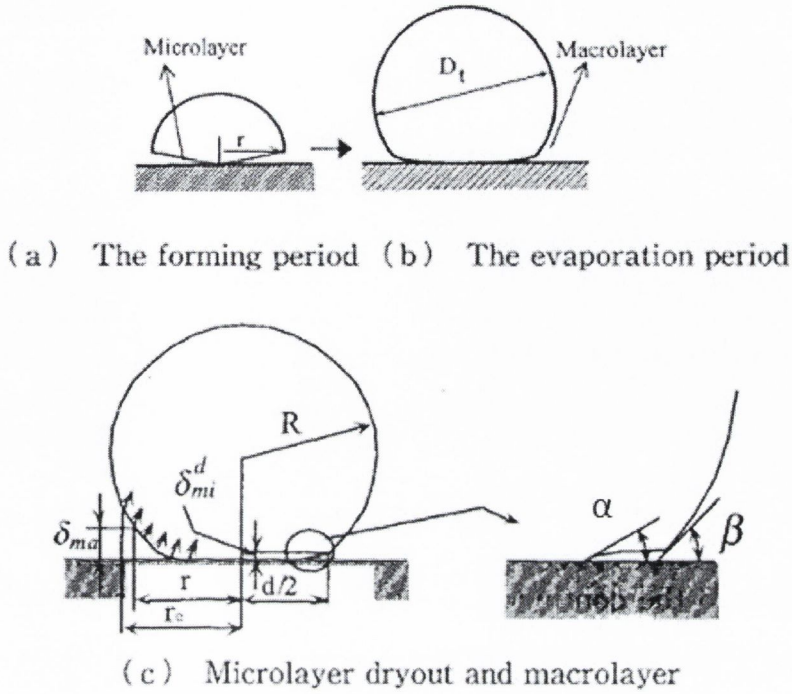
Figure 2.5: Dynamic microlayer (Zhao and Tsuruta, 2002)

When the wall superheat is low, the following approximation was made,

$$\frac{2}{3}\pi R^3 \rho_v h_{fg} = 2\pi k_l \int_0^R \int_0^t \frac{(T_w - T_{sat})}{\delta_{mic}^0} r\, dt\, dr, \ \ 0 \le t \le t_g \tag{2.83}$$

By using the initial thickness of the microlayer $\delta_{mic}^0$ at any point (radius $r$) by Cooper and Lloyd (1969) which is,

$$\delta_{mic}^0 = 0.8\sqrt{\vartheta_l t} = \sqrt{c\alpha.t}, \ \ with\ c = 0.64\, \mathrm{Pr} \ \ \ 0 \le t \le t_g \tag{2.84}$$

the bubble radius expression then was obtained,

$$R = \frac{2k_l(T_w - T_{sat})}{\rho_v h_{fg}\sqrt{c\alpha}} t^{1/2} \tag{2.85}$$

At the end of the initial growth phase of an individual bubble $(t = t_g)$, the bubble diameter $d$ was given by,

$$d = \frac{4k_l(T_w - T_{sat})}{\rho_v h_{fg}\sqrt{c\alpha}} \cdot t^{1/2} \tag{2.86}$$

or the initial growth duration of the individual bubble is given as,

$$t_g = c\alpha \left[\frac{\rho_v h_{fg} d}{4k_l(T_w - T_{sat})}\right]^2 \tag{2.87}$$

(ii)     *Final growth period* $(t_g \leq t \leq t_g + t_e)$

Meanwhile, for the period of final growth due to evaporation of the microlayer $(t_g \leq t \leq t_g + t_e)$, the microlayer was reported not to expand and the shape of the bubble changes from semi-spherical to a spherical segment geometry due to the evaporation of the microlayer as shown in Figure 2.5. At the same time, a liquid layer thicker than the microlayer is formed under the bubble outside the microlayer area which was called the macrolayer. The evaporation time of the microlayer $t_e$ was determined by the conduction equation of the liquid microlayer with the condition,

$$\delta_{mic(r=d/2)} = 0, \quad at\ t = t_g + t_e \tag{2.88}$$

and the following result was given;

$$t_e = \frac{c^2 \alpha h_{fg}^3 \rho_v^2 d^2}{32 c_{pl} k_l^2 (T_w - T_{sat})^3} \tag{2.89}$$

Since the evaporation time of microlayer, $t_e$ is very short and the evaporation heat flux at the microlayer is very high, the effect of condensation heat transfer is small compared to evaporation and can be disregarded. Therefore, after considering a total heat balance, the bubble radius, $R_e$ at the end of the final growth phase was given by,

$$R_e = \left[\frac{c\alpha\rho_l h_{fg}}{(32\beta_1 k_l[T_w - T_{sat}])}\right]^{1/3} . d \qquad (2.90)$$

where;

$c = $ constant $= 0.64 \, Pr$

$d = $ diameter of individual bubble at the end of initial growth

$= \frac{4k_l(T_w - T_{sat})}{\rho_v h_{fg}\sqrt{c\alpha}} . t^{1/2}$

$\beta_1 = \frac{1}{2} + \frac{3}{4}\cos\beta - \frac{1}{4}\cos^3\beta$, $\beta$ is the configuration bubble angle after microlayer evaporation in Figure 2.5

(iii)   *Condensation period* $t_c\left(t_g + t_e \le t \le t_g + t_e + t_c\right)$

After the dryout of the microlayer, evaporation occurs mainly at the macrolayer region. However, the evaporation heat flux is much smaller than that of the microlayer. On the other hand, at the interface of the vapour bubble, the heat transfer due to vapour condensation becomes dominant and the condensation process of the individual bubble is controlled by the equation,

$$\frac{d}{dt}\left[\frac{4}{3}\pi\beta_1 R^3 \rho_v h_{fg}\right] = \int q_{ev}dA_{mac} - 2(1 + \cos\beta)\pi R^2 h_v (T_{sat} - T_\infty) \qquad (2.91)$$

It was considered that the heat transfer of vapour condensation is governed by convection of subcooled liquid, i.e., $\dot{m}h_{fg} = h_v(T_{sat} - T_\infty)$ with $h_v = 10^4$ W/m$^2$.K,

36

which is independent of liquid subcooling. According to Zhao and Tsuruta (2002), the evaporation heat transfer on the macrolayer can be neglected in typical nucleate boiling scenarios since it is only 5% of total heat transfer, therefore,

$$\frac{d}{dt}\left[\frac{4}{3}\pi\beta_1 R^3 \rho_v h_{fg}\right] \cong \int -2(1 + \cos\beta)\pi R^2 h_v(T_{sat} - T_\infty) \qquad (2.92)$$

The condensation period, $t_c$ was derived from Eq. (2.92) and was given by,

$$t_c = \frac{2\beta_1 \rho_v h_{fg} R_e}{(1 + \cos\beta)h_v(T_{sat} - T_\infty)} \qquad (2.93)$$

*(iv)    Waiting time $t_w$*

During this period, the process of supplying subcooled bulk liquid to the heated wall commences immediately after the bubble collapses before the next bubble cycle begins. The thermal boundary layer grows by transient conduction to the subcooled liquid. The temperature profile in the boundary layer was determined by solving the conjugated heat transfer in both the liquid and the heater wall. In this waiting time analysis, Zhao and Tsuruta (2002) have considered two cases, i.e., 'uniform wall heat flux' and 'uniform wall temperature'. In the case of 'uniform heat flux', they considered the heat capacity of the heater wall, $\rho_s c_{ps}\delta_s$ to be very small, so the wall temperature, $T_w$ and the wall heat flux, $q$ were approximately related by,

$$T_w - T_\infty = \frac{2q\sqrt{\alpha t}}{\sqrt{\pi}k_l} \qquad (2.94)$$

The equivalent thickness of the thermal boundary layer and its temperature profile were given by,

$$\delta = \frac{2\sqrt{\alpha t}}{\sqrt{\pi}} \tag{2.95}$$

$$T = T_w - \frac{(T_w - T_\infty)y}{\delta} \tag{2.96}$$

and the nucleation condition for an active cavity with radius, $R_c$ was given by,

$$T_y = T_{sat} + \frac{2\sin\theta.\sigma T_{sat}}{R_c h_{fg}\rho_v} \tag{2.97}$$

As the liquid temperature profile [Eq. (2.96)] becomes the tangent line of Eq. (2.97) the waiting time becomes,

$$t_w = \left[\frac{\pi(1+\cos\theta)\rho_v h_{fg} R_c^2}{4\sin^2\theta.\sigma T_{sat}}\right]^2 \frac{(T_w - T_\infty)^2}{\pi\alpha} \tag{2.98}$$

where $\theta$ is the contact angle. With the cavity radius, $R_c$ taken as,

$$R_c = \left[\frac{2\sigma T_{sat} k_l \sin^2\theta}{(1+\cos\theta)\rho_v h_{fg} q}\right]^{1/2} \tag{2.99}$$

the minimum waiting time becomes,

$$t_w = \left[\frac{\pi k_l}{2q}\right]^2 \frac{(T_w - T_\infty)^2}{\pi\alpha} \tag{2.100}$$

Meanwhile for the case of 'uniform wall temperature', the equivalent thickness of thermal boundary layer was considered same as in Eq. (2.76) by Han and Griffith (1965) and the minimum waiting time was given by,

$$t_w = \left[\frac{8(1 + \cos\theta)\sigma T_{sat}}{\rho_v h_{fg}}\right]^2 \frac{(T_w - T_\infty)^2}{\pi\alpha(T_w - T_{sat})^4} \tag{2.101}$$

### 2.3.2 Experimental Investigations

Ibrahim and Judd (1985) have performed experiments to investigate the growth and waiting times of bubble forming in water boiling on a copper surface. The growth and departure of bubbles forming at seven different naturally occurring nucleation sites was studied in detail for different combinations of heat flux and subcooling. For each experiment performed, a conductance probe capable of sensing the presence of vapour or liquid at the location of the tip was located at a small distance above the surface and the signals corresponding to the growing and waiting times of 5000 successive bubbles were analysed. The analysis of the results obtained at their nucleation Site E at a heat flux of 166 kW/m$^2$ and various levels of subcooling ranging from 0 to 20$^\circ$C is presented in Figure 2.6.

From their observation, the most curious aspect of the results is the manner in which the waiting time results varied with subcooling. Similar variations were found in the waiting time results obtained at the different nucleation sites under different combinations of heat flux and subcooling. As indicated in Figure 2.6, the variation of the growth time result with subcooling is in excellent agreement with the predictions of a theoretical model of Mikic et al. (1970), but the variation of waiting time with subcooling was most unusual. The initial increase in waiting time with increasing subcooling is consistent with classical nucleation theory in that it is apparent that longer waiting times would be required to heat the liquid in the vicinity of a nucleation site to the condition at which a nucleation could occur. However, it was not possible to explain the apparent decrease in waiting time with increasing subcooling at the time that the paper was published.

A subsequent study of the experimental results presented by Ibrahim and Judd (1985) led to the conclusion that nucleation could not be the mechanism responsible for the initial increase in waiting time with increasing subcooling as had been claimed. As seen in Figure 2.7, the waiting time measurements obtained during the formation of bubbles at Site E were almost independent of heat flux under nearly saturated boiling conditions. Based on classical nucleation theory, the bubble waiting time at the higher levels of heat flux should have been much less than that at the lower level of heat flux due to the fact that the temperature of liquid which replaced the previous departing bubble should have increased in temperature much more rapidly at the higher heat flux than at the lower heat flux. Therefore, a shorter period of time is required for a nucleus to begin to grow. From the data which they obtained, it demanded an explanation of something other than nucleation theory to explain both trends of 'upgoing' and 'downgoing' waiting time results. About a decade later, Judd (1999) stated that the measurement technique of bubble waiting time used by Ibrahim and Judd (1985) was not appropriate to measure waiting time in the case of subcooled boiling. According to Judd (1999), failure to understand the way in which subcooling affects bubble growth was responsible for the incorrect interpretation of the values of waiting time reported in Ibrahim and Judd (1985). Therefore, there is still significant work to be done to gain proper understanding of the influence of subcooling on bubble growth dynamics.
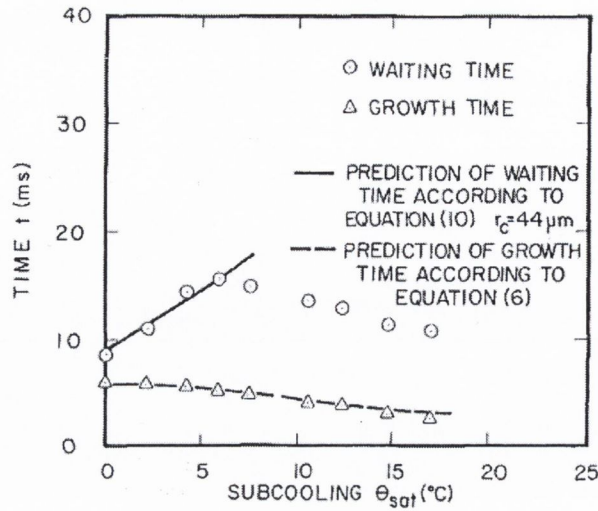
Figure 2.6: Variation of waiting and growing times with subcooling for bubbles forming at Site E [Ibrahim and Judd (1985)]
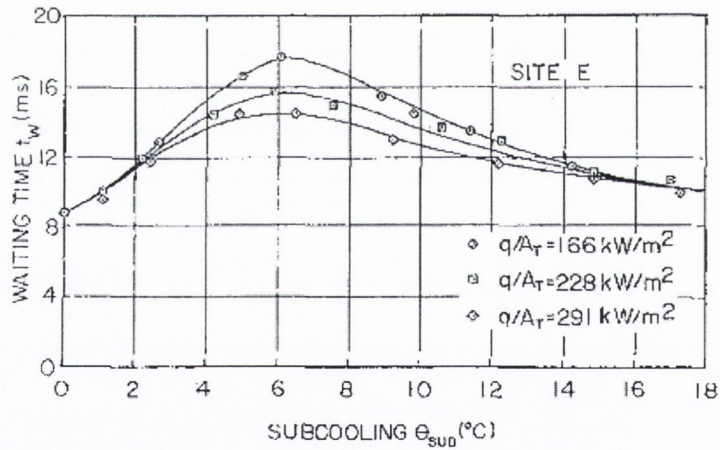


Figure 2.7: Superposition of the waiting time measurements for bubbles forming at site E for all levels of heat flux investigated by Ibrahim and Judd (1985)

By using a high speed camera, Zhao and Tsuruta (2002) performed an experiment to observe vapour bubble behaviour during nucleate pool boiling of subcooled water. The boiling surfaces used were the side surfaces of Pt wires with diameters of 0.3 mm and 0.5 mm. The experiments were performed in the range of water subcooling of 20°C to 60°C at atmospheric pressure. From their observations,

Zhao and Tsuruta presented the wall heat flux and subcooling effects in relation to the bubble lifetime and the conclusions which they have drawn are as follows;

(i)  *Wall heat flux effects*

As the wall heat flux increases, the waiting time and the total period of individual bubbles decrease at the same liquid subcooling for higher wall heat fluxes. Therefore, heat transfer is mainly controlled by the behaviour of individual bubbles. The total latent heat removed by vapour bubbles is smaller as the wall heat flux is increased.

(ii)  *Subcooling effects*

As the subcooling increases, the waiting time becomes much longer. This trend is in contrast to the Ibrahim and Judd (1985) results in which the waiting time decreases with the increasing of liquid subcooling when the subcooling is higher than about 6 K. For a high subcooling of 60 K, the bubble diameter becomes very small even at very high wall heat fluxes and the increasing waiting time trend continued. The total latent heat removed by vapour bubbles becomes smaller as the liquid subcooling is increased. With the trends for bubble diameter, waiting time and latent heat removed by vapour bubbles at high subcooling, it can be concluded that the total heat flux removal is mainly contributed by heat conduction outside the evaporating area as the liquid subcooling become larger. In other words, the enhancement of heat transfer for subcooled boiling is mainly contributed by the augmented heat removal caused by the formation and collapse of individual bubbles.

Demiray and Kim (2004) recently investigated the effects of low and high subcooling on bubbles nucleating from a single site by measuring the heat transfer under the nucleating bubbles using a microheater array with 100 μm resolution. They

used FC-72 as the working liquid. From their observation, the individual bubble departure diameter and energy transfer were larger with low subcooling but the departure frequency increased at higher subcooling, resulting in higher overall heat transfer. They concluded that the majority of the energy for a single bubble event was gained from the superheated liquid layer and not from the wall, indicating that microlayer and contact line heat transfer are not significant. Instead, transient conduction and microconvection are the dominant mechanism of heat transfer.

## 2.4   Summary

From the literature, in the classical analysis of bubble growth the size of the bubble was determined from its radius or diameter which is not an accurate measure of the actual bubble size. Most agree that the shape of bubble of practical importance in boiling is not a perfect sphere, therefore the bubble size is more accurately represented by volume measurement from the actual bubble contour, which will be the technique used in the present study. It is understood that the high technology required for this type of analysis, such as high speed video camera and powerful computers, were not mainstream equipment or mature technologies during those early times. It should be noted that this bubble size measurement technique has been used recently by Siedel et al. (2013) for nucleate boiling and built upon earlier work by Di Bari and Robinson (2013) for adiabatic bubble growth. It can thus be said that this analysis technique is still in the early days of development and that there is still significant work to be done to fully understand bubble dynamics during boiling; these aspects can be technical, such as improvement of bubble image quality (to minimize errors), analytical, such as developing techniques to compensate for the mirage effect, and parametric, such as gaining deeper knowledge of bubble growth characteristics by including the influence of bulk liquid subcooling.

With the global theories and robust empirical formulations of nucleate boiling seeming still to be elusive due to a lack of a complete understanding of the

fundamental physics of bubble dynamics, perhaps the analysis of a single bubble growth could contribute better understanding of bubble dynamics. However, up to now there is still a lack of experimental study of single bubble growth in nucleate boiling for both saturated and subcooled conditions. Therefore, the present experimental study of single bubble growth using the latest technologies would contribute knowledge for deeper understanding of nucleate boiling for both saturated and subcooled conditions.

From the experimental results of waiting time in subcooled boiling presented by Ibrahim and Judd (1985), the trends of 'upgoing' and 'downgoing' of waiting time data with subcooling levels demand an explanation of something other than nucleation theory as suggested by Ibrahim and Judd. Judd (1999) has stated that the measurement technique of bubble waiting time used by Ibrahim and Judd (1985) was not appropriate to measure waiting time in the case of subcooled boiling due to a failure to understand the way in which subcooling affects bubble growth. That being said, there is still much work to be done if we hope to gain a proper understanding of the way in which subcooling affects all aspects of the bubble growth during nucleate pool boiling. Therefore, the present study attempts to make a first step towards an unambigious understanding of subcooling influences on the growth of bubbles.

# CHAPTER 3

# EXPERIMENTAL DESCRIPTION AND DATA ANALYSIS

An experimental apparatus for nucleate pool boiling has been developed with an artificial cavity as a nucleation site. This apparatus is equipped with a subcooling system to subcool the bulk liquid during boiling. The purpose of this experimental facility is to analyse single bubble growth dynamics in pool boiling with and without subcooling. Temperatures and heat fluxes were measured and bubble images were recorded.

In this chapter, the experimental description for the present study is presented. This chapter begins by presenting the experimental set-up describing the vessel, artificial nucleation site, measurement and control equipment, visualization and bulk liquid subcooling. It follows by the experimental procedures, measurement techniques, operating conditions and this chapter will end with a description of the data analysis techniques utilized.

## 3.1    Experimental Set-up

### 3.1.1  Description of the Pool Boiling Facility

In the present study, a pool boiling facility consisting of a sealed cylindrical vessel, as shown schematically in Figure 3.1, has been designed to facilitate observations and video recording of the dynamics of single bubble growth and departure subsequent to nucleation. It is achieved by equipping the vessel with two rectangular windows directly opposite one another. During the experiments, a single bubble event is recorded through one of the windows by using a high speed video camera while the boiling area is illuminated by a light source through the other window.

The working fluid used in this study is HFE-7000. This refrigerant has low boiling point (34°C), good thermal stability, good material compatibility with low global warming potential (GWP) and zero ozone depletion potential (ODP). These properties make it useful as a low temperature heat transfer fluid. Further to this, HFE-7000 is a highly wetting fluid which will cause the bubble foot to remain fixed to the edge of the nucleation site which was desired for this basic study. For these reasons HFE-7000 was selected as the working fluid for the present study.

The vessel is filled with refrigerant until the free surface between the liquid and the vapour phase is at height of about 62 mm from the base of the vessel. In order to maintain the desired saturation and pressure conditions of the working fluid during experiments, a film heater is attached to the outside of the vessel. The boiling surface used in the present study is upward facing in the bulk liquid and it is located in the centre, 30 mm from the base of vessel.
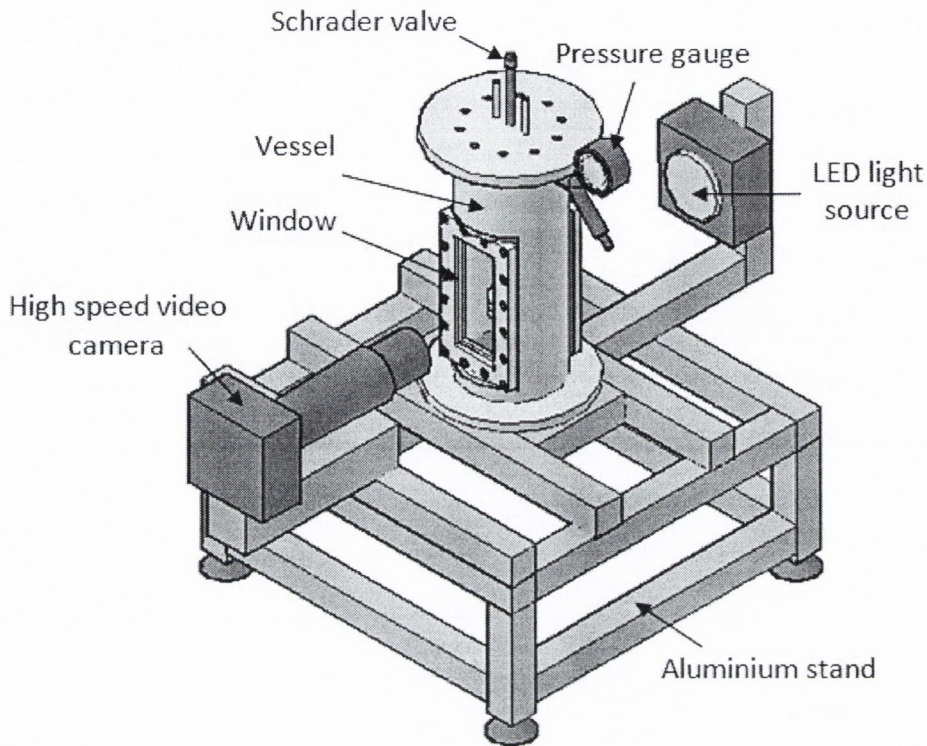
Figure 3.1: Pool boiling facility

### 3.1.2 Pool Boiler

The pool boiler used in the present study is shown in Figure 3.2. The pool boiler is a cylindrical container constructed of stainless steel with the size of 250 x ø80 mm (inner) and wall thickness of 10 mm. The two ends of the cylindrical container are closed by lower and upper flanges and sealed on both ends using a compatible O-ring. The lower flange has a hole to fit the heating element and the upper flange was attached with a Schrader valve which is used during degassing of the liquid and the container.

This pool boiler is equipped with two glass windows to record the bubble images using a high speed video camera and to allow illumination at the boiling surface during visualization and recording of bubble images. The glass is 2 mm in thickness in order to minimize the refraction of light.

Inside and in the centre of the pool boiler, a water coil heat exchanger is placed 15 mm above the heated surface for bulk liquid subcooling experiments. Three T-type thermocouples were placed in the container to measure the bulk liquid temperature and also for bubble size calibration (thermocouple 1 was placed on level and beside the heated surface).
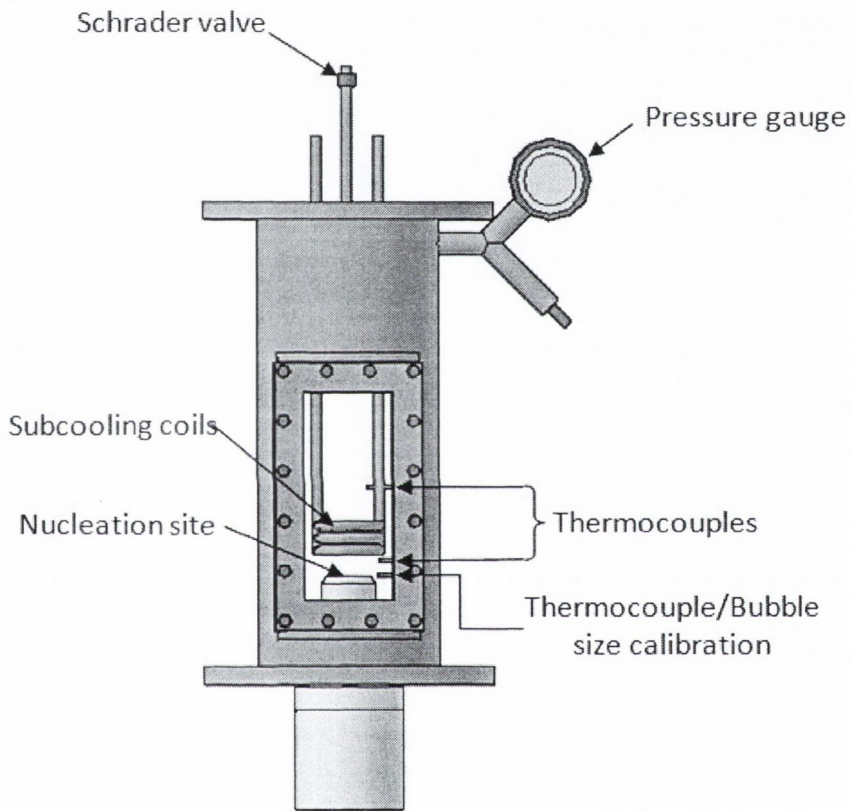


Figure 3.2: Pool boiler

### 3.1.3 Heating Element and Artificial Nucleation Site

A heating element has been built based on the heating element design introduced by Siedel et al. (2008) which is illustrated in Figure 3.3. In the assembly, a cartridge heater is inserted into a 12 mm outer diameter copper rod. The cartridge

heater has dimensions of 50 x ø10 mm and a wattage rating of 150 W and is connected to an AC power supply. The copper tube section narrows over the heater to form a 5 mm diameter and 75 mm long copper rod. This rod is equipped with six T-type thermocouples used to measure the heat flux passing through the rod. From the temperature distribution, the surface temperature is also extrapolated. A 20 mm diameter and 40 µm copper plate with 99.9% purity is bonded with high pressure atop the rod using Araldite thermally conductive adhesive. The assembly is insulated in a PTFE structure using an araldite epoxy resin. The assembly in Figure 3.3 is inserted through the hole of the lower flange of the pool boiler and fastened in place and sealed with a double O-ring seal. At the centre of the copper plate, an artificial nucleation site is created by drilling a hole of approximate depth of 500 µm using a 180 µm ±10 µm drill bit. The drilling process was performed using a programmable micro-drill.
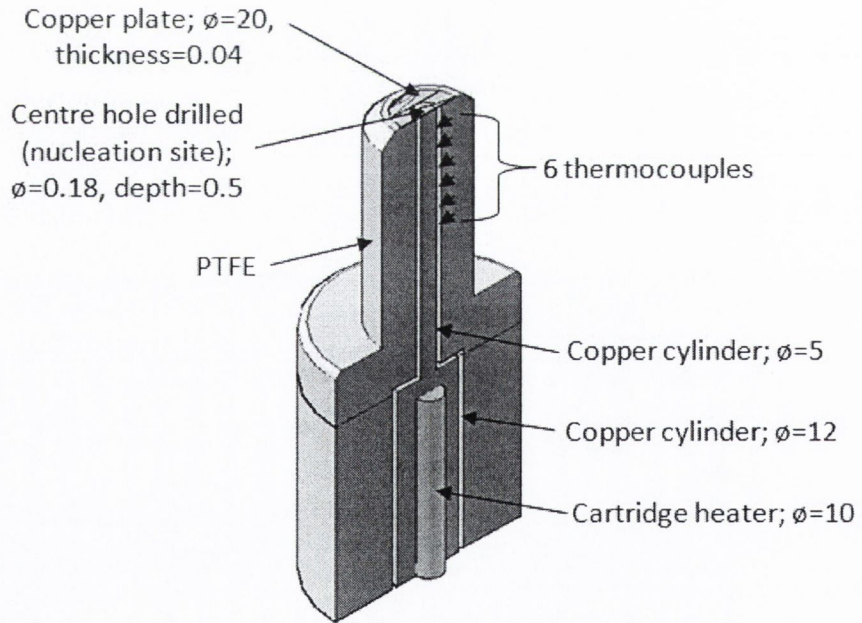


Figure 3.3: Schematic of half slice of heating element and artificial nucleation site

(Unit: mm)

### 3.1.4 Measurement and Control Equipment

*Temperature*

The temperatures at several different locations in bulk liquid have been measured using T-type thermocouples. This type of thermocouples has been chosen due to its high stability of temperature reading relative to other types and its suitability for relatively low temperature measurement as in the present study. Three thermocouples are placed strategically in the bulk liquid to monitor the temperature homogeneity. The first thermocouple is placed near the boiling surface at a distance of 1.5 cm from the nucleation site. The second thermocouple is placed 1 cm above the boiling surface and 1.5 cm away from the boiling surface in order to not affect the formation of the rising natural convection plume at the centre of the plate. The third thermocouple is placed close to the free surface at a distance of 4 cm from the boiling surface. Six 0.2 mm diameter T-type thermocouples are bonded to the copper rod using an Araldite thermally conductive adhesive in order to measure the heat flux dissipated to the liquid as well as the boiling surface temperature. The details of these six thermocouples position are shown in Figure 3.6. All temperature measurements were taken using an Omega temperature data acquisition system.

*Pressure*

A pressure gauge is used for monitoring the pressure inside the system. It also ensures that no non-condensable gases are present in the system and monitors the thermodynamic state. The pressure inside the system should be equal to the saturation pressure corresponding to the saturation temperature. If the pressure is high, most probably non-condensable gases are mixed with the vapour phase or dissolved in the liquid phase.

### Bulk Liquid Temperature Control

The experiments were conducted with the bulk liquid temperature at 34$^{\circ}$C, which is the saturation temperature at atmospheric pressure. In order to maintain this temperature, the bulk liquid is heated by a rectangular polyimide film insulated flexible heater with PSA (pressure-sensitive adhesive) attached to the pool boiler outer wall.

### High Speed Videography

During the experiments, a NAC Hi-Dcam II high speed video camera is used to capture the growth and departure of bubbles with high temporal and spatial resolutions. In all experiments, this video camera has been used with an EX Sigma DG Macro 105mm 1:2.8 lens with magnification, M 1:1. A Kenko extension tube with the length of 80 mm has been added between the video camera and the lens in order to make the lens focus at closer distances and therefore produce higher magnification. The photographic view of the video camera setup is shown in Figure 3.4. In the experiments, the recording frequency is set to 1000 fps with a resolution of 630 x 269 pixels. During recording, the bubbles are illuminated by a high intensity LED light with luminous of 1380 lm.

| Bright LED light | Lens EX Sigma DG Macro | 80 mm Kenko extension tube | Video camera NAC Hi-Dcam II |
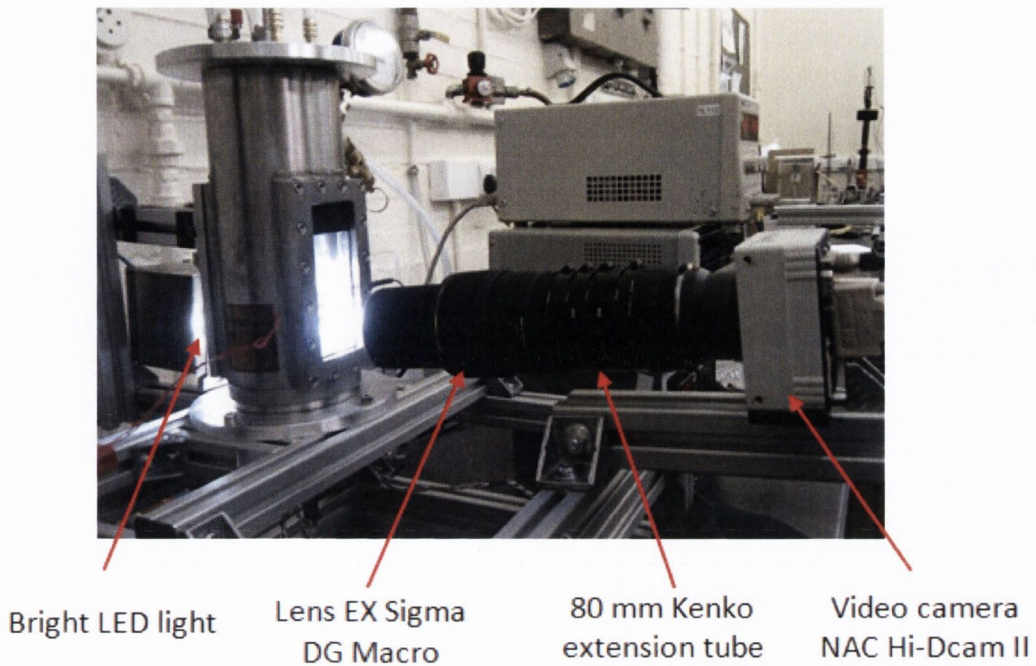
Figure 3.4: Video camera setup

### *Liquid Subcooling*

For the boiling experiments in subcooled liquid, the bulk liquid in the pool boiler has been subcooled by water flowing in a coiled copper heat exchanger (Figure 3.5). This coil is immersed in the bulk liquid at a distance of 15 mm above the boiling surface, as schematically shown in Figure 3.2. During the subcooling experiments, the temperature of water flowing in copper pipe coil is set to a controlled temperature approximately equivalent to the desired level of subcooling. The temperature is controlled with a programmable chiller system.

Figure 3.5: Copper pipe coils for liquid subcooling

## 3.2    Experimental Procedures

After assembling the rig, the surfaces inside the pool boiler including the copper plate, nucleation site and wall were cleaned by using acetone. Subsequent to this all the surfaces were rinsed with distilled water. The vessel was subsequently allowed to dry and was then filled with HFE-7000 as the bulk liquid. The bulk liquid was brought to a temperature corresponding to a pressure of about 1.2 bar and maintained at this temperature for several hours. Regular degassing was performed to ensure that no non-condensable gases were present in the vessel. The bulk liquid was then cooled down and maintained at a temperature of 34°C which corresponds to a saturation pressure of 1 bar.

At this stage, the cartridge heater from the heating element was turned on to superheat the boiling surface. Approximately 20 K of wall superheat was required to initiate boiling at the artificial nucleation site. Bubble activity only occurred at the artificial nucleation site as a result of good care during surface preparation and cleaning.

The single bubble growth and departure events at a particular wall superheat, or at a particular subcooling level in subcooled experiments, were then recorded at 1000 fps. During the video recording stage, particular care is given to avoid mirage effects on the bubble images. Mirage effects occur when the light rays are refracted by passing through a medium of non-constant optical index of refraction. They cause a distortion of the object image and alter the perception of reality. As the optical index usually varies with temperature, mirage effects can be a source of error when studying and observing boiling. A technique of minimizing mirage effects during recording of bubbles was used by Siedel (2012). He suggested that the recording angle has to be modified to allow a $2^o$ to $3^o$ angle with the horizontal plane. This allows the optical path to cross a much thinner superheated layer of liquid, without over-distorting the image. Therefore in the present study, the lens of the video camera was tilted slightly downward to $2^o$ from the horizontal plane during recording of the bubble images.

## 3.3  Measurement Techniques

### 3.3.1  Heat Flux and Boiling Surface Temperature Measurement

The heat flux dissipated to the fluid by the boiling surface as well as the boiling surface temperature were calculated using the six thermocouples bonded along copper rod in the heating element (Figure 3.3). Some assumptions are taken in which; (i) the heat flux across a section of the copper rod is assumed to be uniform i.e. one dimensional heat conduction, (ii) the system is assumed to be axisymmetric, (iii) the radial heat losses through the PTFE are assumed to be uniform along the rod, and (iv) the thermal conductivity of copper is assumed to be constant within the temperature range investigated. The position of the six thermocouples along the rod and an example of temperature data obtain from them is depicted in Figure 3.6.

With the above mentioned assumptions, the temperature along the z-axis of the rod can be regression fit with a polynomial function such as;

$$T(z) = (az^2) - (bz) + c \qquad (3.1)$$

where,

$$b = -\frac{\partial T}{\partial z}\bigg|_{z_0} \qquad (3.2)$$

$$a = \frac{1}{2}\frac{\partial^2 T}{\partial z^2} \qquad (3.3)$$

In this case, $c$ is the boiling surface temperature. With $k_{cu}$ being the thermal conductivity of copper,

$$q_w = bk_{cu} \qquad (3.4)$$

with $q_w$ is the heat flux at the boiling surface, and

$$\frac{\partial q}{\partial z} = 2ak_{cu} \qquad (3.5)$$

where $\frac{\partial q}{\partial z}$ is the rate of heat dissipation along the rod. To determine the coefficients $a, b$ and $c$, a second order polynomial regression fit is used on the six temperature measurements.
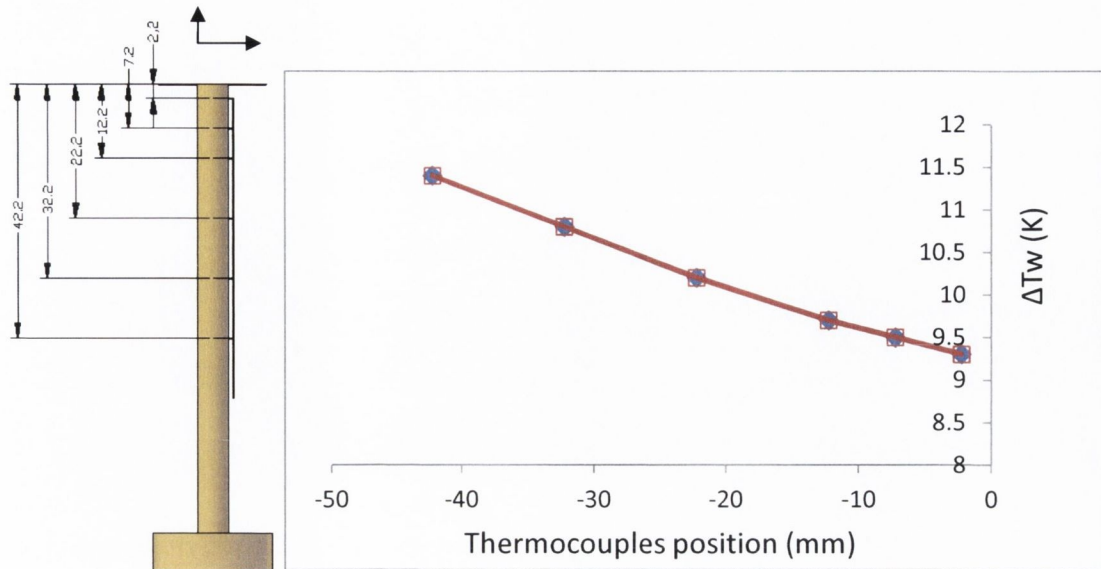
Figure 3.6: Thermocouples position in mm and its temperature example

### 3.3.2 Image Processing

An open source image editor software, IrfanView, as well as the commercial software Matlab is used for image processing in order to define the relevant bubble characteristics such as bubble volume and position of the centre of gravity. The image processing code is attached in Appendix A. The steps of the image processing are described as follows;

a) The size of a pixel in the image is measured by using an image of thermocouple 1 (bubble size calibration) recorded with the same magnification as shown in Figure 3.7. This measurement has been done in the IrfanView software.
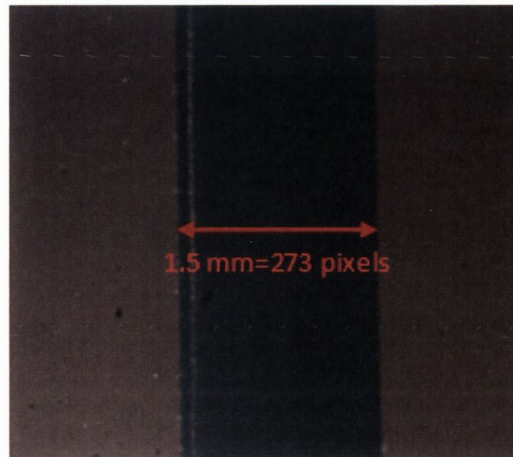
Figure 3.7: Image of thermocouple part for bubble size calibration

b)      The batch of images is cropped by keeping the area of interest only. Particular care should be taken when cutting the bottom of the image exactly on the nucleation site. This image cropping process has been done in the IrfanView software [Figure 3.8 (a) and Figure 3.9 (a)].

c)      The images are then pre-processed by increasing the contrast and setting an appropriate brightness. The values that have been chosen for contrast and brightness are then applied to the entire batch [Figure 3.8 (b) and Figure 3.9 (b)].

d)      The highest grey gradients are then detected by using the Sobel method which is a written script with the commercial Matlab software located in the Image Processing Toolbox.

e)      All objects of white and black in the picture are analysed to detect the bubbles from other contours [Figure 3.8 (c) and Figure 3.9 (c)].

f)      Once the contour of a bubble is detected, the geometric parameters of the bubble are then computed [Figure 3.8 (d) and Figure 3.9 (d)].
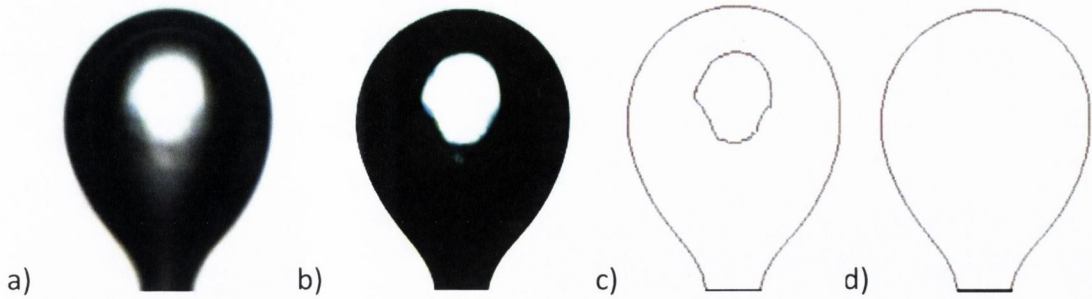
Figure 3.8: Sequence of single bubble image processing for saturated boiling
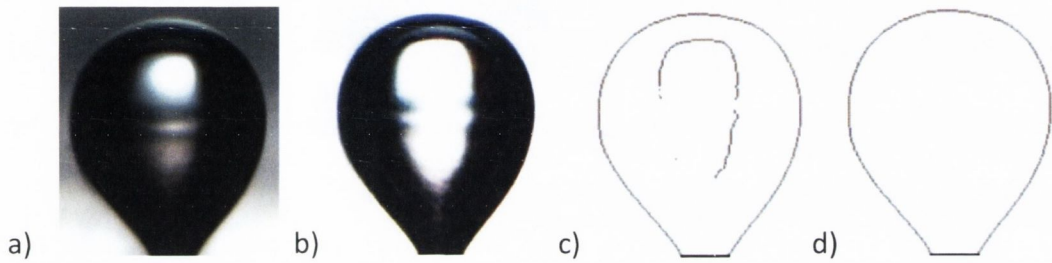


Figure 3.9: Sequence of single bubble image processing for subcooled boiling

In the calculations of the bubble volume, the bubble is divided into slices of 1 pixel height by considering that each slice as a cylinder (axisymmetric), and the volume is the total of the cylindrical section. This volume calculation method is considered more precise since the whole contour is taken into account rather than simplifying the bubble as a sphere or a truncated prolate spheroid. A prolate spheroid approximation would have as much as 20% error on the volume determination when the bubble has a neck at the base. Moreover, the bubble volume is not considered as fully axisymmetric when calculated using this method to offer a better calculation for an oscillating bubble, thus the volume determination error remains small.

In the calculation of the height of the centre of gravity, $h_{cg}$, it is assumed that the density is homogeneous inside the bubble. By using the same calculation method

of the bubble volume, the volume is divided in half and the height of both lower and upper volume is determined.

### 3.3.3 Experimental Accuracy and Uncertainty

The uncertainty of wall superheat, $\Delta T_w$ is estimated from the plotted temperature drop across the layer of Araldite thermal conductive adhesive (Figure 3.10). The gap between the copper disk and the copper rod is considered to be approximately 25 μm so that the uncertainty of the wall superheat is estimated to range from 2.7% for low wall superheat up to 5.9% for high wall superheat.

The estimation of heat flux uncertainty depends on the distribution of the temperature measurements within the copper rod (Figure 3.6), in particular the magnitude of the slope $b$ in Eq. (3.2). The larger the slope, which corresponds with a higher heat flux, the lower the level of uncertainty. A more detailed description of the heat flux uncertainty estimation can be found in the recent study of Siedel (2012). It is estimated to be $\pm47\%$ for low heat flux levels and it reduces to $\pm15\%$ for high heat flux levels. However, since the wall superheat is the important parameter with regard to bubble growth, the high uncertainty on the heat flux is still acceptable [Siedel et al. (2008)].

The uncertainty on the volume and height of centre of gravity determination is difficult to assess. The distortion of the image due to the mirage effect or the whole optical system cannot be estimated analytically. To ensure the realness of the bubble images the best possible care should be taken during recording. The uncertainty due to the contour determination can be then estimated to 1 pixel normal to the surface. The uncertainty on the volume is approximately 3% before bubble detachment (high image sharpness) and more than 20%, just after bubble nucleation when the bubble is still small (low image sharpness).
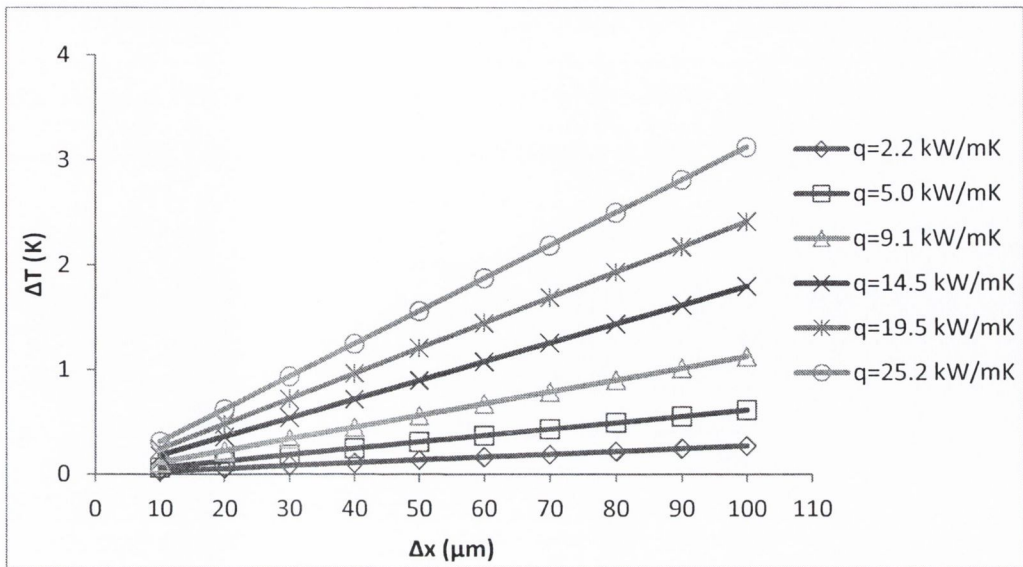
Figure 3.10: Estimation of temperature drop across the layer of Araldite thermal conductive adhesive

## 3.4    Operating Conditions

All the experiments were conducted at atmospheric pressure (1 bar). The fluid that has been chosen is HFE-7000. It is a non-flammable and low global warming potential (GWP) heat transfer fluid. In all experiments, the liquid level in the pool boiler is set at 42 mm from the boiling surface. The thermodynamics properties of saturated HFE-7000 at atmospheric pressure are shown in Table 1.

Table 1: Properties of HFE-7000 at atmospheric pressure [3M (2014)]

| Properties | Value | Unit |
|---|---|---|
| Boiling point, $T_{sat}$ | 34 | °C |
| Liquid density, $\rho_l$ | 1400 | kg/m$^3$ |
| Vapour density, $\rho_v$ | 8 | kg/m$^3$ |
| Kinematic viscosity, $v$ | 0.32 x 10$^{-6}$ | m$^2$/s |
| Latent heat of vaporization, $h_{fg}$ | 142 | kJ/kg |
| Specific heat, $c_p$ | 1.3 | kJ/kg.K |
| Surface tension, $\sigma$ | 0.0124 | N/m |
| Thermal conductivity, $k$ | 0.075 | W/m.K |
| Coefficient of Expansion, β | 0.00219 | K$^{-1}$ |

## 3.5 Data Analysis

### 3.5.1 Heat transfer coefficient

The heat transfer coefficient is ostensibly a measure of the thermal conductance due to convective heat transfer at the boiling surface and is defined as;

$$h = \frac{q''}{\Delta T_w}$$  (3.6)

with $\Delta T_w$ being the wall superheat and $q''$ being the heat flux.

### 3.5.2 Bubble equivalent diameter

The bubble equivalent diameter is defined as the diameter that a spherical bubble would have if its volume were the same as that of the real bubble. It is thus defined as;

$$D_{eq} = \left(\frac{6V}{\pi}\right)^{\frac{1}{3}}$$

(3.7)

### 3.5.3 Dimensionless time and volume

For displaying bubble growth data it is often convenient to display the data non-dimensionally by choosing an appropriate normalising parameter. In this work the time is made non-dimensional by normalizing it with the measured departure time;

$$t^* = t/t_d$$

(3.8)

Likewise, the bubble volume is made non-dimensional by normalizing it with respect to the calculated departure volume;

$$V^* = V/V_d$$

(3.9)

### 3.5.4 Bubble growth curve

Bubble growth is generally described by a non-dimensional power law. Therefore, the bubble growth curves are given as:

$$V^* = C.t^{*n}$$

(3.10)

where $C$ is a constant and $n$ is the power law exponent. Both of these are determined by regression fitting the growth curves.

### 3.5.5 Non-dimensional parameter of shape and oscillation

A non-dimensional parameter which describes the shape of the bubble and its oscillation is considered in the analysis. This parameter $A_s$ was introduced by (Siedel et al., 2008) and is defined as:

$$A_s = \frac{h_{cg}}{R_{eq}}$$

(3.11)

where,

$$R_{eq} = \left(\frac{3V}{4\pi}\right)^{\frac{1}{3}}$$

(3.12)

with the definition;

(a) If $A_s = 1$, the bubble is sphere

(b) If $A_s < 1$, the bubble is truncated sphere

(c) If $A_s > 1$, the bubble has a neck form

(d) If $\frac{dA_s}{dt} > 0$, an oscillation elongates the bubble in the vertical direction

(e) If $\frac{dA_s}{dt} < 0$, an elongation tends to flatten the bubble

### 3.5.6 Forces acting on a growing bubble

In the calculation of forces acting on a growing bubble, a control volume is used as depicted in Figure 3.11. The bubble images from the experiment have been processed to get its contour using image processing [Figure 3.8 and Figure 3.9]. The control volume is defined by the volume of bubble excluding the volume of the nucleation site.
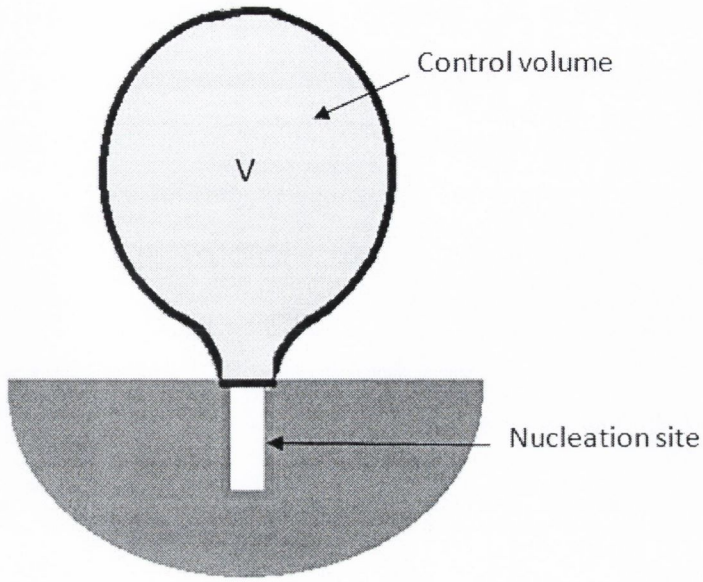
Figure 3.11: Schematic of control volume

A specific subdivision of the control volume will be used for the resolution of the momentum equation. The different volumes, surfaces and lines involved are described in Figure 3.12.
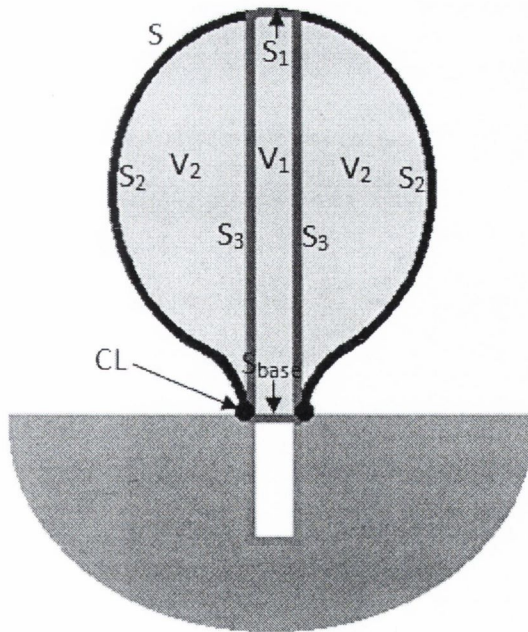


Figure 3.12: Schematic of volumes, surfaces and lines involved

The momentum conservation law states that within a control volume, the variation of momentum is equal to the sum of the external forces applied to this control volume. It emphasizes that the momentum is an integral value and the integral form of the momentum equation is considered as:

$$\frac{d}{dt} \iiint_V \rho_v u_v \, dV = F_{li} + F_{buoy} + F_{\sigma} \tag{3.13}$$

where $F_{li}$, $F_{buoy}$ and $F_{\sigma}$ are the resultant of the liquid inertia, the buoyancy and the surface tension forces. The information about a change of mass of the control volume or a motion of its centre of gravity can be provided, but does not indicate a change of shape as long as the centre of gravity remains at the same location.

### 3.5.6.1    *Momentum variation*

The derivative with time of the momentum can be considered as the resultant of the static and dynamic forces. As the momentum variation is analogous to a force, then the momentum forces, $F_{mom}$ is:

$$F_{mom} = \frac{d}{dt} \iiint_V \rho_v u_v \, dV \tag{3.14}$$

where the velocity vector is equal to the velocity of the centre of gravity, $u_{cg}$

$$F_{mom} = \frac{d}{dt} \left( \rho_v u_{cg} \times \iiint_V dV \right) \tag{3.15}$$

65

$$F_{mom} = \frac{d}{dt}\left(\rho_v u_{cg} \times V\right)$$ (3.16)

$$F_{mom} = \rho_v u_{cg}\frac{dV}{dt} + \rho_v V \frac{du_{cg}}{dt}$$ (3.17)

By considering $h_{cg}$ as the height of the centre of gravity and assuming its motion to be vertical,

$$F_{mom} = \rho_v \frac{dh_{cg}}{dt}\frac{dV}{dt} + \rho_v V \frac{d^2 h_{cg}}{dt^2}$$ (3.18)

where $h_{cg}(t)$ and $V(t)$ are measured from the recorded images.

### 3.5.6.2    *Liquid inertia and added mass force*

The liquid inertia and added mass force is the liquid reaction to its acceleration caused by the motion of the interface. Its expression is similar to the momentum variation except for two differences;

i.    The density considered is the liquid density, and

ii.   Each term is weighted by a coefficient usually referred to as added mass coefficient:

$$F_{li} = K_1 \rho_l \frac{dh_{cg}}{dt}\frac{dV}{dt} + K_2 \rho_l V \frac{d^2 h_{cg}}{dt^2}$$ (3.19)

The value of the added mass coefficients, $K_1$ and $K_2$ depend on the bubble shapes and the conditions of bubble growth. Magnaudet et al. (1995) have given both coefficients to be equal to 0.5 for the case of a spherical bubbles growing in an infinite liquid while

for the case of a hemispherical bubble growing on a wall, Klausner et al. (1993) and Legendre et al. (2008) give $K_1 = 2$ and $K_2 = 4$. Since in this study the bubble dynamics is somewhere in between the two scenarios, values of $K_1 = K_2 = 1$ have been used in order to gauge the magnitude and thus importance of the liquid inertia force.

### 3.5.6.3    *Buoyancy force*

The buoyancy force is due to the vertical pressure gradient caused by gravity. It can be considered as the resultant of the hydrostatic pressure forces on the bubble surface which are the hydrostatic liquid pressure on the outward surface $S$, the hydrostatic vapour pressure on the inward surface $S$ and the vapour pressure on both sides of the surface $S_{base}$ as illustrated in Figure 3.12. In the calculation, the buoyancy force is equal to the integral over the bubble surface of the vertical component of the hydrostatic pressure force. The calculation approach includes the influence of the presence of the contact area at the base of the bubble. To facilitate this the bubble is divided into separate volumes and areas as shown in Figure 3.12 as proposed by Siedel et al. (2013)

By considering homogeneous liquid and vapour densities, the buoyancy has been broken into three terms as follows [Siedel et al. (2013)];

$$F_{buoy,1} = (\rho_l - \rho_v)Vg \tag{3.20}$$

$$F_{buoy,2} = -(\rho_l - \rho_v)V_1g \tag{3.21}$$

$$F_{buoy,3} = \frac{2\sigma}{R}S_{base} \tag{3.22}$$

where $R$ is the radius of the tip of the bubble. The total of buoyancy force is;

$$F_{buoy} = F_{buoy,1} - F_{buoy,2} + F_{buoy,3} \qquad (3.23)$$

with $F_{buoy,1}$ being the buoyancy force of the bubble which is fully immersed in the liquid, $F_{buoy,2}$ being a first correction term on the buoyancy to take into account only the part of the bubble which has liquid below and above, and $F_{buoy,3}$ being a second correction term on the buoyancy (also known as contact pressure) which considers the pressure difference across the interface area located above the nucleation site.

### 3.5.6.4      *Triple line surface tension and adhesion forces*

The analysis of triple line surface tension and adhesion forces involve three different phases at the contact line. The forces are governed by both the surface tension between the liquid and vapour phases and the wettability of the liquid over the solid surface. The wettability is usually characterized by contact angle, $\alpha$. The resultant of the triple line forces is generally known as surface tension force and is expressed as follows;

$$F_\sigma \vec{k} = \int_{CL} \sigma \vec{t} \, dl \qquad (3.24)$$

where $\vec{t}$ is the unit vector tangential to the interface in the meridian plane and at the contact line. With the base of the bubble, which is axisymmetric, the term can be expressed as;

$$F_\sigma = -2\pi R_{base} \sigma \sin \alpha \qquad (3.25)$$

with $2\pi R_{base}$ being the perimeter of the triple line of radius, $R_{base}$ and $\alpha$ is the contact angle which is the angle between the interface at the triple line and the horizontal plane.

### 3.5.7 Bubble Curvature

In the buoyancy force calculation an important parameter is the bubble tip radius, which is the inverse of the bubble tip curvature. With the bubble assumed as axisymmetric, the curvature $C$ of the bubble at any point depends on the two curvatures $C_1$ and $C_2$ related to the two principle radii of curvature $R_1$ and $R_2$ at a point on the vapour-liquid interface as described follows;

$$C = C_1 + C_2 \tag{3.26}$$

with

$$C_1 = \frac{1}{R_1} \ and \ C_2 = \frac{1}{R_2} \tag{3.27}$$

The two circles which approximate the bubble surface at a point at the interface lie on two orthogonal planes as illustrated in Figure 3.13. The circle with curvature $C_1$ (blue circle) passes through three consecutive data points, for instance $j-1$, $j$, $j+1$ on the vertical plane whilst $C_2$ (red circle) is a circle passing through the point $j$ lying on the orthogonal plane of $C_1$ with the centre of the circle $C_2$ is on the symmetrical axis.
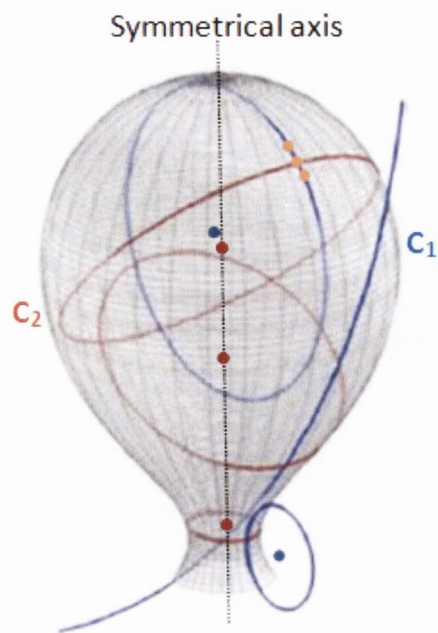
Figure 3.13: Two principle radii at three selected points in a 3-dimensional reconstruction bubble[Di Bari and Robinson (2013)]

At the tip of the bubble, $C_1=C_2$ due to axisymmetry.

Very detailed description of the bubble shape for quasi static bubbles can be found in the recent studies of Di Bari and Robinson (2013), Lesage et al. (2013) and Siedel et al. (2014).

# CHAPTER 4

# RESULTS AND DISCUSSION

In this chapter, data from the experiment of pool boiling with saturated liquid as well as subcooled liquid are analysed, further presented and discussed. The case of saturated liquid is the main discussion and analysis and the initial results on the effects of subcooled liquid on bubble dynamics will be discussed at the end of this chapter. This chapter begins with an introduction section (Section 4.1) which briefly presents the experimental conditions in the form of various dimensionless numbers for fluid dynamics and heat transfer studies. This will give an overview in term of physical phenomenon for single bubble growth and will guide the discussion. This section also presents a set of images of single bubble evolution and emphasizes a clear change of bubble shape between the bubble incipience and the bubble near departure.

Next, this chapter will present the heat flux analysis of the heated surface (Section 4.2) before going further into the bubble dynamics discussions. It follows with sections on bubble waiting and growth times (Section 4.3) and bubble departure characteristics (Section 4.4); volumetric growth rates (Section 4.5); energy transfer at the interface (Section 4.6); shape and oscillation analysis (Section 4.7); contact angle and forces analysis (Section 4.8) and will end the chapter with the effects of liquid subcooling (Section 4.9).

## 4.1 Introduction

The study of single bubble growth from an artificial nucleation site in saturated pool boiling has been carried out experimentally at atmospheric pressure using refrigerant HFE-7000, which has the properties shown in Table 1 in section 3.4. The experiment has been conducted with the surface (wall) excess temperature to the saturation temperature of the fluid (34°C) in the range from 2.2°C to 11.8°C. These will be termed the wall superheat.

By using HFE-7000 as a fluid, it should be noted that compared to water the density difference between liquid and vapour phases is higher and the surface tension is about six times smaller. This will lead to a lower capillary length, $L_c$ defined as:

$$L_c = \sqrt{\frac{\sigma}{(\rho_l - \rho_v)g}} \approx 0.953\ mm \qquad (4.1)$$

To consider the type of heat absorption during the experiments, i.e., sensible versus latent heat, the Jakob number, $Ja$ is calculated and defined as:

$$Ja = \frac{\rho_l c_{pl}(T_w - T_{sat})}{\rho_v h_{fg}} \qquad (4.2)$$

In the present study, the Jakob numbers, $Ja$ ranges between $3.5 \leq Ja \leq 18.9$. According to Cole and Shulman (1966), this $Ja$ range is considered as low. It can thus be considered that the majority of heat is absorbed by vapour (latent heat) instead of by the liquid (sensible).

In order to measure the instability of the liquid thermal boundary layer due to differences of temperature (surface and fluid temperatures) and density (liquid density dependence on temperature), the Rayleigh number, $Ra$ has been used and is defined as:

$$Ra = Gr.Pr \qquad (4.3)$$

where the Grashof number, *Gr* is defined as,

$$G_r = \frac{g\beta\Delta T_w D^3}{\vartheta^2} \qquad (4.4)$$

and the Prandtl number, *Pr* is

$$Pr = \frac{\mu c_p}{k_l} = 7.76 \qquad (4.5)$$

with the diameter of the copper disk, *D* being the characteristic length. It has been calculated that, for the range of wall superheats that have been investigated in this study, i.e., $\Delta T_w$=2.2 K to 11.8 K, *Ra* is between 2.9 x $10^7$ to 1.5 x $10^8$ which is relatively high and can be considered as turbulent convection [Niemela et al. (2000)].

A growing bubble in boiling experiences the effects of both surface tension and buoyancy forces which depend on the properties of working fluid HFE-7000. To have a sense of which effect is dominant, the Bond number, *Bo* is calculated and is defined as:

$$Bo = \frac{(\rho_l - \rho_v)gr^2}{\sigma} \qquad (4.6)$$

with the radius of the artificial nucleation site being the length scale. Here, $Bo \approx 0.0089$ which indicates that for a growing bubble in liquid HFE-7000 at atmospheric pressure, surface tension is dominant over buoyancy. As discussed by Lesage et al. (2013), the bubble can be expected to be the shape of a spherical section since it is below the cut-off Bond number of *Bo*=0.06032 over which bubbles can be expected to be deformed considerably by hydrostatic pressure forces.

73

To classify whether bubble growth would be expected to be diffusion controlled or inertial influenced, which is associated with whether the kinetic energy of the surrounding liquid would be the dominant influence, Robinson and Judd (2004) have proposed a criterion as follows;

$$I_R = \left(\frac{4}{27}\right)\left(\frac{\sigma}{\rho_l \alpha_l^2}\right)\frac{R_c}{Ja^2} \begin{cases} \ll 1 \text{: Inertial controlled} \\ \gg 1 \text{: Diffusion controlled} \end{cases} \qquad (4.7)$$

where $R_c$ is the bubble radius at nucleation which is taken here as the cavity radius. In the present study, with the Jakob numbers $3.5 \leq Ja \leq 18.9$, $I_R$ lies between $5.7 \times 10^3$ and $1.9 \times 10^2$ in which range, according to Robinson and Judd (2004), the bubble growth is controlled by thermal diffusion and inertial influences can be neglected.

In order to have adequate analysis of single bubble growth dynamics, a clear and sharp image of bubbles growing on the heated surface is vital. Figure 4.1 shows a photographic sequence of a bubble evolution at $\Delta T_w = 9.1$ K. In this figure, it shows that the bubble evolution consists of three principal stages. At the early stage, which is a very short period, ($t < 5$ ms), the shape of bubble growing from the nucleation site is a truncated sphere. At the middle stage ($5$ ms $< t < 85$ ms) as the volume increases, a larger portion of the bubble is acted upon by buoyancy. When this portion becomes large enough, the bubble becomes more elongated as the buoyancy force tends to lift the upper portion of the bubble with the bubble foot being attached to the mouth of nucleation site. At the final stage ($t > 85$ ms) when the bubble is just about to depart, a neck is formed at the bubble base. Subsequent to this, the neck begins curving inward as the bubble volume increases and causes the upper region of the bubble to accelerate upward prior to departure. It is noticed that the buoyancy effects have a large influence on this phenomenon. The magnitude of buoyancy force is believed to increase with the progression of the necking process causing a positive feedback effect which accelerates the departure process, as discussed by Di Bari and Robinson (2013).
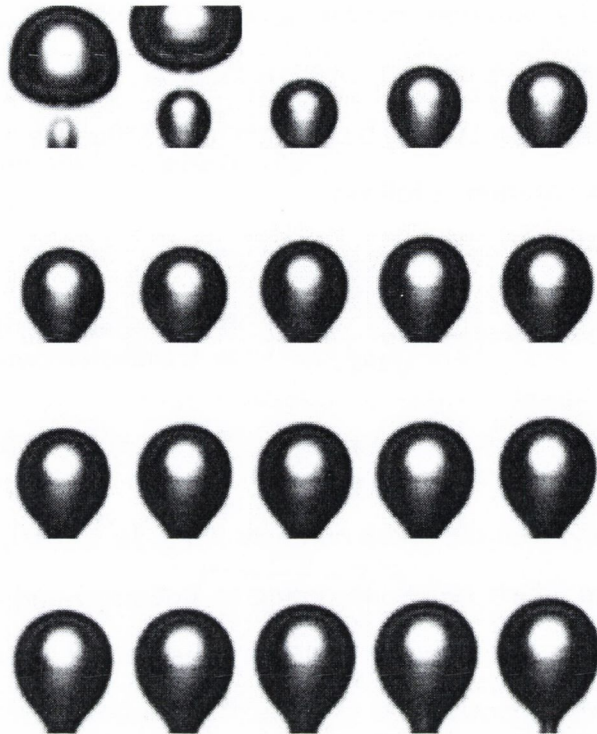
Figure 4.1: Bubble growth at $\Delta T_w = 9.1$ K with $\Delta t = 5$ ms between the images

## 4.2 Heat Flux at the Heated Surface

As mentioned in the previous chapter, the total heat flux transmitted to the fluid is calculated from the temperatures measured inside the copper heating element. The heat flux versus wall superheat is shown in Figure 4.2. It is clearly shown that the relation between heat flux and wall superheat is relatively linear for the range of superheats tested. At the maximum heat flux tested, i.e., $q'' = 46.3 \frac{\text{kW}}{\text{m}^2}$, the surface produces 20 K of wall superheat whereas at the minimum heat flux $q'' = 2.2 \frac{\text{kW}}{\text{m}^2}$, the wall superheat is only 2.2 K.
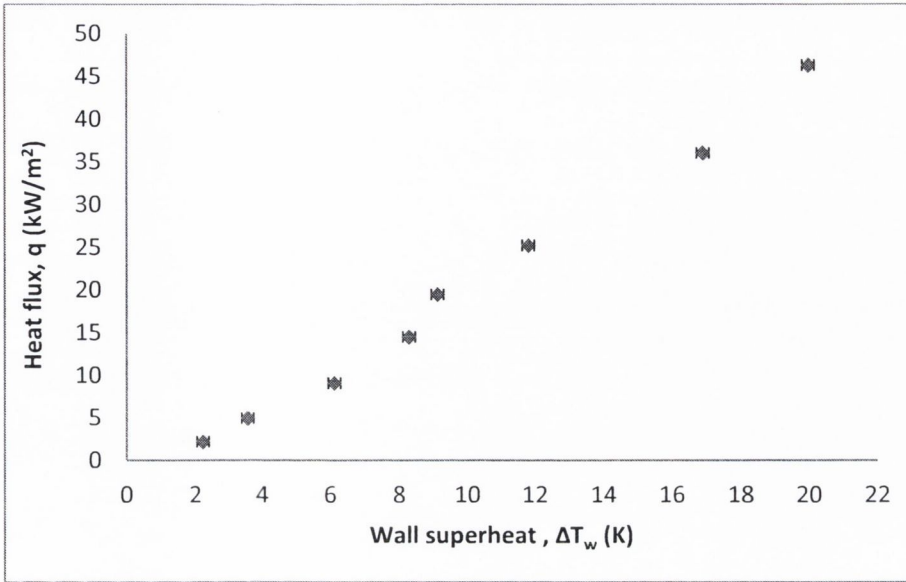
Figure 4.2: Heat flux at various wall superheats

Figure 4.3 shows the heat transfer coefficient versus wall superheat of the present work (nucleate boiling) together with the natural convection correlation suggested by Kobus and Wedekind (2001) for small heated surfaces. Kobus and Wedekind (2001) have calculated the heat transfer coefficient $h = \frac{Nu.k}{D}$ by using the classical correlation, i.e., $Nu = C.Ra^n$, in which they proposed the values of $C$ and $n$ as 0.9724 and 0.194 respectively for the case $10^4 \leq Ra \leq 3 \times 10^7$. For the present experiment, the heat transfer coefficient has been defined in Eq. (3.6). From the figure, it shows a very large difference between the measured heat transfer coefficient and that predicted for natural convection. This shows that the bubble agitation caused by the nucleating bubbles is an effective mechanism of heat transfer compared with buoyant natural convection. For the present work, it indicates that the increasing trend of heat transfer coefficient is asymptotic with a value of about 980 W/m$^2$.K at a superheat of 2.2 K, levelling off at about 2300 W/m$^2$.K at a superheat of 20 K. It is observed that the rate at which the heat transfer coefficient increases is large for the superheat range of 2.2 K $\leq \Delta T_w \leq$ 8.3 K. This is believed to be due to the frequency of bubble growth on the heated surface and will be discussed further in

76

a following section. Meanwhile, if only natural convection was occurring on the heated surface, according to the correlation of Kobus and Wedekind (2001), the heat transfer coefficient would be about 100 $W/m^2.K$ at wall superheat of 2.2 K with a moderate increase to about 150 $W/m^2.K$ at a wall superheat of 11.8 K. Since the bubble nucleation on the heated surface shows a high positive impact on transferring the heat, the dynamics of bubble growth is clearly worthwhile investigating.
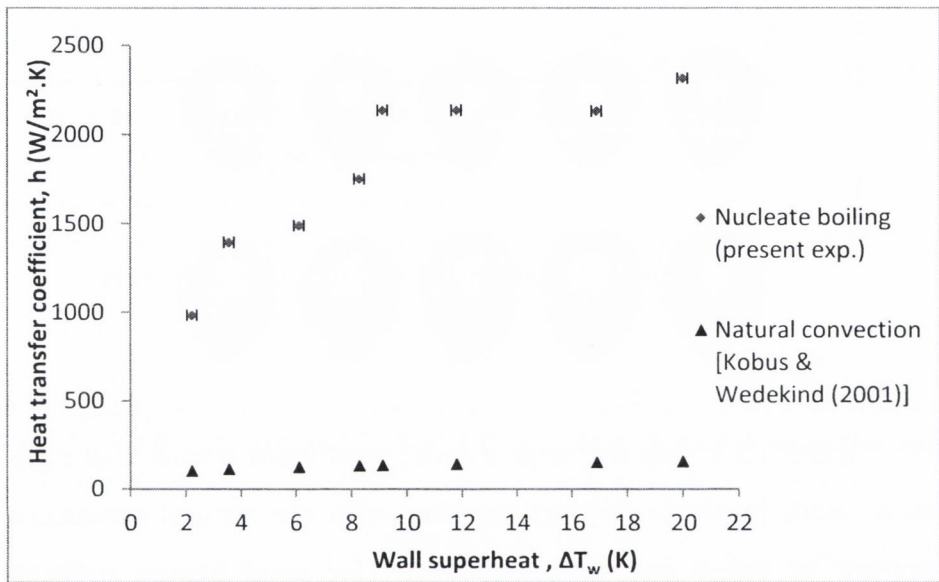


Figure 4.3: Nucleate boiling versus natural convection correlated by Kobus and Wedekind (2001)at various wall superheats

## 4.3 Waiting and Growth Times

### 4.3.1 Waiting time

The bubble waiting time is defined as the period of time elapse during which transient conduction into the liquid occurs, but no bubble growth takes place. In other words, it is the time interval between the departure of the previous bubble and the nucleation of a new bubble. Figure 4.4 is an example of a photographic sequence of a bubble waiting period for a superheat of 2.2 K.
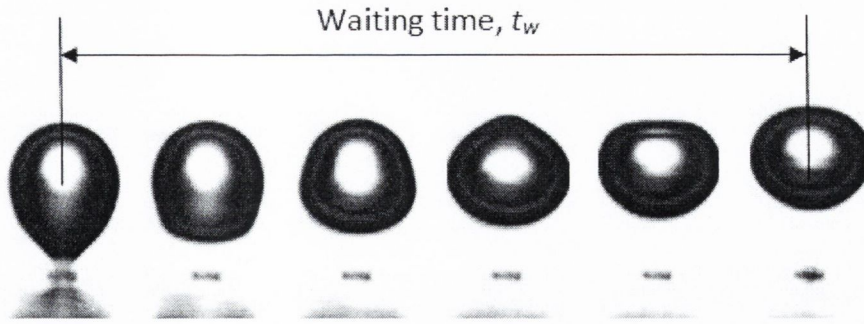
Figure 4.4: Determination of bubble waiting time $t_w$ for wall superheat, $\Delta T_w = 2.2$ K, with $\Delta t = 1$ ms between the images

The waiting time of six successive bubbles at the different wall superheats is shown in Figure 4.5 for the range of wall superheats tested in this investigation. It shows that the bubble waiting time for low to medium wall superheats, ($\Delta T_w$ =2.2 K, 3.5 K, 6.1 K and 8.3 K) is very consistent over the six bubble events. For the case of higher wall superheats, ($\Delta T_w$=9.1 K and 11.8 K), there is a variation of $\pm 1$ ms in the bubble waiting time for the six successive bubbles.
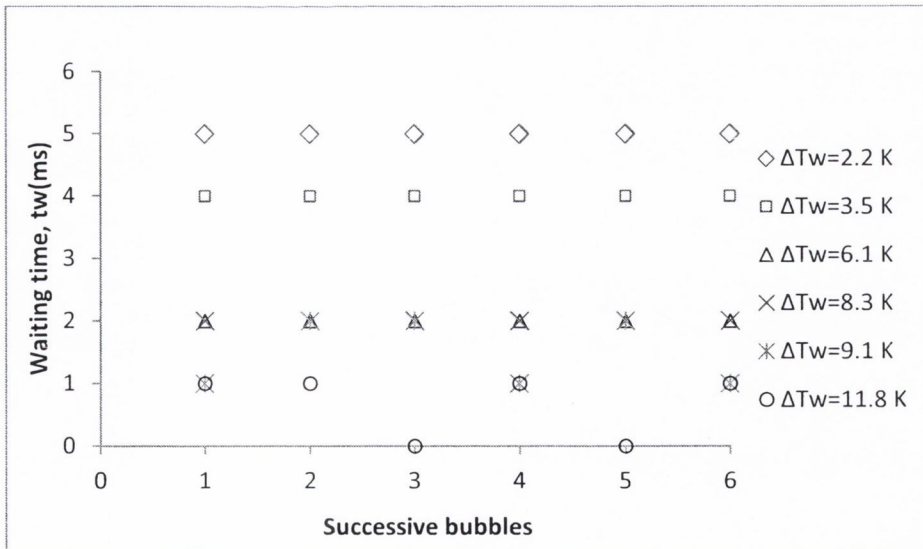


Figure 4.5: Waiting times, $t_w$ of six successive bubbles for the range of wall superheats tested

Figure 4.6 shows the waiting time for the average of the six successive bubbles at various wall superheats. The bubble waiting time is found to decrease exponentially with increasing of the wall superheat. It clearly shows that a rapid decrease of waiting time occurs between $2.2\text{ K} \leq \Delta T_w \leq 6.1\text{ K}$. The waiting time correlations by Mikic and Rohsenow (1969) and Han and Griffith (1965), using in Eq. (2.80) and Eq. (2.81) respectively, also predict a decreasing trend of waiting time with wall superheat, though with a smaller slope. It is noticed that the waiting time correlation by Mikic and Rohsenow (1969) for the low wall superheat, i.e., $\Delta T_w$=2.2 K is just within the experimental uncertainty of the present measurements. However, for the medium and high superheats both of the classical nucleation theories over predict the measured waiting times.

Immediately after a bubble departs, cooler bulk liquid replaces the space left by the departed bubble near the nucleation site due to conservation of mass. This liquid is then heated by transient conduction from the heated surface. For lower wall superheats the rate at which heat is transferred into the liquid is lower and as such the rate at which the thermal boundary layer grows is lower as well. Thus, the decreasing waiting time with increasing superheat shown in Figure 4.6 is consistent with the notion that for a bubble to nucleate a prescribed temperature must be reached at the tip of the bubble. To initiate a new bubble from the cavity after the previous bubble has departed, classical theories dictate that a sufficient thickness of the thermal boundary layer near the cavity is needed and the growth of the thermal boundary layer is calculated using a constant surface tension of fluid. Figure 4.6, shows that of the two generally accepted classical theories, the Mikic and Rohsenow (1969) theory is in reasonable agreement with the present data, especially at low superheats. When the fluid surface tension is dependent on temperature, whereby the surface tension decreases with increased temperature, it could be argued that this would cause a more pronounced decrease of waiting time as the wall superheat increases, as is observed here. This hypothesis may require further investigation and is

beyond the capabilities of the current apparatus and thus outside of the scope of the current investigation.
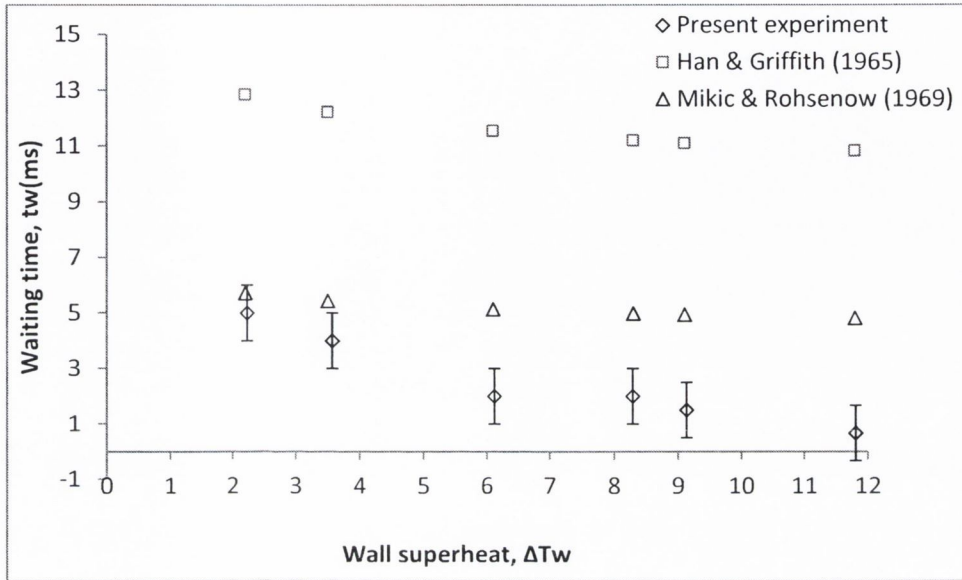


Figure 4.6: Waiting time, $t_w$ for the average of six successive bubbles at various wall superheats

## 4.3.2 Growth time

The growth time of a bubble is defined as the time interval between when the bubble embryo emerges from a nucleation site after the waiting time and the moment that it detaches from the nucleation site. Figure 4.7 shows the growth times of six successive bubbles for the range of wall superheats investigated. The absolute deviation of the bubble growth times is within 5% for all wall superheats tested and the smallest absolute deviation which is about 0.3% for the wall superheat 11.8 K. This illustrates the excellent repeatability of the bubble growth measurements with the current apparatus.
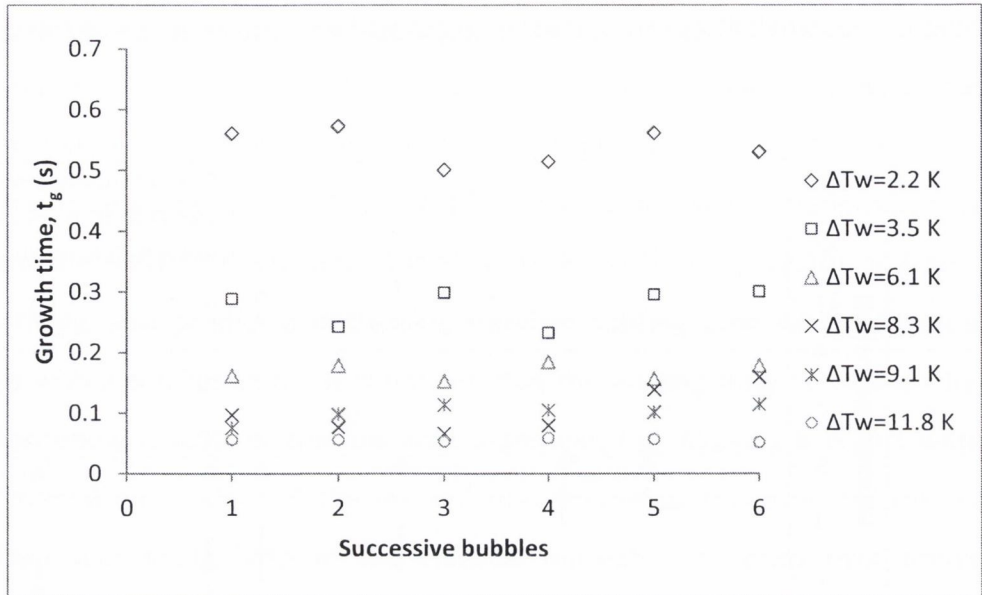
Figure 4.7: Growth times, $t_g$ of six successive bubbles

Growth times for the average of six successive bubbles at the various wall superheats are shown in Figure 4.8. Similar to the bubble waiting time, the bubble growth time also decreases exponentially with increasing wall superheat. It clearly shows that a rapid decrease of the growth time occurs between $2.2 \text{ K} \leq \Delta T_w \leq 6.1 \text{ K}$ whereas it decreases less steeply from $6.1 \text{ K} < \Delta T_w \leq 11.8 \text{ K}$. During bubble growth, energy is transported into the bulk liquid in the thermal boundary layer by conduction from the heated surface. Bubble growth is driven by the temperature difference between the superheated liquid surrounding the bubble and the saturated vapour within the bubble. This sensible energy is used to vaporize the liquid and cause bubbles to form and grow. Since increasing the superheat increases the driving temperature difference for vaporization, it is expected that the bubble growth times decrease with increased wall superheat. The figure also shows the growth time data from Siedel et al. (2008). This data is very consistent with the current measurements even though it was for a different working fluid and a cavity of different yet similar size. Predicting the growth time is difficult, however, since it requires the prediction of the initial thermal field, the heat transfer rate into the bubble as it is growing and

bubble departure criterion. Although modelling these aspects is beyond the scope of this study, the excellent repeatability of the current measurements along with the validation of the trends with the only other study of its kind makes these measurements very useful for the validation of future theoretical studies.
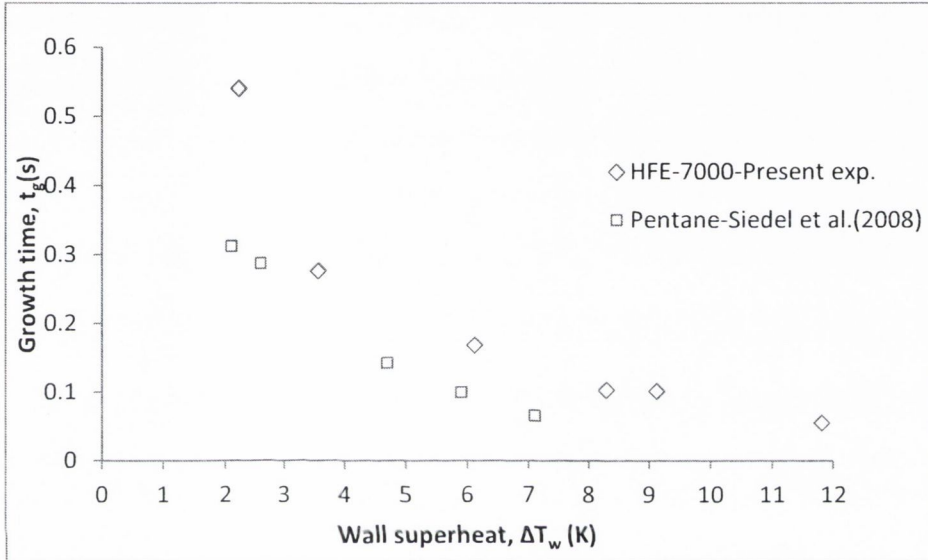


Figure 4.8: Growth time, $t_g$ for the average of six successive bubbles at various wall superheats

## 4.4 Bubble at Departure

In nucleate boiling, the departure rate of the formed bubble is intimately linked with the heat transport rate. This departure rate is often referred to as the bubble departure frequency and it is calculated as the reciprocal of the summation of bubble waiting time, $t_w$ and bubble growth time, $t_g$;

$$f_d = 1/(t_w + t_g) \tag{4.8}$$

Figure 4.9 shows the bubble departure frequency for different wall superheats for the average of six successive bubbles. In the figure, it shows the bubble departure frequency increases with a somewhat parabolic profile with wall superheat. The bubble departure frequency shows a gradual and nearly linear increase for $2.2\,\text{K} \leq \Delta T_w \leq 9.1\,\text{K}$, from 1.8 Hz to 9.6 Hz, after which the rate increases reaching $f_d \approx 17.6\,\text{Hz}$ at $\Delta T_w = 11.8\,\text{K}$. The figure also shows the bubble departure frequency data for Pentane from Siedel et al. (2008). Compared with the present study, the bubble departure frequency data from Siedel et al. (2008) are generally higher with the linearly increasing trend with wall superheat.  However, these differences are not surprising since no measurable waiting time was reported in their study.
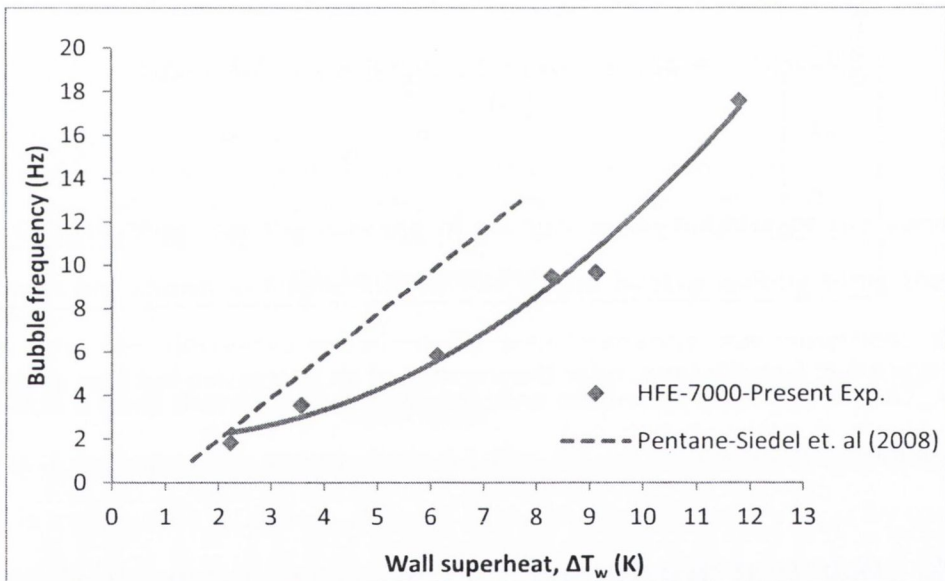


Figure 4.9: Bubble departure frequency at various wall superheats for the average of six successive bubbles

The frequency of bubble release depends on how large the bubble must become for departure to occur, and as a consequence, on the rate at which the bubble can grow to this size. This is of course related to the wall superheat since it in part determines the growth rate. The departure volume for six successive bubbles is shown in Figure 4.10. In the figure, the departure volume for each of the six successive

bubbles shows a small scatter for the respective superheat. Overall, the bubble departure volumes for all bubbles tested is within ±10% of the average which illustrates the good repeatability of the measurements. Deviations from the average would be related to experimental uncertainty of the processing and calculation of the volume as well as with the frame rate of the camera, i.e., pinpointing of the exact moment of departure.
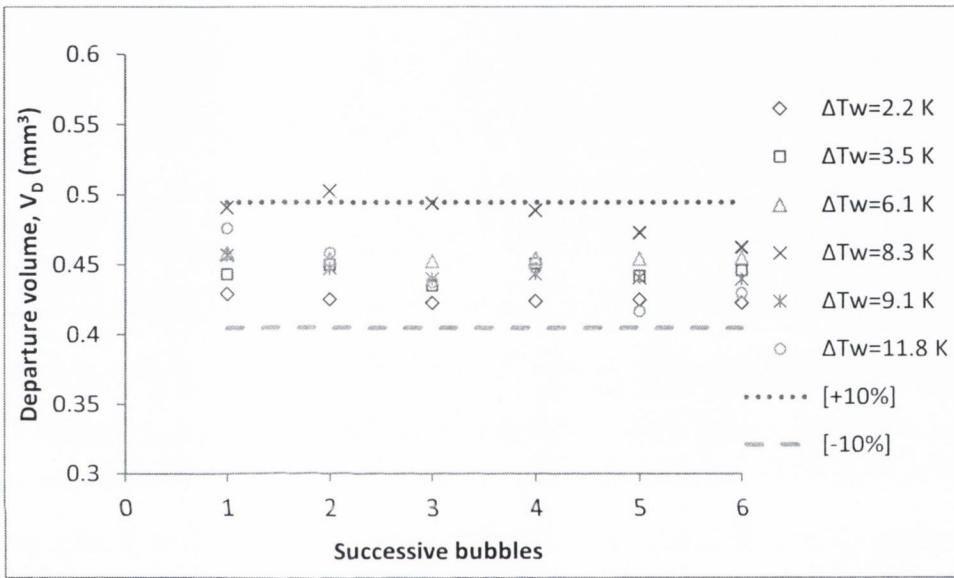


Figure 4.10: Departure volume, $V_D$ of six successive bubbles

A very recent correlation for predicting bubble departure volumes for quasi static bubbles has been developed by Di Bari and Robinson (2013) in which the Tate Volume [Tate (1864)] and the ratio ($d_o/L_c$) have been taken into account. The correlation was developed for adiabatic bubbles formed by gas injection through a submerged orifice and is given as;

$$V = 0.6863 \left(\frac{d_o}{L_c}\right)^{-0.116} V_T \tag{4.9}$$

where the working fluid capillary length, $L_c$ is defined in Eq. (4.1) which is $L_c \approx$ 0.953 mm and $d_o$ is the orifice diameter, i.e., $d_o = 0.18$ mm. $V_T$ is the Tate Volume [Tate (1864)] which is defined as;

$$V_T = \frac{\pi d_o \sigma}{(\rho_l - \rho_g)g} \tag{4.10}$$

Figure 4.11 shows the departure volume for the average of six successive bubbles for the range of superheats tested in this investigation. The figure shows fairly good consistency of the departure volume both for successive bubbles at a given superheat as well as for all bubbles over the range of superheats tested (within 5% of the mean). For the superheat of $\Delta T_w = 8.3$ K there is some discrepancy in the volume compared with the other superheats, though they are within 10% of the mean of all bubble departure volumes calculated. As mentioned, this is within the experimental uncertainty which arises from pinpointing of the exact moment of departure along with that associated in the calculation of the volume. It can thus be said that, for these experiments, the departure volume is constant with wall superheat, which is in fact expected for quasi static bubble growth when the bubble foot remains attached to the rim of the nucleation site. The figure also shows the departure volume data (Pentane) from Siedel et al. (2008) and the departure volume correlation by Di Bari and Robinson (2013). With the same type of working fluid, i.e., wetting fluids, the data by Siedel et al. (2008) shows fairly constant departure volumes with the wall superheats tested, but the departure volumes are found to be about 20% larger than the present study. The prediction of bubble departure volumes by the Di Bari and Robinson correlation well predicts the present data and is within the experimental uncertainty. It can be concluded that the Di Bari and Robinson correlation of bubble volume for adiabatic gas injection from orifices is also suitable for this case of diabatic bubble growth in nucleate boiling when the bubble grows quasi-statically and the bubble foot

remains fixed to the rim of the cavity. This indicates that the adiabatic experiments and associated development of the the correlation well considered the complexity of bubble growth.
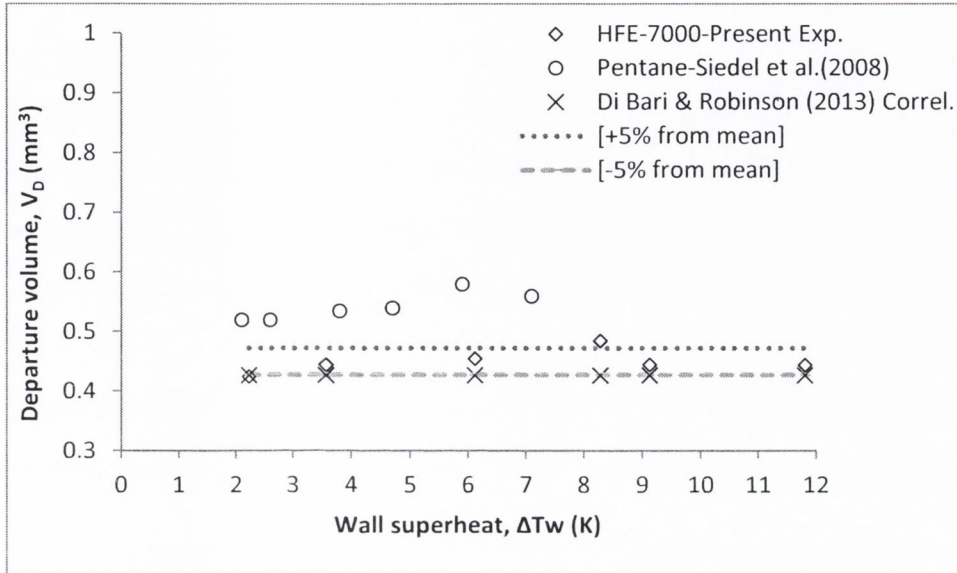


Figure 4.11: Departure volume for the average of six successive bubbles at various wall superheats

In nucleate boiling, the diameter of the bubbles at departure has historically been used to explain bubble departure behaviour. Here, the equivalent bubble departure diameter is determined from the actual volume of bubbles using the equivalent volume of a sphere [Eq. (3.7)], and its value for the six consecutive bubbles is shown in Figure 4.12 for each superheat tested. The departure diameter trends are of course similar to the trends of the departure bubble volume as depicted in Figure 4.10. The variations of the mean values are shown to be very repeatable and are all within ±3% of each superheat's respective mean, with a ±10% variation across all of the superheats.

Bubble departure diameters for the average of the six successive bubbles at each wall superheat tested are shown in Figure 4.13. The present study with HFE-7000 shows a maximum deviation of ±3% for all wall superheats with the mean value found

to be $D_b$=0.597 mm. From the plotted data, bubble departure diameter can be considered as having a very small dependence on wall superheats and this is supported by the work of Yang et al. (2000). The bubble departure diameters from the experiment of Siedel et al. (2008) using pentane as a working fluid are also plotted in Figure 4.13, and are also independent of the wall superheat. Of course this is related to the fact that inertial forces are negligible and the bubbles are growing in a quasi-static manner. For Siedel et al. (2008), by using pentane with a larger capillary length ($L_c \approx 1.56$ mm) and lower Bond number ($Bo \approx 0.0033$) as a working fluid, they have found the mean bubble departure diameter ($D_b \approx 0.635$ mm with absolute deviation ≈2.7%) is larger compared with the present study ($L_c \approx 0.953$ mm). In this figure, correlations for predicting bubble departure diameter by Fritz (1935), Kiper (1971) and Di Bari and Robinson (2013) are also shown. The Fritz (1935) correlation of bubble departure diameter is given as;

$$D_b = 0.0208\alpha \sqrt{\frac{\sigma}{g(\rho_l - \rho_g)}} \tag{4.11}$$

in which the contact angle, $\alpha$ is specified to be equal to 35°C for liquids other than water, as proposed by Stephan and Abdelsalam (1980). As shown in Figure 4.13, prediction of the bubble departure diameter using this correlation is found to over-predict the present experiment data by about 16%. The Kiper (1971) correlation for the bubble departure diameter is given as;

$$D_b = 2.7Ja \tag{4.12}$$

where $Ja$ is the Jakob number. The prediction of bubble departure diameter using the Kiper correlation appears to be quite inappropriate considering it has a linear dependence on wall superheat and the experimental data shows no dependence. It is noted that in the case of Kiper (1971), inertial forces were considerable during bubble

growth which is not the case of the present study. Therefore, it can be concluded that the bubble departure theories or correlations for bubbles with inertial forces should not be used in quasi-static bubble cases. Since the bubble volume at departure by Di Bari and Robinson correlation is well predicted as shown in Figure 4.11, similarly, good prediction of bubble diameter at departure is expected as well, as seen in Figure 4.13.
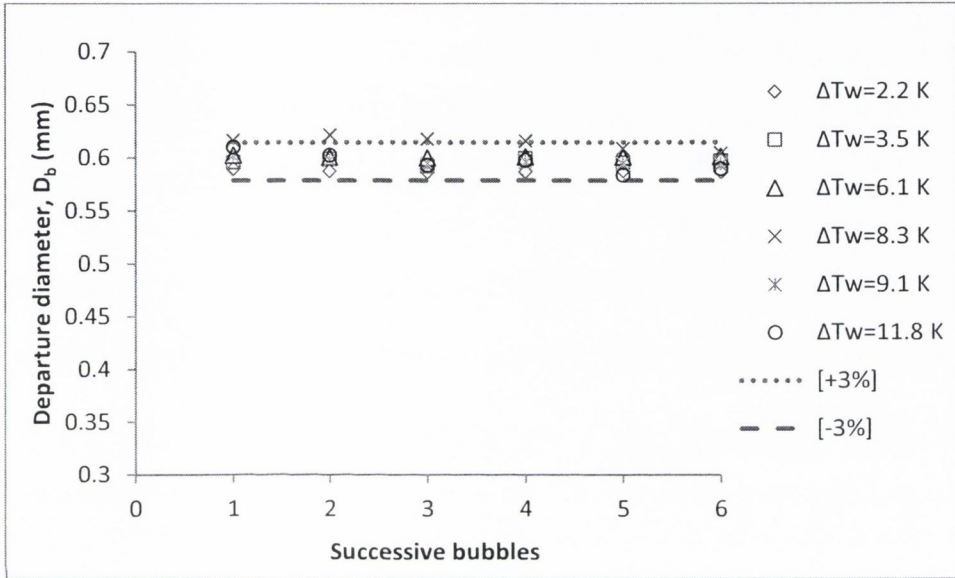


Figure 4.12: Bubble departure diameter, $D_b$ of six successive bubbles
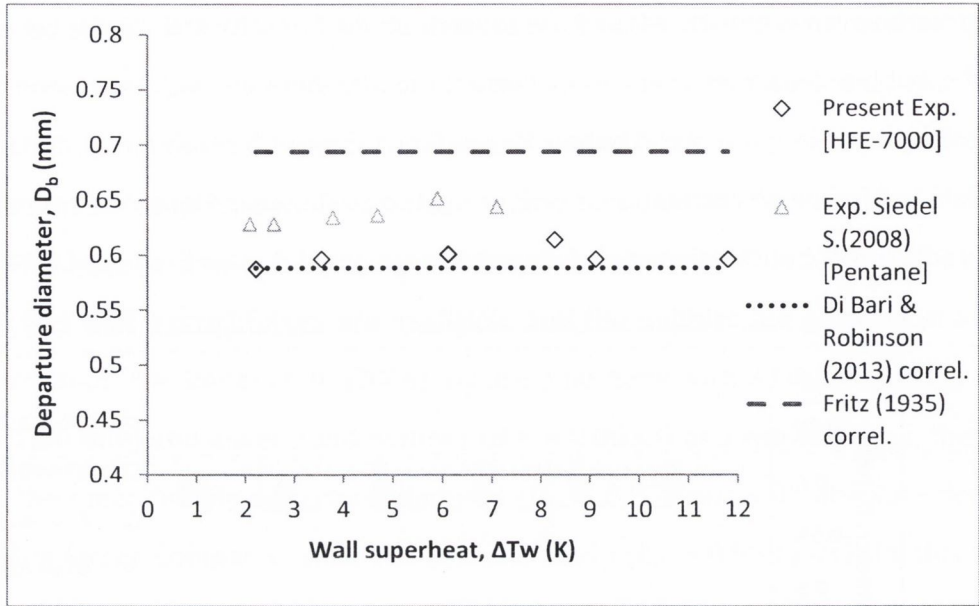
Figure 4.13: Departure diameters for the average of six successive bubbles at various wall superheats

The relationship between the bubble departure diameter and the bubble departure frequency for the present experiment is shown in Figure 4.14. The trend in this figure is similar to the trend of bubble departure volume at different wall superheats (Figure 4.11) since the bubble departure diameter is calculated from the volume of an equivalent sphere [Eq. (3.7)] and the bubble departure frequency exponentially increases with the wall superheats.
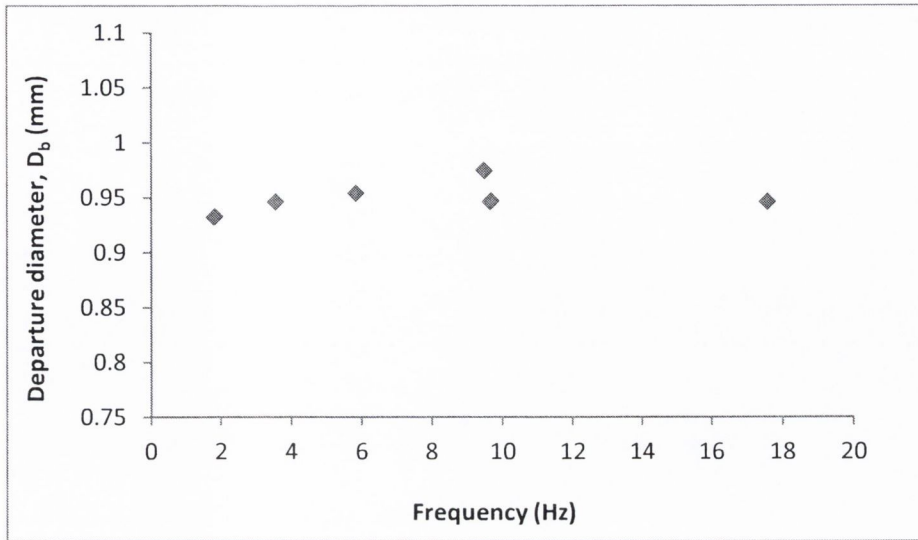
Figure 4.14: Relationship of equivalent bubble departure diameter and bubble departure frequency

In historical bubble departure analyses the bubble departure diameter, $D_b$ and bubble frequency, $f$ are often considered together in the form of the product $f.D_b$. This is done since the product $f.D_b$ can be considered as an estimate of the vapour flow rate which is thought to be related to the effectiveness of the heat transfer. Figure 4.15 shows $f.D_b$ for various wall superheats. The figure also shows the prediction of $f.D_b$ using the correlations by Jakob and Fritz (1931) and Zuber (1963). As stated by Kim and Kim (2006), the Jakob and Fritz correlations for $f.D_b$ is given a constant value, i.e., $f.D_b = 0.078$ whilst the Zuber correlation is given by Eq. (2.68). The correlations of Jacob & Fritz and Zuber predict that $f.D_b$ is independent of wall superheat ($f.D_b$ = constant) which is in contrast to the present work where $f.D_b$ increases by an order of magnitude over the range of superheats tested. The trends clearly show that the present study of quasi-static bubble growth contradicts the notion that the bubble departure size is related to the departure frequency. The correlations of Jakob & Fritz and Zuber each show about 70% and 80% over-prediction compared with the maximum $f.D_b$ of the present experiment data.
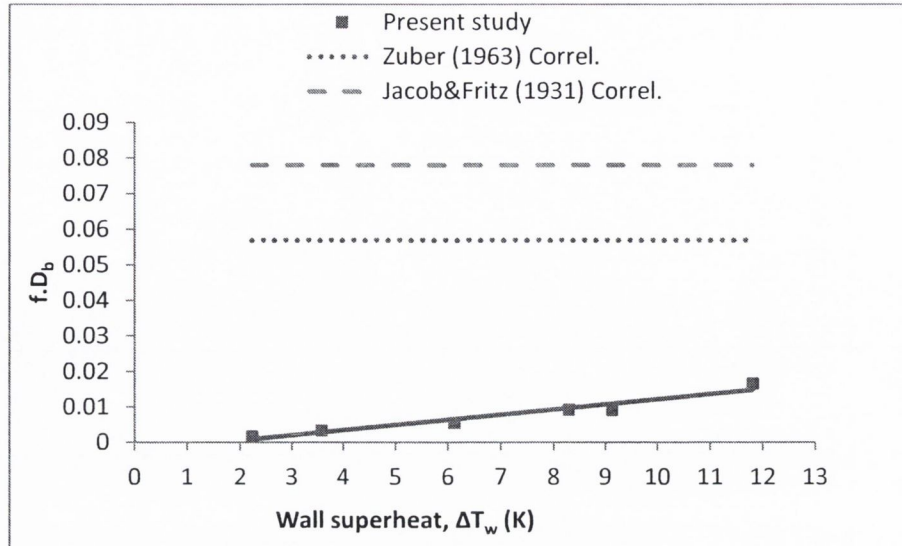
Figure 4.15: Bubble departure frequency-diameter at various wall superheats

## 4.5 Volumetric Growth

Various features of bubble growth, such as waiting and growth times, departure frequency and size, have been discussed above. The global trends were presented and compared with classical theories in order to gauge their relevance and appropriateness. However, actual bubble dynamics, growth histories and related analysis have not yet been discussed. Historically, less attention has been given to the deep analysis of the bubble dynamics, compared with global bubble features, since it is not easily incorporated into predictive models for heat transfer. However, the non-universality of the classical theories and their relatively poor predictions for even the simplest pool boiling scenario illustrate that there is still a lack of understanding with regard to isolated bubble growth in boiling.

The bubble which nucleates, grows and leaves the surface is subsequently replaced by a new bubble nucleating at the same nucleation site. From a viewpoint of experimental repeatability, it is necessary to investigate if any significant differences exist between the bubble events for a given wall superheat. Figure 4.16 plots the six bubble growth curves for the successive bubbles at $\Delta T_w = 11.8$ K. It indicates that the

shapes of each bubble, as quantified by the bubble volume, are generally the same with the volume at departure of each bubble being within ±5% of one another, whereas for the bubble growth time, the dispersion interval is within 20%. The small difference in the departure volume is due to the fact that the bubbles are quasi-static as discussed above. The larger variation in the growth time is likely due to differences in the initial thermal field at nucleation.
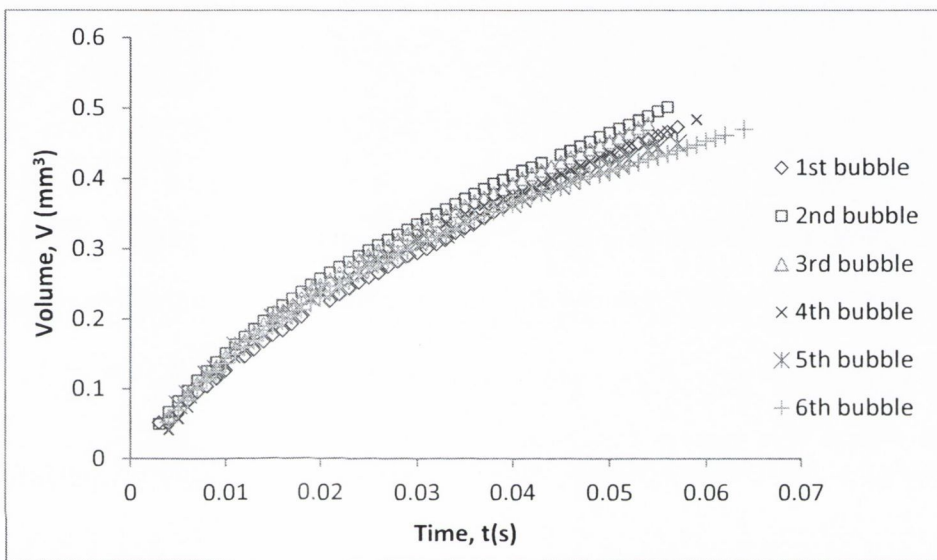


Figure 4.16: Growth curves of six successive bubbles at $\Delta T_w = 11.8$ K

Bubble growth curves at various wall superheats for the average of six successive bubbles are plotted in Figure 4.17. In this figure, bubble growth curves at various wall superheats have a similar shape though the bubble growth times are significantly reduced with increasing wall superheat. This trend is clearly depicted in Figure 4.8 and the physical phenomenon was discussed earlier in terms of the higher wall superheat providing a higher driving potential for bubble growth. A more meaningful comparison is provided in Figure 4.18 where the growth curves are transformed into dimensionless form by dividing the time by the total growth time ($t^* = t/t_d$) and the volume by the departure volume ($V^* = V/V_d$). It is clearly shown that the growth curves collapse very well onto a single curve illustrating that the non-

dimensional growth can be considered independent of wall superheat for the range of Jakob numbers tested in the present study.

To describe volumetric growth curve, an empirical growth law, i.e., power law [Eq. (3.10)] is usually used. As depicted in Figure 4.18, the non-dimensional growth curves of the present experiment can be described as follows;

$$V^* = \begin{cases} 2.5 \times t^* \text{ for } t^* < 0.1 \\ t^{*0.6} \quad \text{ for } t^* > 0.1 \end{cases}$$

This bubble growth law is relatively well described by the recent results of Siedel et al. (2008) using Pentane as a working fluid. A rapid volumetric growth at the initial stage can be explained due to the high level of sensible energy in the superheated thermal boundary layer causing a rapid volumetric growth rate. At the later stage, energy in the superheated liquid layer has been largely been depleted causing a slower volumetric growth rate. However, at the early stage of bubble growth ($t^* < 0.2$), Siedel et al. (2008) have found a lower growth rate, $V^* = 2 \times t^*$. This difference could be due to the lower amount of thermal energy stored in the thermal boundary layer since no waiting times were evident in the Siedel et al. (2008) experiments, which is not the case here. Another possibility for the difference is the influence of surface tension of the fluid used. The surface tension will affect the process of pushing the fluid layer above the cavity during early growth. In the present experiment with HFE-7000 as a working fluid the Bond number is $Bo = 0.0089$ whilst for the Pentane experiments of Siedel et al. (2008) it was $Bo = 0.0033$. Fluids with a larger Bond numbers will have lower surface tension effects and it can be argued that, for similar initial conditions, it will result in faster volumetric growth rate during the early stage of growth when there is plenty of sensible energy available for vaporization. This suggests that the properties of fluid used should be taken into account for the growth law at the early stage of bubble growth.

The empirical growth laws of the present study are notably different from the classical growth laws in analytical studies, including Plesset and Zwick (1954), Forster

and Zuber (1954), Scriven (1959) and Cooper and Lloyd (1969). The classical growth laws are generally stated in the form $R = Ct^{0.5}$ and this would result a volume growth of the form $V^* = t^{*1.5}$, as depicted in Figure 4.18. The discrepancy is quite striking and shows that their models are quite over simplified since they neglect physical aspects of bubble growth which may be dominant, such as the fact that bubbles are not perfect spheres during growth. For the volume growth power law, $V^* = t^{*1.5}$, the trend of the volume curve is concave-shaped (as depicted in Figure 4.18) meaning that the net heat transfer rate must in fact be increasing as the bubble grows. The present study and that of Siedel et al. (2008) have both determined a predominantly convex-shaped trend of volume growth law, i.e., $V^* = t^{*0.6}$. This power law trend is highly relevant and a more physical description of bubble growth since it considers volumetric bubble growth, as opposed to bubble radius models of perfect spheres.
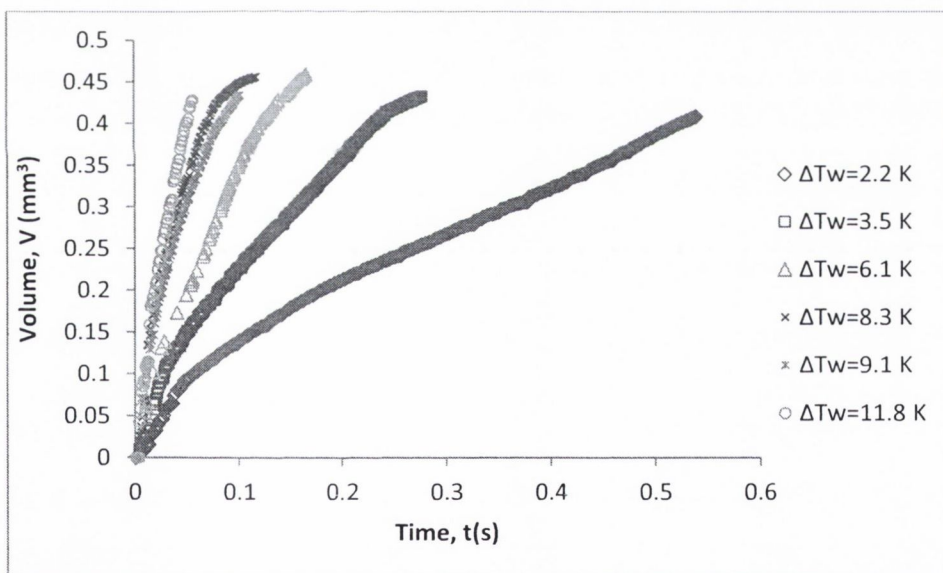


Figure 4.17: Average of six bubbles growth curves at various wall superheats
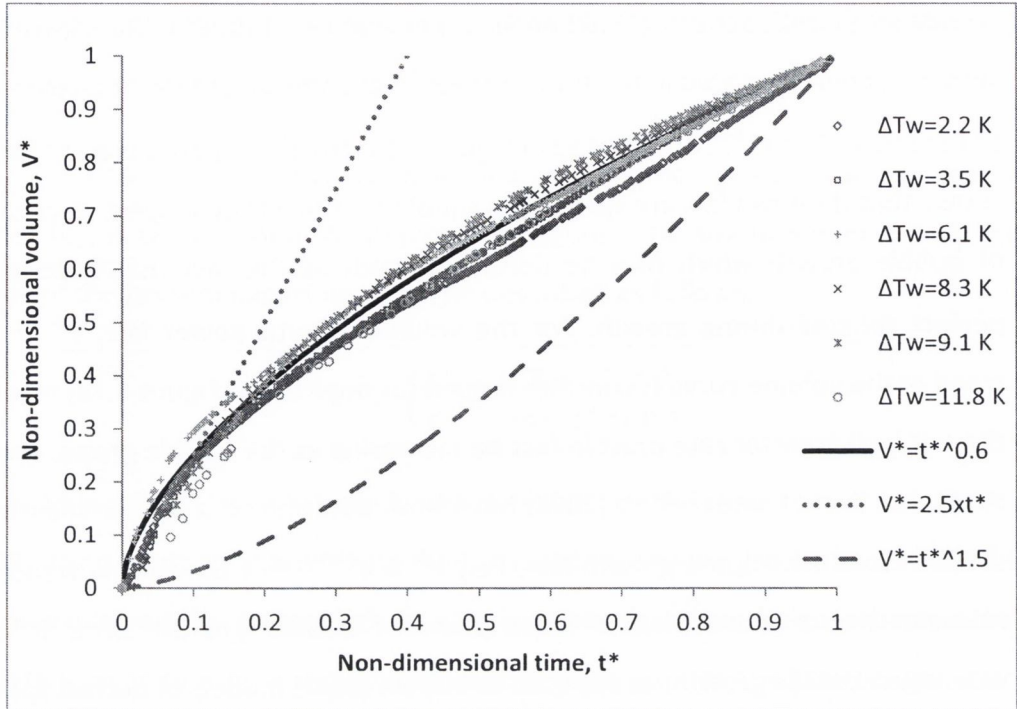
Figure 4.18: Average of non-dimensional six bubbles growth curves at various wall superheats

## 4.6    Energy Transfer at Liquid-Vapour Interface

Once a bubble nucleates it continually depletes the sensible energy stored within the liquid surrounding it. As a result, the volumetric growth rate trend is asymptotic. The present study and that of Siedel et al. (2008) have in fact predicted the same asymptotic volume growth law, i.e., $V^* = t^{*0.6}$. This begs the question as to why there is such a large discrepancy between this work and classical theories.

In order to better understand the differences between the growth law of the present study and the classical growth law, the energy balance at the liquid-vapour interface will be considered. By treating the bubble as a control volume, the transfer of latent heat by vapour production into the bubble is equal to the overall heat transfer into the bubble by conduction within the liquid phase. The energy balance at the liquid-vapour interface is expressed as;

$$\rho_v h_{fg} \frac{dV}{dt} = \int_A k \frac{\partial T}{\partial \eta} dA \qquad (4.13)$$

where $A$ is the instantaneous bubble surface area and $\partial T/\partial \eta$ is the local instantaneous temperature gradient in the liquid normal to the interface. In this equation it is clear that the rate of change of the bubble volume depends on the rate of energy transfer into the bubble. If the overall rate of heat transfer to the bubble decreases, so should the volumetric growth rate. It should be noted that Eq. (4.13) assumes a constant vapour density, which is a good assumption if the vapour pressure is more or less constant and equal to the saturation pressure, i.e., $P_v \sim P_\infty$. Considering the Young-Laplace equation, i.e., $P_v - P_\infty = 2\sigma/R$, the bubble radius $R$ must be large enough that the capillary pressure is small. The minimum radius the bubble will have is that of the cavity (90 µm) which gives a capillary pressure of 275 Pa, which several orders of magnitude smaller than the vapour and ambient pressures so the assumption is reasonable.

The rate of change of bubble volume, i.e., $dV^*/dt^*$ is shown in Figure 4.19. For the case of the present study, the trend $(dV^* / dt^*)$ is constant for $t^* < 0.1$ and decreasing for $t^* > 0.1$. At the initial growth stage ($t^* < 0.1$) where $dV^*/dt^* \sim 2.5$, the volume growth is sustained in this region when there is a lot of energy stored in the superheated layer. Here, the increasing surface area compensates for the decreasing rate of heat transfer due to the depletion of the sensible energy in the superheated layer around the bubble. At the later growth stage ($t^* > 0.1$), where $dV^*/dt^* \sim 0.6/t^{*0.4}$, the volumetric growth rate is decreasing with time, indicating that even though the surface area is increasing, it is no longer increasing at a rate that can compensate for the decreasing rate of heat transfer. The end result is that the volumetric growth rate decreases with time, i.e., it decelerates.

For the case of classical volume growth laws, i.e., $V^* = t^{*1.5}$ where $dV^*/dt^* \sim 1.5t^{0.5}$, volumetric growth rate increases with time. The fact that the energy

in the superheated layer is depleting while the bubble is growing means that the rate of heat transfer is decreasing with time as well. From the classical volume growth theories, the reason that the volume growth is predicted to continuously increase is because the surface area increases at a faster rate than the rate at which the heat transfer is decreasing [Eq. (4.13)]. However, the present experimental data contradicts this and indicates that after $t^*>0.1$ the surface area no longer increases at a rate that can compensate for the decreasing rate of heat transfer. Therefore, the current data casts doubt regarding the validity of classical bubble growth theories which are founded on idealized bubble geometries and heat transfer conditions.
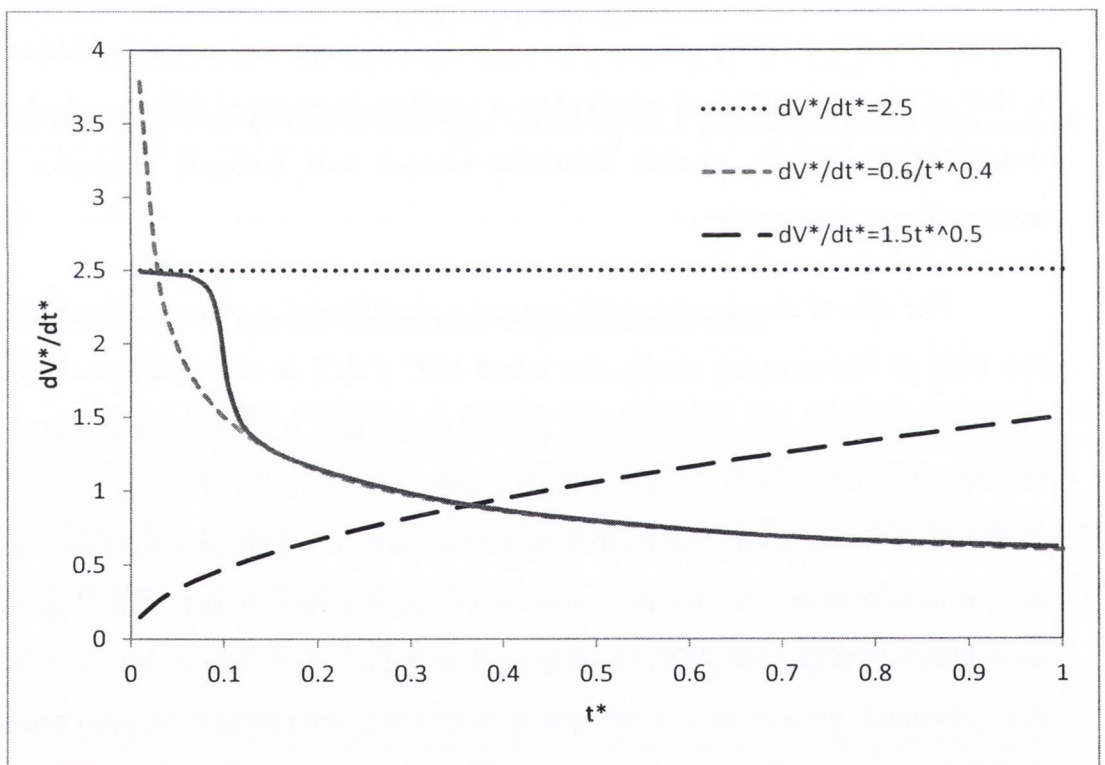


Figure 4.19: Rate of bubble volume change

## 4.7    Bubble Shape and Oscillations

### 4.7.1  Aspect ratio

The bubble aspect ratio $AR$ ($h/w$) is a dimensionless parameter often used as a very simple parameter to describe the bubble shape. The classifications of bubble aspect ratio can be described as follows: if $AR > 1$ the bubble is elongated in the vertical direction whilst if $AR < 1$, the bubble shape is a truncated segment. The aspect ratio of single bubble growth for different wall superheats is shown in Figure 4.20. It is first noted that the profile histories of the bubble aspect ratio collapse very well onto a single profile confirming that that the shape of quasi-static bubbles can be considered independent of wall superheat. After bubble incipience, the bubble shape stays close to a spherical truncated shape for a very short period ($0 < t^* < 0.05$). After $t^* > 0.05$, the bubble begins to elongate gradually in vertical direction where $AR > 1$. It is also noted that the profile of the bubble aspect ratio for high wall superheats, i.e., $\Delta T_w$=9.1 K, 11.8 K, is seen to experience oscillations for the growth interval $0.05 < t^* \leq 1$. The oscillations of the bubble shape are due to the interaction of the growing bubble with the previous bubble. Here, the bubble waiting time plays an important role. As has been discussed the waiting time decreases with wall superheat, and this gives less time for the previous bubble to rise before nucleation of the next bubble, as depicted in Figure 4.21 and Figure 4.22. For the case of the wall superheat of $\Delta T_w$=2.2 K (Figure 4.21) which has a relatively long waiting time ($t_w \approx 5$ ms), it clearly shows the previous bubble having enough time to rise upward before a new bubble comes out of the nucleation site. Here there is no interaction between the two bubbles. For case of the wall superheat of $\Delta T_w$=11.8 K (Figure 4.22), it is evident that the bubble has a very short waiting time ($t_w \leq 1$ ms). Here, there is an observable interaction between the growing and rising bubbles. Thus it can be stated that the low waiting times and high growth rates associated with the higher superheats combine in such a way that there are observable and measurable interactions between growing and rising bubbles.
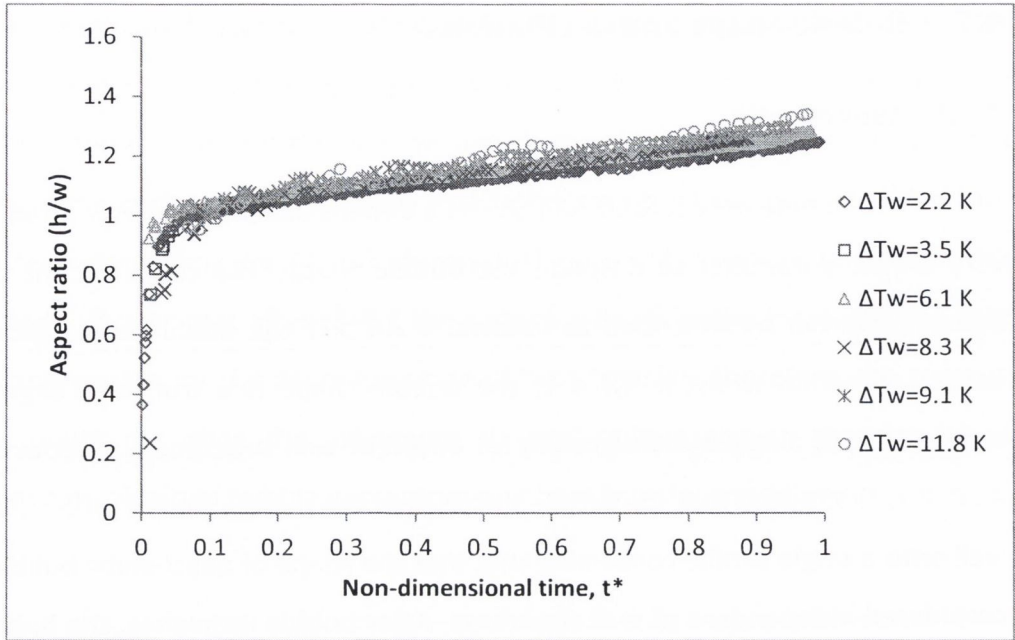
Figure 4.20: Bubble growth aspect ratios ($h/w$) at various wall superheats
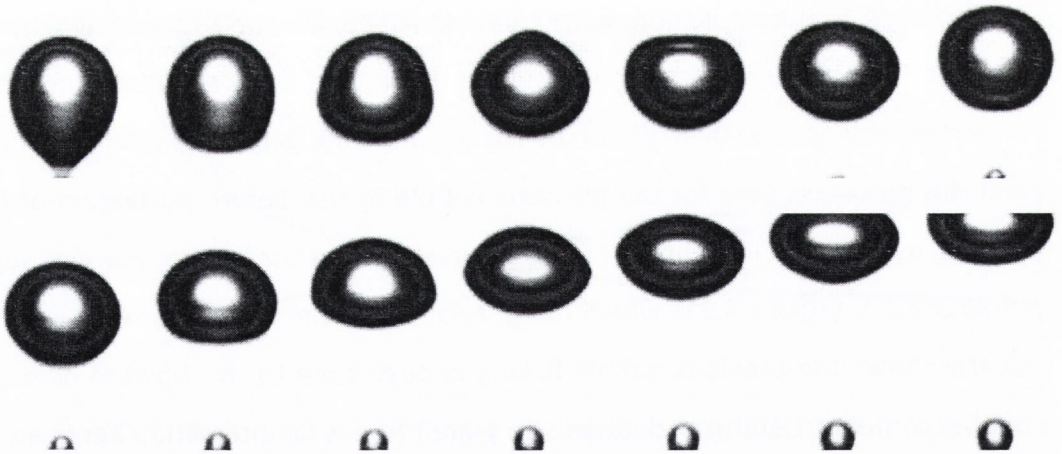


Figure 4.21: Early stage of bubble growth after departing last bubble for $\Delta T_w$=2.2 K with $\Delta t = 1$ ms
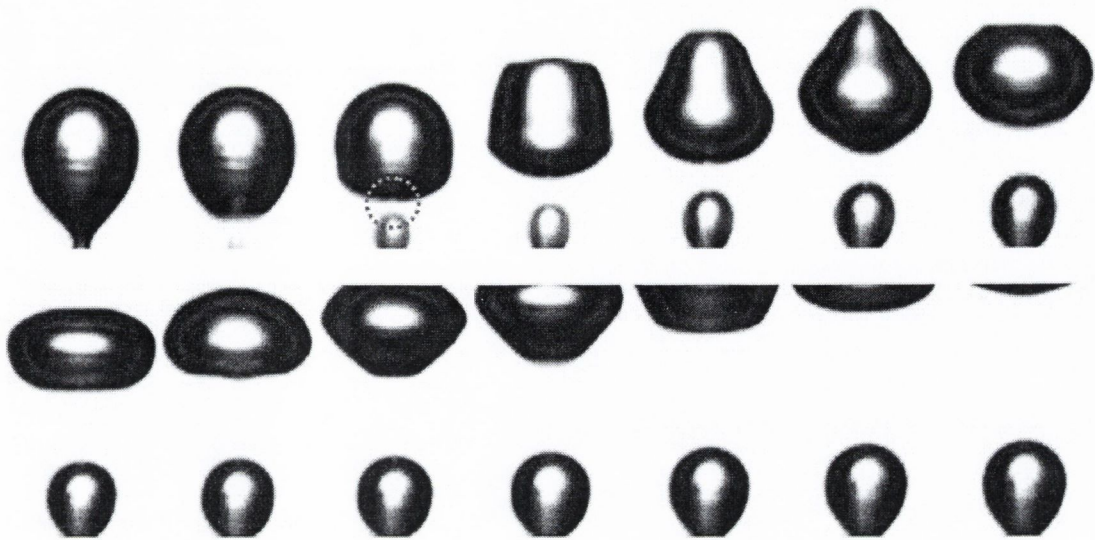
Figure 4.22: Early stage of bubble growth after departing last bubble for $\Delta T_w$=11.8 K with $\Delta t = 1$ ms

The shape changes and subsequent oscillations are due to expansion and compressive forces opposing each other during bubble growth. From observation, there is a clear downward force (compressive force) due to the resistance offered by the rising bubble (Figure 4.22) as the rapidly growing bubble bumps the slowly moving rising bubble. This changes the bubble shape by flattening it somewhat, i.e., the aspect ratio decreases. However, during bubble growth, surface tension acts as a restoring force which tries to minimize the surface area of the bubble. This restoring action acts in such a way as to increase the aspect ratio, thus establishing the oscillations. It should be noted that in some instances vertical coalescence of the two bubbles was observed during bubble growth for the wall superheat $\Delta T_w$=11.8 K and this is shown in Figure 4.23. Thus, it can be presumed that the wall superheat $\Delta T_w$=11.8 K is the approximate transition between the isolated bubble growth regime and bubble column regime.
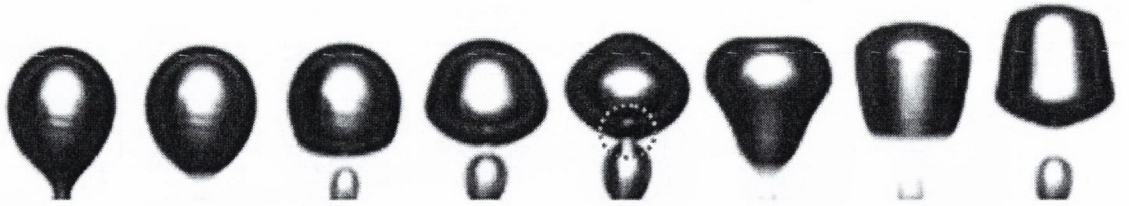
Figure 4.23: Vertical coalescence of two successive bubbles for the case of $\Delta T_w$=11.8 K

### 4.7.2 Height of centre of gravity

The height of centre of gravity of a bubble is also useful in describing the bubble growth dynamics and oscillations. From a bubble dynamics standpoint, the rise of the centre of gravity is related to the bubble momentum. Figure 4.24 shows the centre of gravity histories during bubble growth at various wall superheats. The figure shows that the rate of change of the centre of gravity increases with wall superheat. For the range of wall superheats tested (2.2 K $\leq \Delta T_w \leq$ 11.8 K) and for these low Jakob number experiments, the height of centre of gravity, $h_{cg}$ only increases by 0.052 mm (8.5%) from lowest to highest superheat. Although this shows some indication of bubble elongation with wall superheat, the difference is within experimental uncertainty so the difference cannot be commented upon with certainty.

The history of bubble height of the centre of gravity during bubble growth in non-dimensional time for different wall superheats is shown in Figure 4.25. In the figure, a fairly uniform profile of the bubble centre of gravity for all wall superheats is observed. For $t^* \leq 0.1$ it rapidly rises and this can be described by considering the trend of the volumetric growth law at the initial stage, as discussed in Section 4.5, i.e., $V^* = 2.5t^*$ for $t^* \leq 0.1$. Here the bubble is surrounded by a superheated thermal boundary layer with sufficient energy to accelerate bubble growth for this short period. Subsequent to this, there is a sharp deceleration of the bubble growth with a nearly constant rate of change of the centre of gravity until departure. During this

phase the rate of bubble growth is decelerated due to a depletion of the energy in the liquid surrounding the bubble.

Although the bubble height of the centre of gravity profiles for the different superheats appear to cluster quite well up to $t^* \approx 0.5$, they do have the appearance of diverging from each other closer to the departure stage. This may be experimental uncertainty and repeatability or may be due to the higher superheats causing the bubbles to interact with the slow rising previous bubble which holds them to the surface allowing more time to grow compared with the case when there was no interaction. Evidence of this is supported by the fact that bubbles that are found to oscillate at the high wall superheats ($\Delta T_w$=9.1 K and 11.8 K), have oscillation amplitudes that increase with increasing wall superheat and the higher oscillations are associated with larger departure centres of gravity.
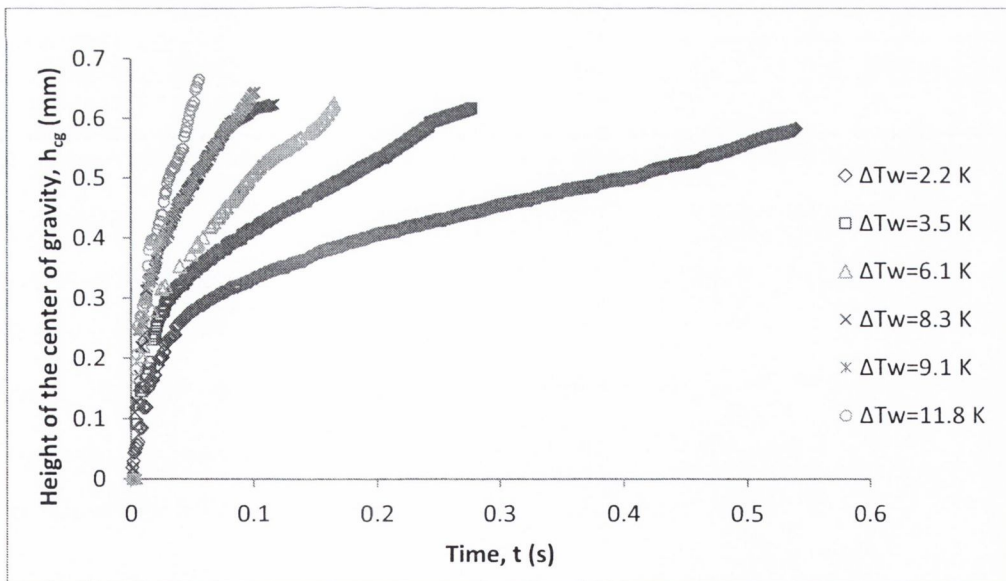


Figure 4.24: Bubble height of centre of gravity histories at various wall superheats
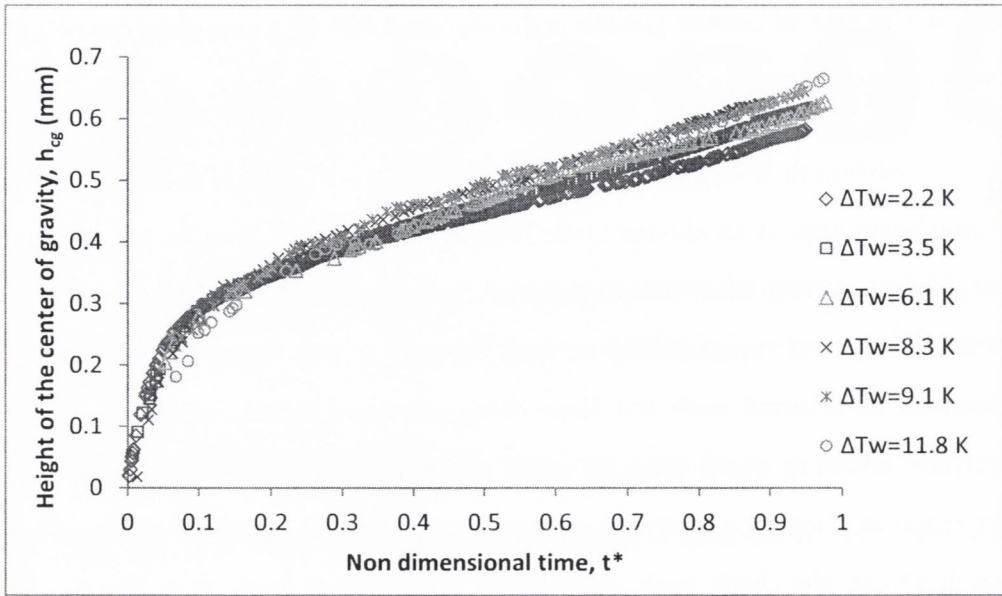
Figure 4.25: Bubble height of the centre of gravity histories at non dimensional time for different wall superheats

The upward velocity of a bubble is characterized by the first derivative of centre of gravity with time ($dh_{cg}/dt$). It is also related to the momentum variation and inertia of the bubble through Eqs. (3.18) and (3.19). Figure 4.26 shows a velocity profile of the centre of gravity for the range of wall superheats tested. In general, the upward velocity of the bubble is proportional to the wall superheats throughout the growth process. At the beginning of growth, the bubble grows upward and has the highest velocity for all wall superheats. For each bubble there is then a rapid deceleration which slows the upward motion of the bubbles. For the case of the lowest wall superheat, $\Delta T_w$=2.2 K, the velocity is lowest of all superheats. It starts at approximately 10 mm/s and sharply drops at around $t^* \approx 0.15$ and is seen to be nearly constant after this, with a slight rise near departure due to the necking process. For the case of a moderate wall superheat, $\Delta T_w$=6.1 K, the velocity profile trend is found to be similar yet with higher velocities in general. For the case of high wall superheats, i.e., $\Delta T_w$=9.1 K and 11.8 K (rapid growing bubble), an undulating profile is obtained throughout the growth period. In both cases, the higher amplitudes are

generally observed earlier during growth and decline towards departure. Also, it is clear that the higher superheat of $\Delta T_w$=11.8 K has associated with it higher oscillation amplitudes.

The acceleration and deceleration of the bubbles are also related to the momentum variation and inertia [Eq. (3.18) and (3.19)] and are depicted in Figure 4.27. The acceleration and deceleration is determined from the second derivative of height of centre of gravity with time ($d^2h_{cg}/dt^2$). Figure 4.27 shows the acceleration and deceleration of the centre of gravity for the wall superheats tested. In the figure, both low ($\Delta T_w$=2.2 K) and moderate ($\Delta T_w$=6.1 K) wall superheats show a deceleration trend from the bubble incipience until $t^*\approx0.15$. After this there is no measurable acceleration or deceleration. This is due to the height of the centre of gravity increasing linearly with time, as depicted in Figure 4.25.

For both high wall superheats ($\Delta T_w$=9.1 K and 11.8 K), the bubble experiences both acceleration and deceleration during growth with observed undulating profiles. Overall, the case of the highest wall superheat, $\Delta T_w$=11.8 K, has higher amplitudes of acceleration and deceleration compared with that of $\Delta T_w$=9.1 K. Furthermore, the amplitudes are noticed to be highest at the initial growth stage and decline gradually until departure, apart from a short acceleration phase at the end due to the necking process. This is evidence that there is more significant interaction between the rising bubble and the growing bubble during the early stage of growth.
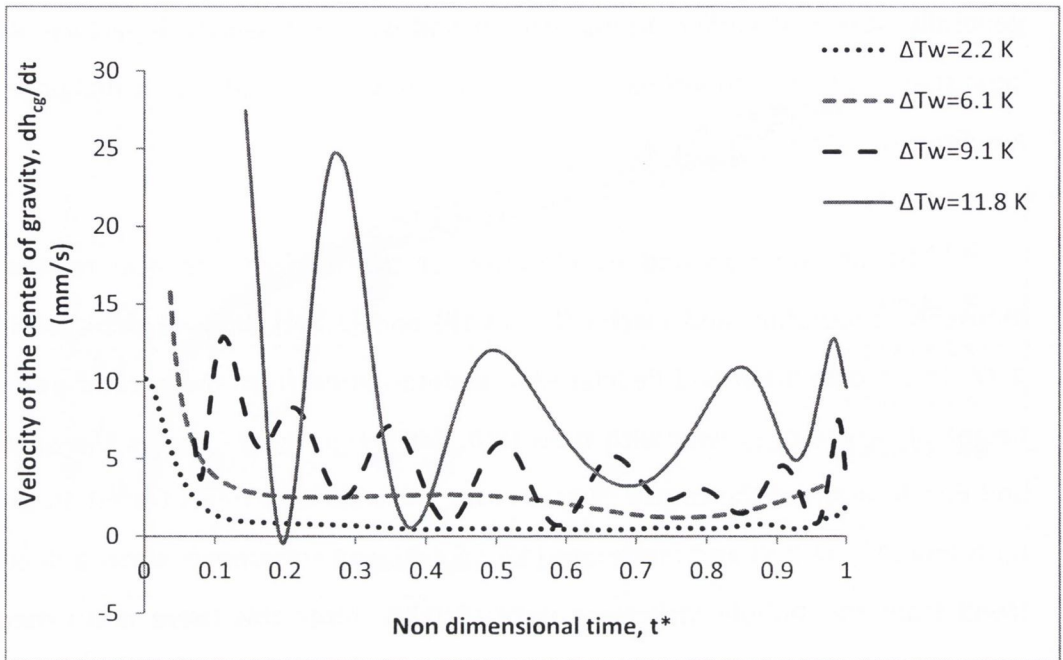
Figure 4.26: Velocity of the centre of gravity ($dh_{cg}/dt$) of bubble growth for different wall superheats
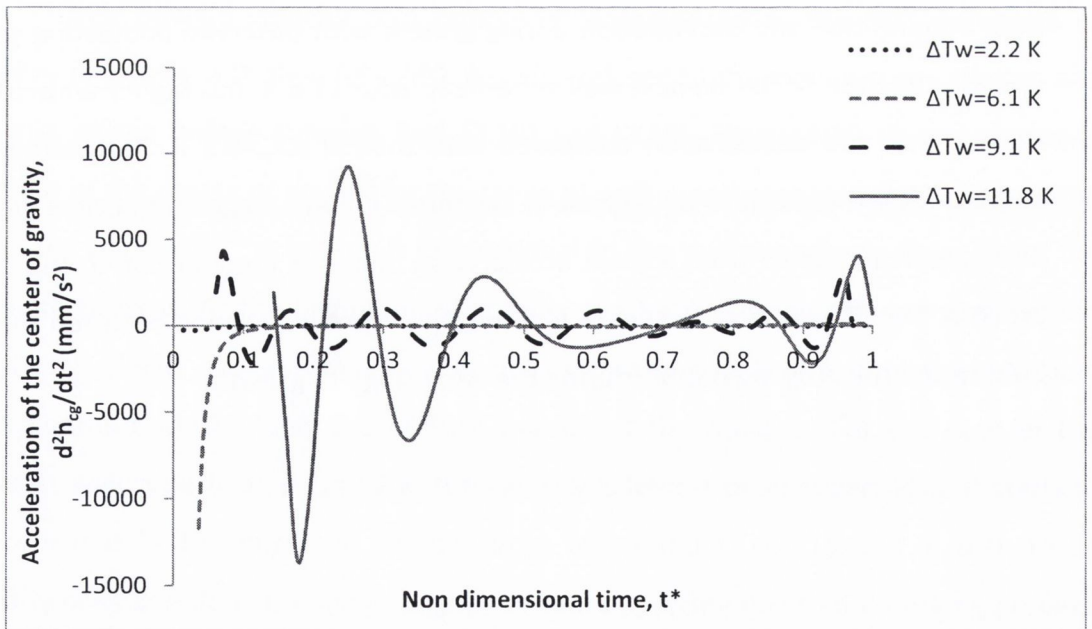


Figure 4.27: Acceleration of the center of gravity ($d^2h_{cg}/dt^2$) of bubble growth for different wall superheats

### 4.7.3 Non dimensional description of shape and oscillations

A non-dimensional parameter $A_s$ for describing together the shape and oscillations of a bubble during growth was introduced by Siedel et al. (2008) and the definition is discussed in Section 3.5.5. This parameter will show evidence of the arguments of shape and oscillation that have been discussed in the previous sections. The evolution of the non-dimensional parameter $A_s$ for various wall superheats is shown in Figure 4.28 and its first derivative is depicted in Figure 4.29. Analysis of the shape as depicted in Figure 4.28 indicates that the bubble is growing as a truncated sphere ($A_s < 1$) for $t^* < 0.05$ and the neck has begun to form after $t^* \approx 0.05$, where $A_s > 1$. For the analysis of the oscillation, as shown in Figure 4.29, the bubble oscillations experienced during the early stage of growth ($t^* < 0.1$) tend to elongate the bubble in the vertical direction, which may be due to the pulling of the growing bubble within the wake of the rising previous bubble. At the later stage, the oscillations tend to elongate or flatten the bubble due to more direct collision-types of interactions with the slow rising bubble. Oscillations of the bubble growth for the case of high wall superheats, i.e., $\Delta T_w$=9.1 K and 11.8 K, appear to cause the bubbles to elongate marginally compared with bubbles at lower wall superheats.
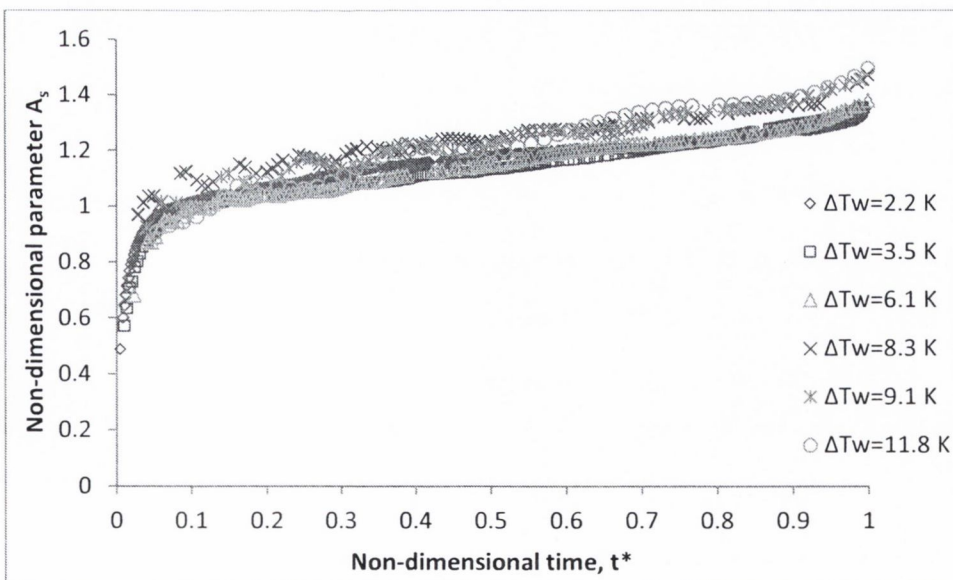


Figure 4.28: Evolution of non-dimensional parameter $A_s$ for various wall superheat
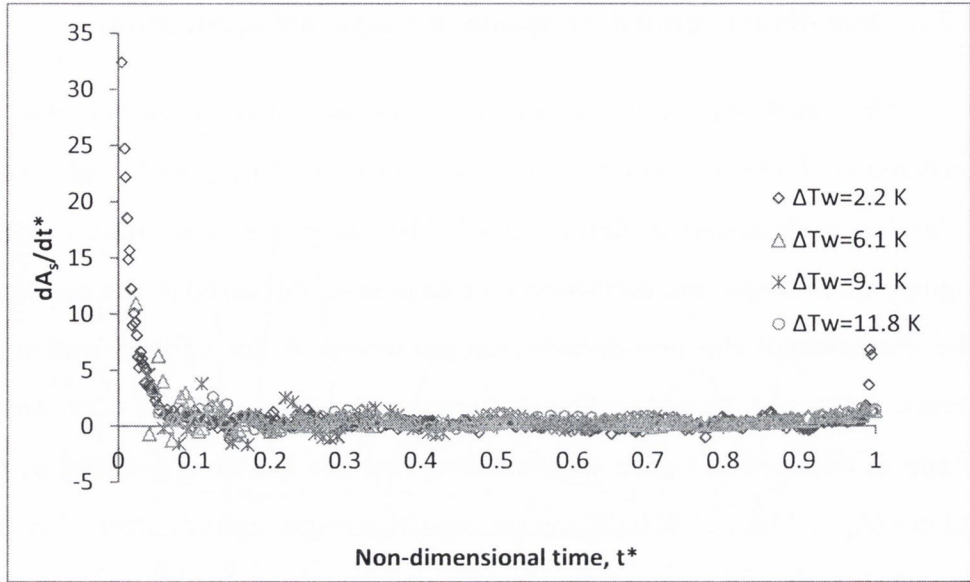
Figure 4.29: First derivative of non-dimensional parameter $A_s$ for various wall superheats

### 4.7.4 Bubble tip and curvature

Figure 4.30 shows the bubble shapes for early, mid and late growth for a low superheat and high superheat case. The details of bubble shape have been studied extensively recently [Siedel et al. (2014), Di Bari and Robinson (2013) and Lesage et al. (2013)] and will not be discussed in detail here. With respect to bubble forces, the bubble tip curvature is one of the most relevant shape parameters as it is required in the calculation of the contact pressure force [Eq. (3.22)]. For bubbles with higher curvature (lower radius) there is a higher pressure difference between the vapour and liquid. This assumes that hydrodynamic liquid pressures are small compared to hydrostatic ones which is the case for quasi static bubble growth. This being the case the vapour to hydrostatic liquid pressure difference is simply given by the relation:

$$P_v - P_l = 2\sigma/R_{tip} = 2\sigma C_{tip}.$$

Figure 4.31 shows the evolution of radius of the bubble tip for low, moderate and high wall superheats. Overall, the results line up fairly well, though there is some

107

scatter in the data. The radius at the tip for all wall superheats shows a trend with an initial sharp increase if it is noted that the minimum radius would be approximately the cavity radius of 90 μm at $t^*=0$ ($R_{tip}$ could not be measured accurately for $t^*<0.1$ due to the small size of the bubble compounded by the influence of the mirage effect). At $t^* \approx 0.4$, the bubble tip radius changes marginally until the bubble departs. This trend indicates that the vapour pressure sharply decreases until near the middle of the growth stage and then remains more or less constant until departure. This has repercussions with regard to the contact pressure force which will be presented in detail in Section 4.8.2.
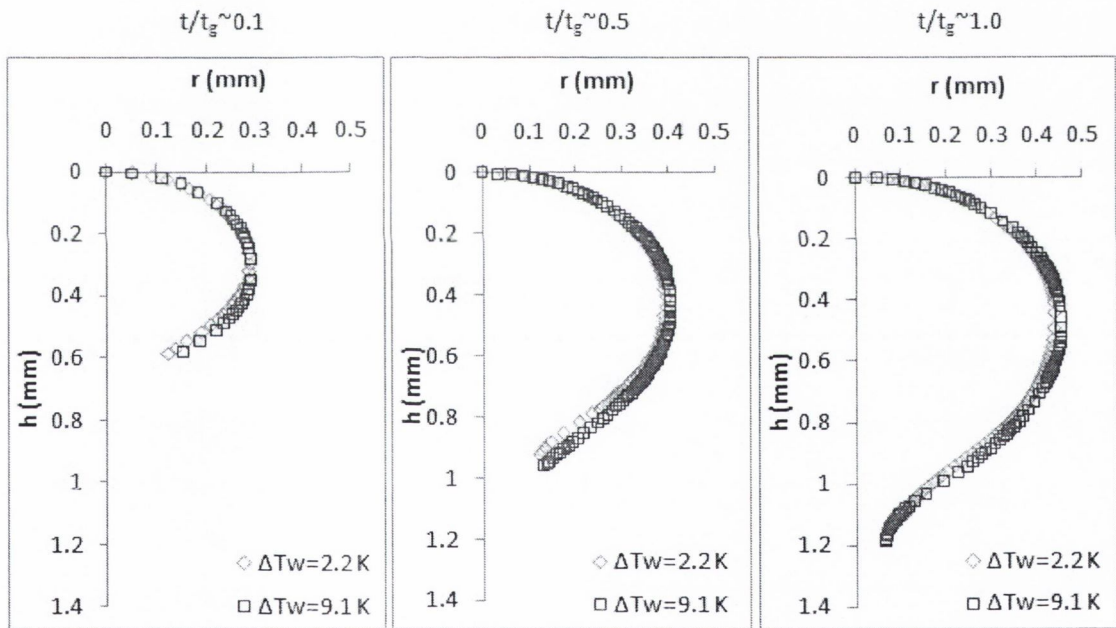


Figure 4.30: Evolution of bubble shape for low and high wall superheats
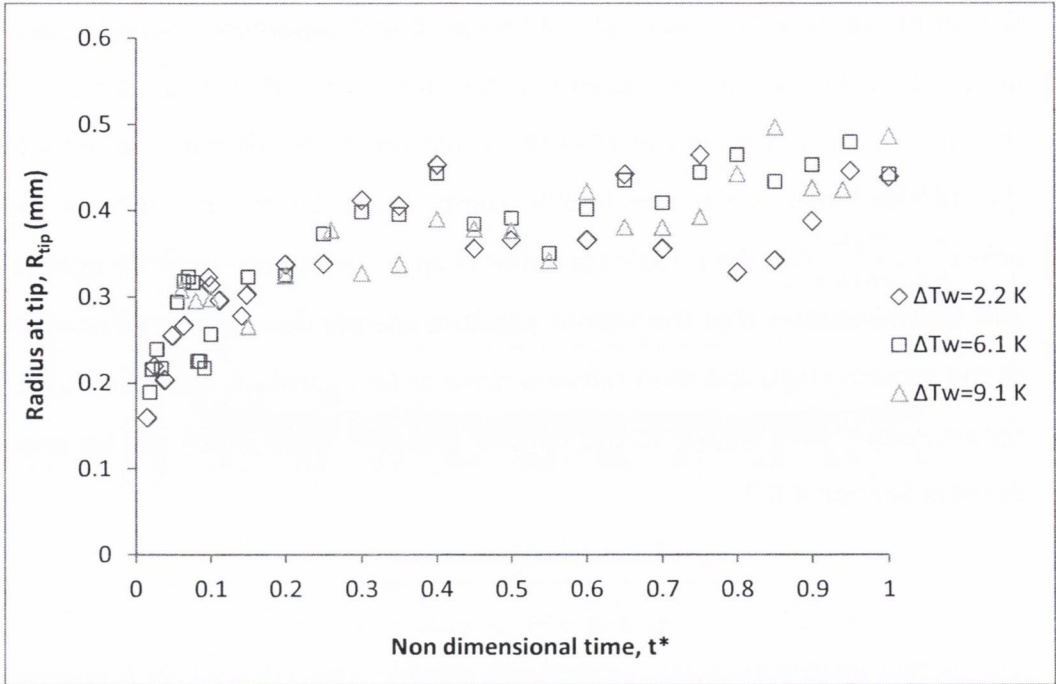
Figure 4.31: Evolution of radius at bubble tip for low, moderate and high wall superheats

## 4.8    Contact Angle and Forces Analysis

### 4.8.1    Contact angle development

The contact angle, $\alpha$ is the angle between the interface at the triple line and the horizontal plane (surface) and it is defined in the liquid phase as illustrated in Figure 4.32. The contact angle is calculated from the two data points of the smoothed interface that are located closest to the surface as depicted in Figure 4.33. The liquid-vapour interface at the bubble base experiences dynamic contact angles at the wall during bubble growth and departure stages (Figure 4.35). The surface tension force acting at the bubble base depends on the dynamic contact angle [see Eq. (3.25)].

However, the measurement of the contact angle in the present experiment is considered to have a non-negligible error, which likely over-estimated the value due to the following

109

(i) The single bubble growth was recorded with a camera inclination of 2° with the horizontal surface in order to avoid the mirage effect over the majority of the bubble surface [Cooper (1983)].

(ii) Even still, the high temperature gradients at the heated surface will still distort the bubble image due to the mirage effect and this will occur most drastically where the contact angle is being measured.
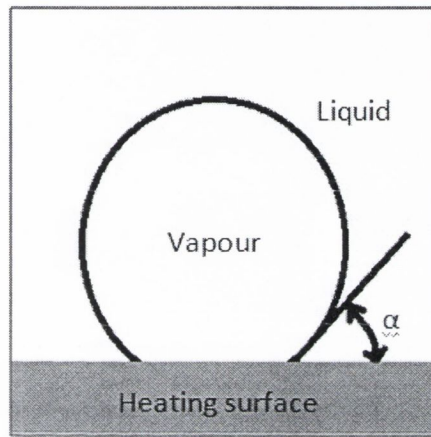


Figure 4.32: Definition of contact angle, $\alpha$



Figure 4.33: Calculation of contact angle, $\alpha$ at the liquid-vapour interface

Figure 4.34 shows a large scatter of measured contact angles with time and this was consistent with the other wall superheats tested. The figure also shows the contact angle for this wall superheat. Siedel et al. (2013) corrected for the mirage effect by solving the capillary equation for the given bubble volume. They showed that by using the calculated contact angle, as opposed to the measured one, the vertical force balance on the bubble was satisfied throughout the growth phase, whereas with the mea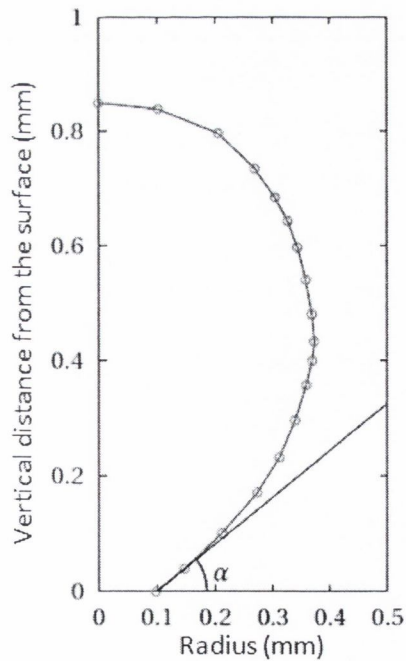sured contact angle there was a large residual on the force balance. Following on from the Siedel et al. (2013) study, this work corrects the contact angle for the mirage effect by calculating the value which would satisfy the vertical force balance. Since these are all quasi static bubbles, the method should give the same contact angle history for each superheat tested.

A photographic sequence illustrating the contact angle dynamics for the wall superheat $\Delta T_w$=2.2 K is shown in Figure 4.35. The percentage difference between the measured and the corrected contact angle is still considerable, as high as 43%, at the early growth of the bubble but the difference is relatively low ($\approx$8%) at the near departure stage. This would drastically influence the calculated surface tension adhesion force and any subsequent analysis. The contact angle has the highest value at initial bubble growth ($\alpha_{measured}$$\approx$109° and $\alpha_{corrected}$$\approx$77°) and steeply decreases to about $\alpha_{measured}$$\approx$55° ($\alpha_{corrected}$$\approx$29°) during the initial nearly spherical growth phase, until $t^* \approx 0.1$. Subsequent to this, the contact angle increases at what can be considered a low rate to measured values of around 65° ($\alpha_{corrected}$$\approx$37°) to 70°($\alpha_{corrected}$$\approx$46°). This is then followed by a phase when it begins to increase as the centre of gravity begins to accelerate as the bubble neck is formed ($t^* \geq 0.9$). Comparison of corrected contact angle histories for low and high wall superheats is presented in Figure 4.36. The respective scatter in the measured contact angles is shown in Appendix C. In the figure, the corrected contact angles for all wall superheats are very close to one another, indicating that the contact angle can be described independently from wall superheat and confirming the correctness of the technique used for its correction.
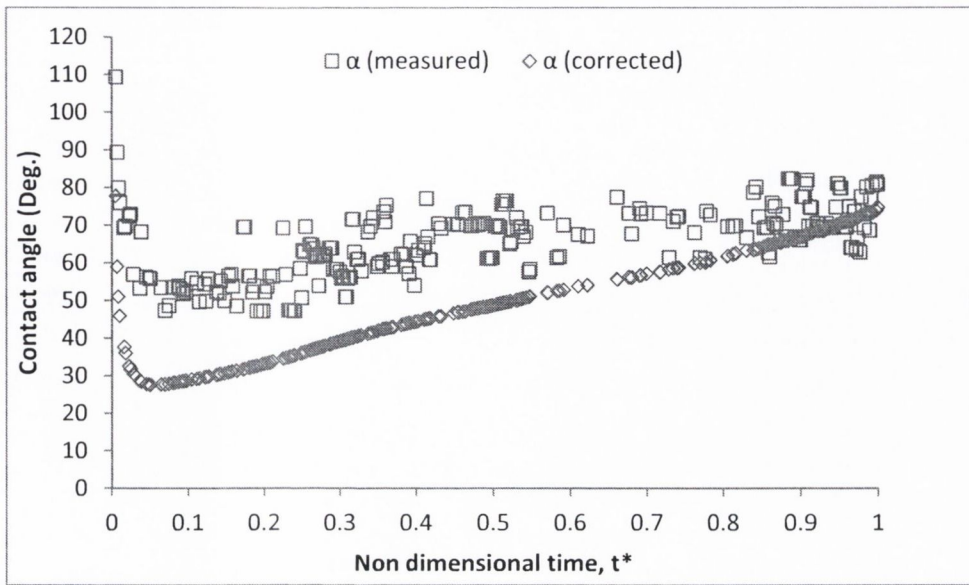
Figure 4.34: Contact angle histories for wall superheat, $\Delta T_w$=2.2 K
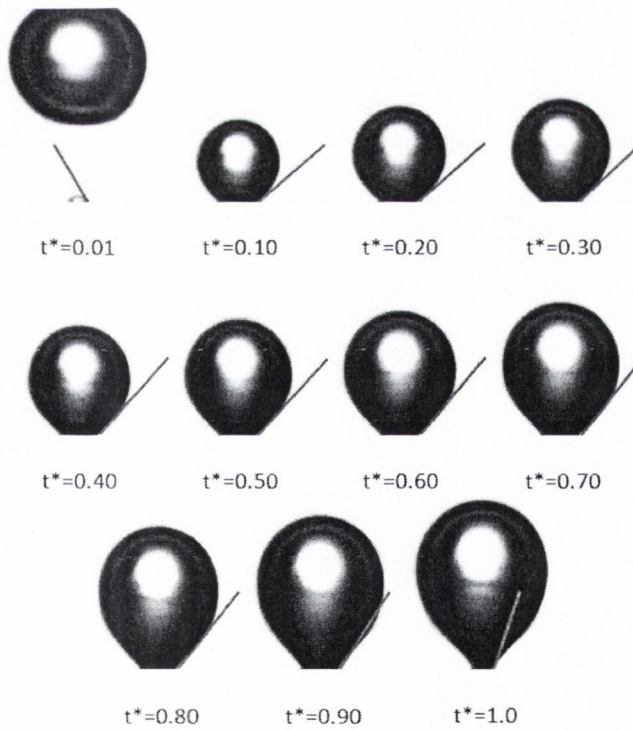


Figure 4.35: Video sequence of bubble growth for wall superheat, $\Delta T_w$=2.2 K
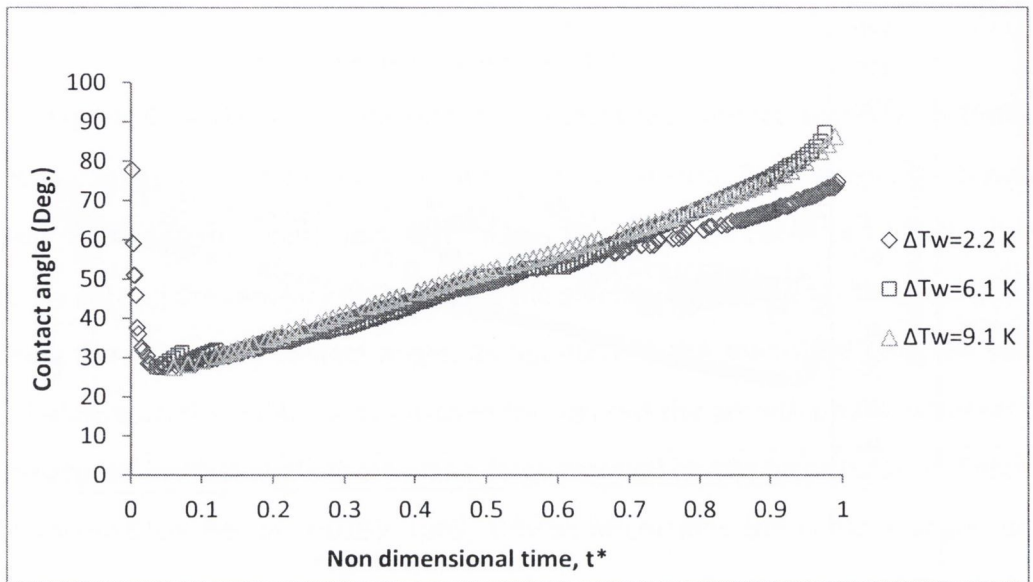
Figure 4.36: Contact angle (corrected) histories for low, moderate and high wall superheats

### 4.8.2  Forces acting on a growing bubble

The details of various forces acting on a growing bubble have been investigated recently by Di Bari and Robinson (2013) and Siedel et al. (2013). As discussed earlier the forces include the momentum, liquid inertia, buoyancy and surface tension forces. The descriptions of these forces including the methods of calculation are explained in Section 3.5.6. These forces influence the evolution of the bubble shape and its motion as well as the bubble condition during departure from heated surface. Therefore, an analysis of the forces acting on growing bubbles will help provide a better understanding of the bubble dynamics and the bubble at departure, which in turn play a very significant role in boiling heat transfer.

A low, moderate and high wall superheat, i.e., 2.2 K, 6.1 K and 9.1 K have been chosen in the force analysis and are shown in Figure 4.37, Figure 4.38 and Figure 4.39 respectively. Figure 4.37 shows the uncorrected surface tension force and the very high residual on the force balance as a consequence. The figure also shows the

corrected surface tension force which results by balancing the upward forces with the downward ones.

In all cases, it clearly shows that the buoyancy force acting on a growing bubble can be considered as independent of wall superheat. This is expected for quasi static bubbles with approximately the same shape. However, since the bubble grows much slower for the 2.2 K superheat case, more bubble measurements are available at the low dimensionless times so this case will be discussed in more detail.

Referring to Figure 4.37 the buoyancy force, $F_{bouy1}$ akin to the Archimedes force, is an upwardly directed force and it increases steadily with the growth of the bubble since it is proportional to the bubble volume. The magnitude of this buoyancy force acting on bubble at departure is approximately 5.8 µN. The so-called contact pressure force, $F_{bouy,3}$, begins high since the bubble curvature is high when the bubble is small. This force decreases sharply as the bubble expands rapidly, decreasing its curvature, up to $t^* \approx 0.1$ after which it decreased gradually until the bubble departs ($F_{bouy,3} \approx 1.33$ µN at departure). For this superheat both $F_{li}$ and $F_{mom}$ are negligible, except for a slight increase in the predicted $F_{li}$ near departure as the bubble neck pinches. Finally, the only downwardly directed force is that of surface tension. This force decreases in magnitude as the contact angle initially decreases, reaches a minimum and subsequently begins to increase in magnitude as the contact angle increases. It reaches a value of $F\sigma \approx -6.7$ µN at departure.

For the analysis of the liquid acceleration and deceleration reactions caused by the motion of the interface, i.e., liquid inertia force, $F_{li}$, it appears this force is significant at high wall superheats, i.e., $\Delta T_w = 9.1$ K with an undulating profile. However, the predicted magnitude of $F_{li}$ reaches levels approaching ±2 µN, which is of the same order as the buoyancy and surface tension forces. Since this is a prediction and is very sensitive to the added mass coefficient, which is not known, it is likely that this force is over estimated. If the presented forces were accurate one would then expect severe variations in the measured contact angle, which was not the case. More

work is required to better understand the liquid inertia forces acting on bubbles, possibly using computational fluid dynamics. For this high superheat case the momentum variation, i.e., momentum force, $F_{mom}$ appears to be becoming noticeable, with magnitudes exceeding 0.25 μN. This order of magnitude seems reasonable in light of the primary forces acting on the bubble.
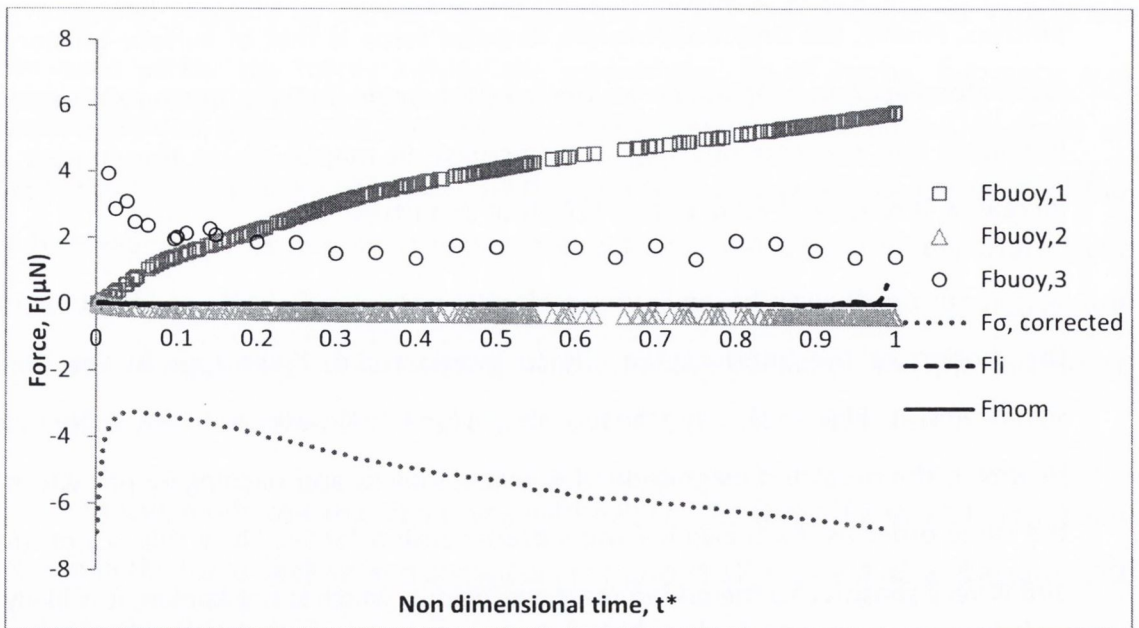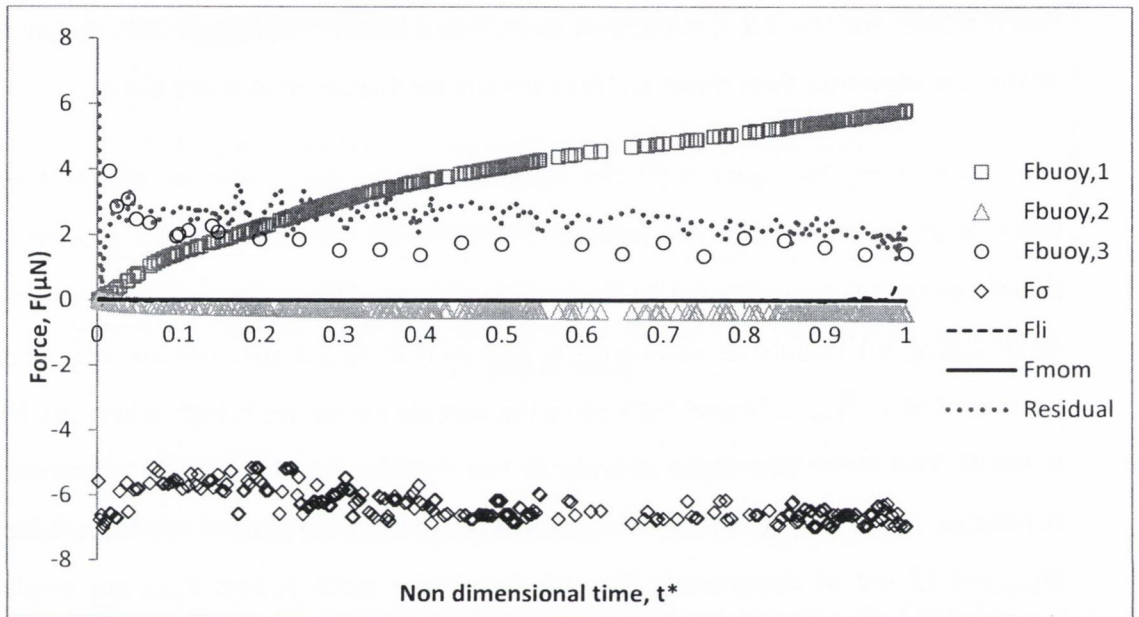


Figure 4.37: Various forces acting on a growing bubble at wall superheat $\Delta T_w$=2.2 K: (top) uncorrected contact angle, (bottom) corrected contact angle
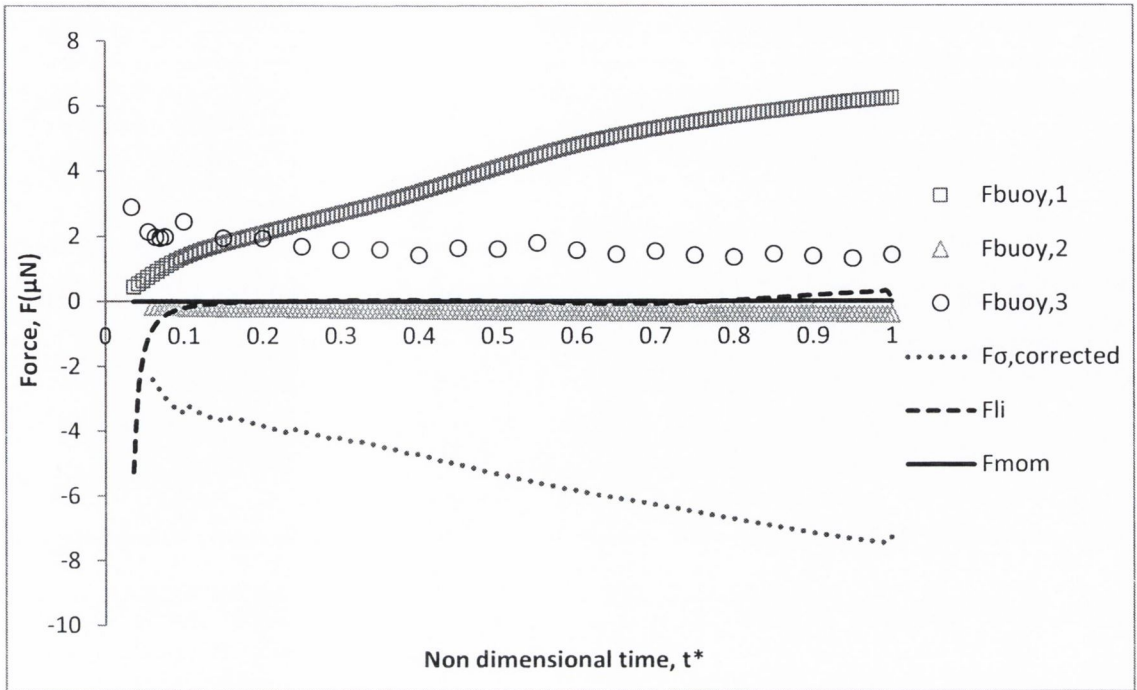
Figure 4.38: Forces acting on a growing bubble at wall superheat, $\Delta T_w$=6.1 K
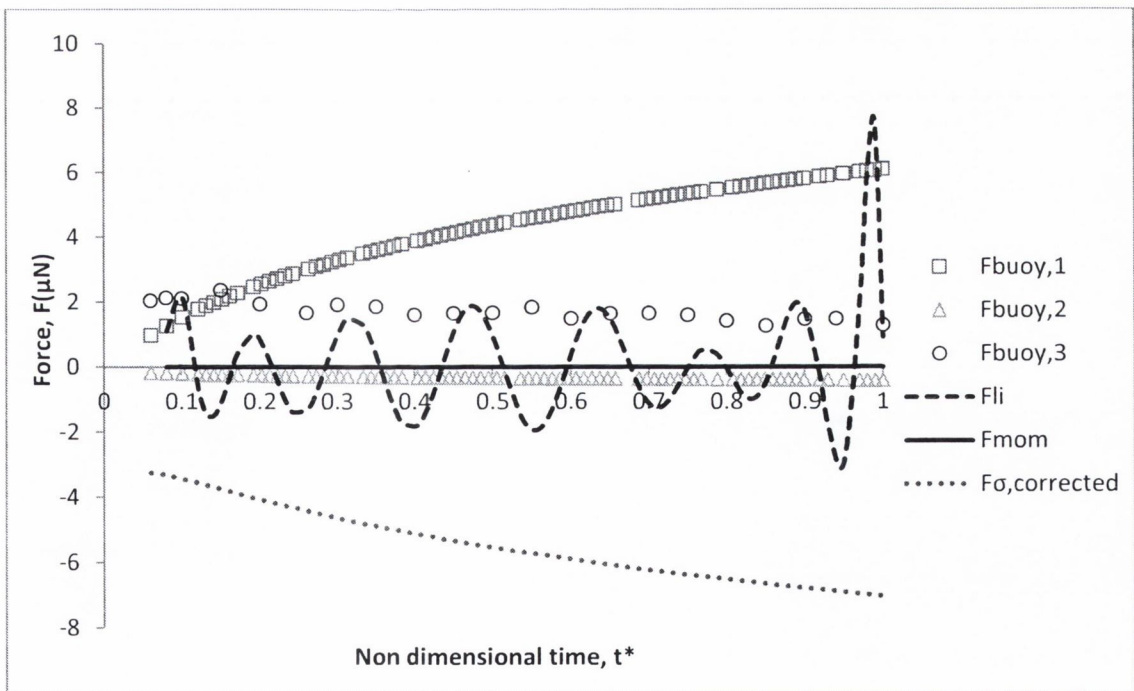


Figure 4.39: Forces acting on a growing bubble at wall superheat, $\Delta T_w$=9.1 K

## 4.9    Effects of Liquid Subcooling

Subcooling of the surrounding liquid pool below saturation generally shifts the boiling curve upward because the driving temperature difference increases with increasing subcooling [Carey (2008)]. In subcooled boiling, the liquid is evaporated in the region of the bubble close to the heated surface and condensed in the upper region exposed to the subcooled liquid, especially during the collapse phase of the bubble [Bode (2008)]. This significant change compared with saturated boiling is expected to affect the mechanisms of heat removal from the heated surface. According to Judd et al. (1991), the rate of heat removal from the heated surface during subcooled boiling is completely determined by the mechanisms of enthalpy transport, microlayer evaporation and natural convection. Natural convection is considered less significant in saturated boiling due to a reduction in the driving temperature differential between the superheated wall and the bulk liquid and the larger area coverage associated with bubbles. In addition, condensation at the interface of vapour bubbles occurs at some stage during growth, as suggested by Zhao and Tsuruta (2002). Considering these, the behaviour of bubble growth in subcooled conditions may be significantly different compared to the saturated condition. A few analytical studies have been carried out on bubble growth dynamics in subcooled boiling, including Kang et al. (1993) and Zhao and Tsuruta (2002), but they lacked the careful experimental studies required for correct validation.

The present study and related experimental technique is capable of providing images of bubble growth with high temporal and spatial resolution and will reveal more clearly some of the important aspects in subcooled boiling, e.g., bubble inception, evolution, frequency, departure size, volumetric growth and action of forces on a growing bubble. The present experiment of pool boiling with subcooled liquid was performed with a fixed heat flux of $q'' = 36$ kW/m$^2$ and subcooling levels ranging from 3 K to 10 K. For this work, the three different subcooling levels are categorized and referred to as: low subcooling ($\Delta T_{sub}$=3 K), mid subcooling ($\Delta T_{sub}$=6 K and 8 K) and high subcooling ($\Delta T_{sub}$=10 K). The present analysis of vapour bubble

growth in subcooled pool boiling is limited to the isolated bubble regime. The data and discussion are mainly focused on comparative analysis of bubble growth characteristics during pool boiling between subcooled conditions and the saturated condition. For the comparison two things must be noted; (i) the heat flux level required for stable bubble growth cycles was higher for the subcooled cases. The lowest level achieved, $q'' = 36\,\text{kW/m}^2$, would cause vertical bubble coalescence for saturated conditions. As a result it was not possible to perform a like-for-like comparison between saturated and subcooled bubble growth for a given fixed heat flux, (ii) higher subcooling and heat fluxes increases the mirage effect considerably which limits the range over which these parameters can be varied and those chosen were determined to give acceptable results.

### 4.9.1 Isolated bubble: Inception, evolution and frequency of departure

Since the experiments have been performed at a relatively high heat flux, i.e., $q'' = 36\,\text{kW/m}^2$, the waiting time is quite small, i.e., less than 1 ms for the subcooling range tested. However, with the bulk liquid subcooled, there is an interesting interaction between the nucleating and departed bubbles which was not observed for the saturated cases. Figure 4.40 shows the sequence of bubble images between the end of one stable growth cycle and the next for isolated bubbles with subcooling levels $\Delta T_{sub}$=3 K, 6 K, 8 K and 10 K. In the figure, it shows that the new bubble grows fast enough for the lower levels of subcooling that vertical coalescence occurs between the early growing bubble and the departing bubble. The departing bubble is seen to pull the fast growing bubble off of the surface prematurely and the bubble merges vertically forming a vapor column. This is of course indicative of the mechanism which inhibits stable bubble growth cycles at the saturated condition for this heat flux.

For the case of low subcooling ($\Delta T_{sub}$=3 K), the time elapsed between the two stable cycles of isolated bubble growth is approximately 5 ms with two coalescence

events occurring. For the case of mid subcooling ($\Delta T_{sub}$=6 K and 8 K), the time elapsed reduces to approximately 3 ms with one coalescence event. For the case of highest subcooling ($\Delta T_{sub}$=10 K), the time gap is approximately $t \approx 2$ ms with no coalescence event. The amount of energy stored in the thermal boundary layer above the cavity to be used for nucleation and growth of the new bubble reduces with increasing subcooling. As the wall superheat decreases with increasing subcooling natural convection plays a more important role as suggested by Judd et al. (1991). Bubble coalescence is more prominant at lower subcooling levels because the growth rates are higher due to the higher driving temperature differential resulting in higher heat transfer rates. This is outlined in Table 2 which shows that the wall superheat increases with decreased subcooling. This suggests that a higher degree of subcooling will slow the processes of nucleation and growth of a new bubble, consistent with the analytical study of Zhao and Tsuruta (2002).

Table 2: Superheat-subcooling relationship

| $\Delta T_{sub}$ | 3 K | 6 K | 8 K | 10 K |
|---|---|---|---|---|
| $\Delta T_{sup}$ | 16.6 K | 16.4 K | 15.2 K | 13.3 K |
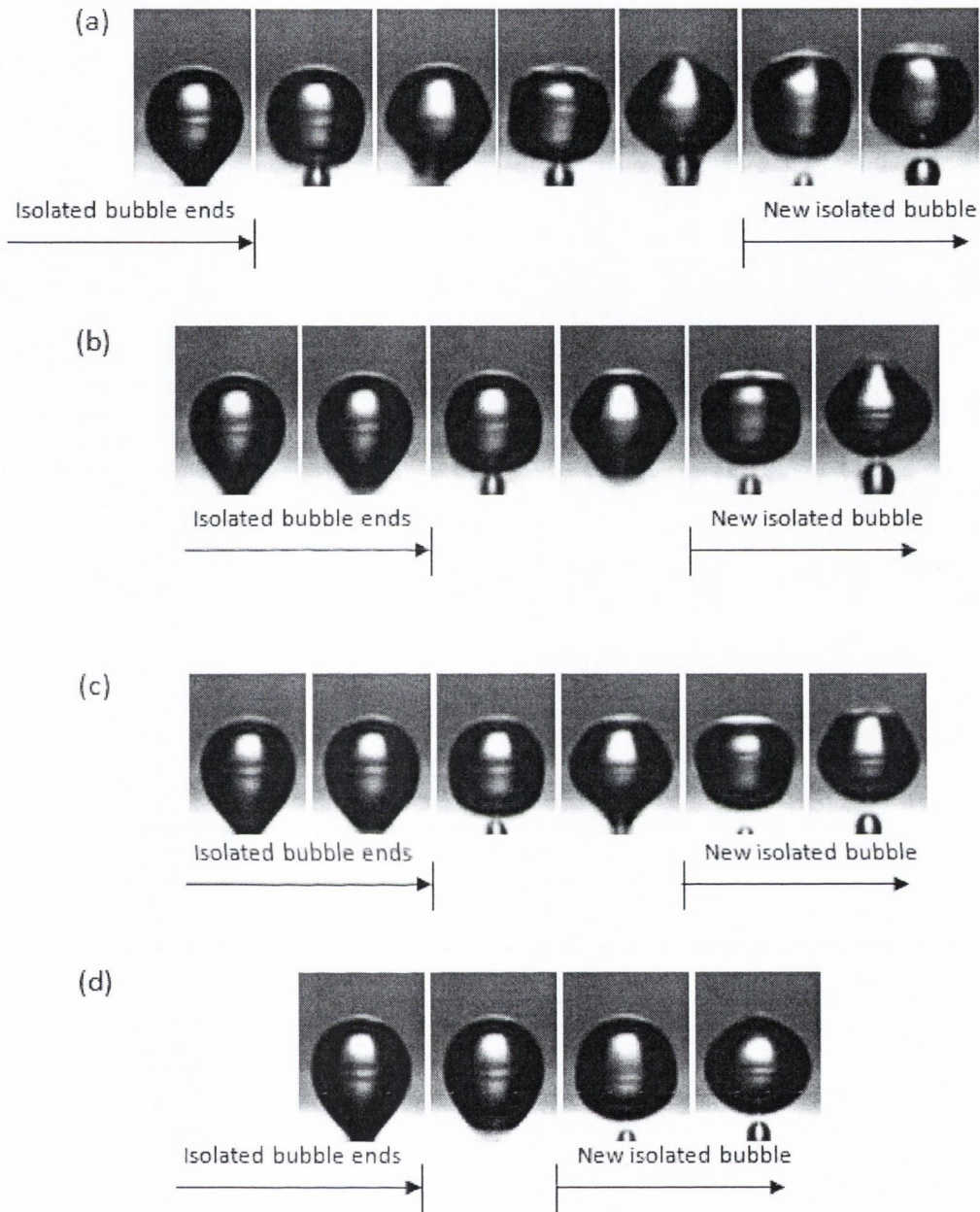
Figure 4.40: Sequence of bubble images of two-cycle of isolated bubbles for subcooling levels: (a) $\Delta T_{sub} = 3$ K, (b) $\Delta T_{sub} = 6$ K, (c) $\Delta T_{sub} = 8$ K, (d) $\Delta T_{sub} = 10$ K with $\Delta t = 1$ ms between the images

Figure 4.41 shows a sequence of bubble images and presents an example of the evolution of a bubble growing in subcooled boiling, in this case for $\Delta T_{sub} = 8$ K. In the figure, the growth process of an individual isolated bubble is divided into two

stages i.e. the initial growth phase and the final growth phase. The shapes of the bubble for the entire bubble growth are very similar for the range of subcooling tested as shown in Figure 4.42. During the initial growth phase ($0 \leq t^* \leq 0.05$), the bubble grows with a truncated-spherical shape then the shape of the bubbles change from truncated-spherical to a distorted geometry due to the action of hydrostatic pressure at the final growth period ($t^* > 0.05$). For the comparative analysis of two different liquid temperatures, the shapes of the bubbles for both subcooled boiling and saturated boiling are similar at the growth stage $t^* \leq 0.1$, as depicted in Figure 4.43. However in the later stage, the bubble for the case of subcooled boiling is less elongated compared to the case of saturated boiling (Figure 4.43). From the contact angle development (Figure 4.48), the histories of bubble shape difference between those two cases are illustrated. It appears that that the bubble has experienced a downward force, possibly by the fluid moving downward as a result of higher density difference, similar to predictions by Chen et al. (1996).
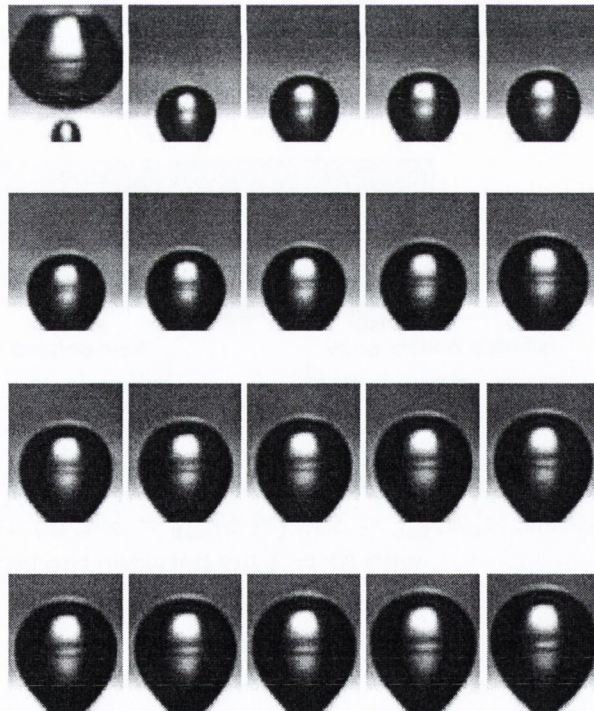


Figure 4.41: Evolution of a bubble in subcooled boiling with $\Delta T_{sub} = 8$ K for heat flux, $q'' = 36$ kW/m$^2$ with $\Delta t = 20$ ms between the images
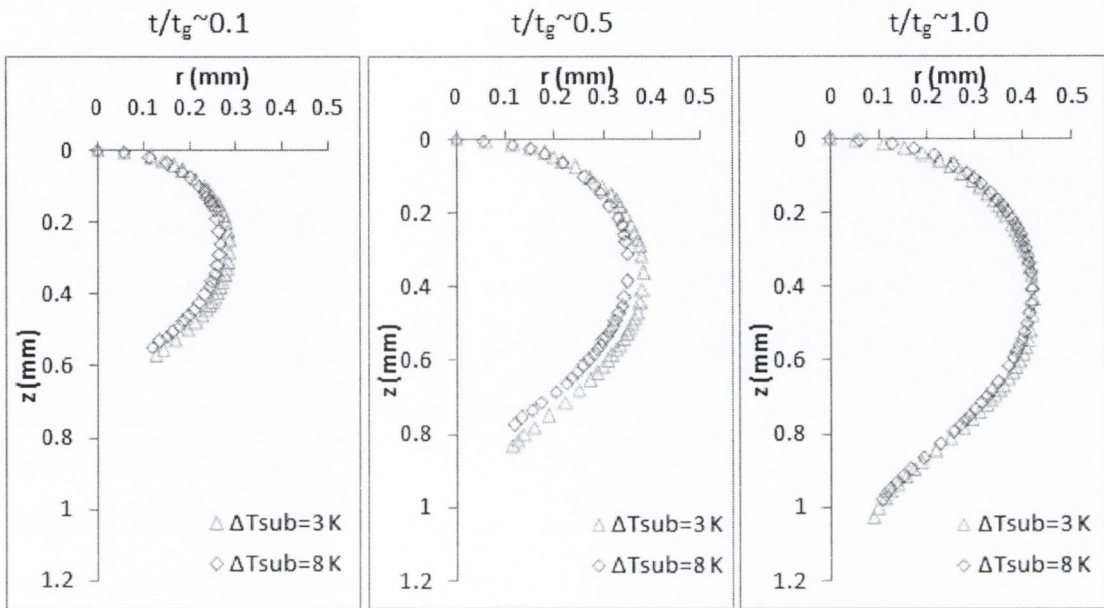
Figure 4.42: Evolution of bubble shape for $\Delta T_{sub} = 3$ K and $\Delta T_{sub} = 8$ K
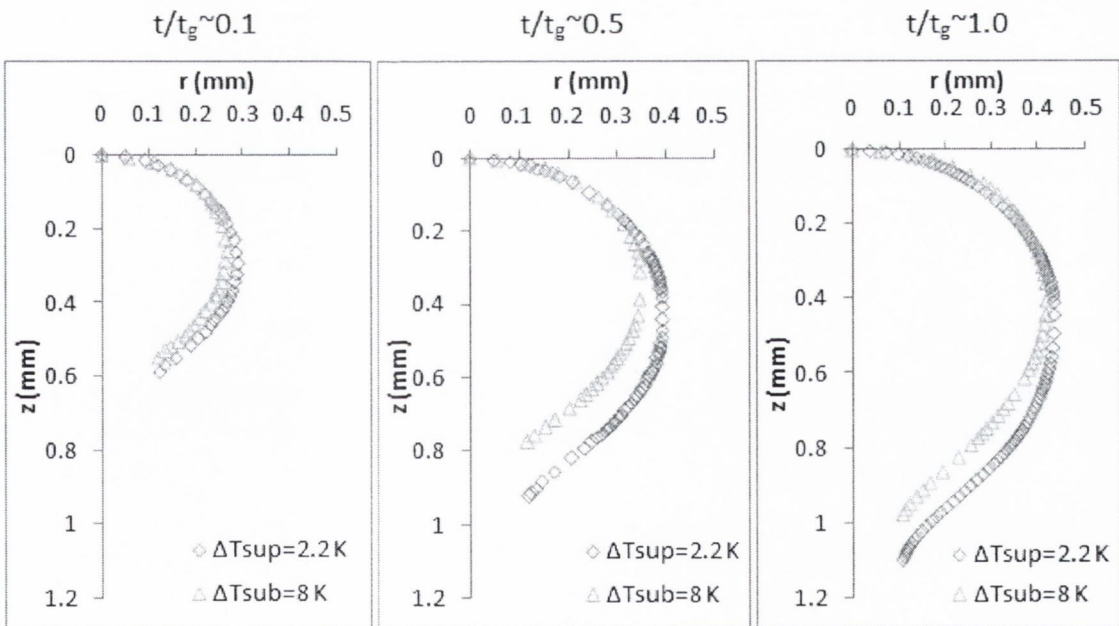


Figure 4.43: Comparative evolution of bubble shape for subcooled boiling ($\Delta T_{sub} = 8$ K) and saturated boiling ($\Delta T_w = 2.2$ K)

Bubble departure frequency for various levels of subcooling is shown in Figure 4.44. Since no notable waiting time has been observed for the subcooling range tested, the departure frequency is only considered as the inverse of growth time of the bubble ($f = 1/t_g$). In the figure, it shows that the bubble departure frequency is relatively high for low subcooling ($\Delta T_{sub}$=3 K) and decreases sharply as the subcooling increased. At low subcooling ($\Delta T_{sub}$=3 K), the bubble departure frequency is approximately $f_d \approx 10.3$ Hz whereas it decreases to $f_d \approx 0.38$ Hz in the case of high subcooling ($\Delta T_{sub}$=10 K).This trend is consistent with Zhao and Tsuruta (2002) but contrary to the study of Demiray and Kim (2004). As discussed earlier, bubble nucleation and growth rates are completely dependent on transferring the energy from the thermal boundary layer to the bubble. As there is less energy in the boundary layer for subcooled conditions, the growth rates of the bubble are affected. Since the temperatures of the liquid vary with the subcooling level, the growth rates may also be affected by the surface tension variations with temperature.
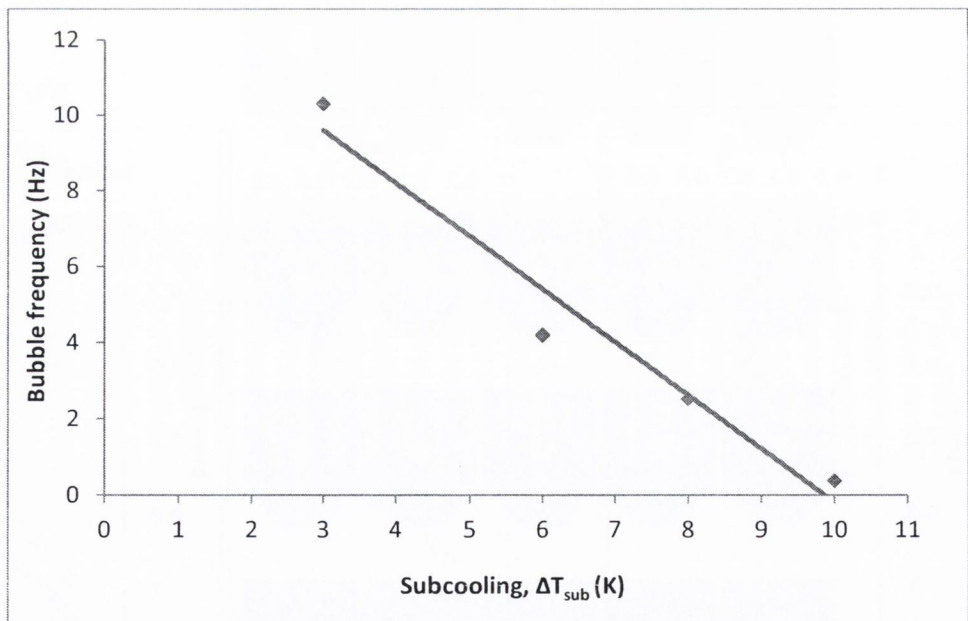


Figure 4.44: Bubble departure frequency for various subcooling levels

### 4.9.2 Volumetric growth and interface heat transfer

Bubble volumetric growth curves at various subcooling levels are plotted in Figure 4.45. In the figure, the mean volume of the bubble at departure for all ranges of subcooling tested is 0.32 mm$^3$ with a variation of $\pm 5$ % from the mean. This bubble size is about $\approx$ 29% smaller compared to the mean volume of bubbles at departure ($V_{d,mean} \approx 0.45$mm$^3$) for the case of saturated boiling (see Figure 4.17). It is believed that the smaller size of the bubbles with subcooling is due to the growing bubble experiencing condensation at its top. Similar results were found in the experiment by Demiray and Kim (2004).

Generally, the bubble growth times are found to increase with increasing subcooling (Figure 4.45) and the increase of the bubble growth time between the mid subcooling and high subcooling cases is quite large. Such a result is in contrastto observations of Ibrahim and Judd (1985) in which the bubble growth time decreases with increasing subcooling. The present experimental result can be explained as follows: the higher subcooling will cause less energy to be stored in the superheated layer. Thus, a bubble growing in highly subcooled bulk liquid has to grow over a longer period of time because of the time required to restore the depleting energy to sustain growth until the bubble size is sufficient for bouyancy (proportional to bubble size) to overcome the adhesive force (surface tension) to enable departure.

In Figure 4.45, the bubble growth curves show notable differences between the three levels of subcooling, i.e., low, mid and high subcooling. For the low subcooling ($\Delta T_{sub}$=3 K), there is a more continuous growth curve, closer to what was observed for the saturated case. For the mid-subcooling cases ($\Delta T_{sub}$=6 K and 8 K), the growth curves begin in the same manner as the others, but then an abrupt change in the growth curve is observed. This initial inflection in the growth curve is due to the superheat being depleted over a portion of the bubble and condensation commencing. From this point onward, bubble growth is governed by the competing influences of evaporation and condensation which makes the growth curve quite

different compared with the saturated cases. This trend is also true for the $\Delta T_{sub}$=10 K case except that it oscillates. The bubble oscillation is probably driven by heat transfer in which the growing and collapsing of the bubble is related to the positive and negative net mass/heat fluxes. Demiray and Kim (2004) also observed bubbles to shrink numerous times before lift-off at high subcooling. The shrinking bubble is due to high condensation occuring over the bubble cap as it grows beyond the superheated layer into the highly subcooled bulk liquid.
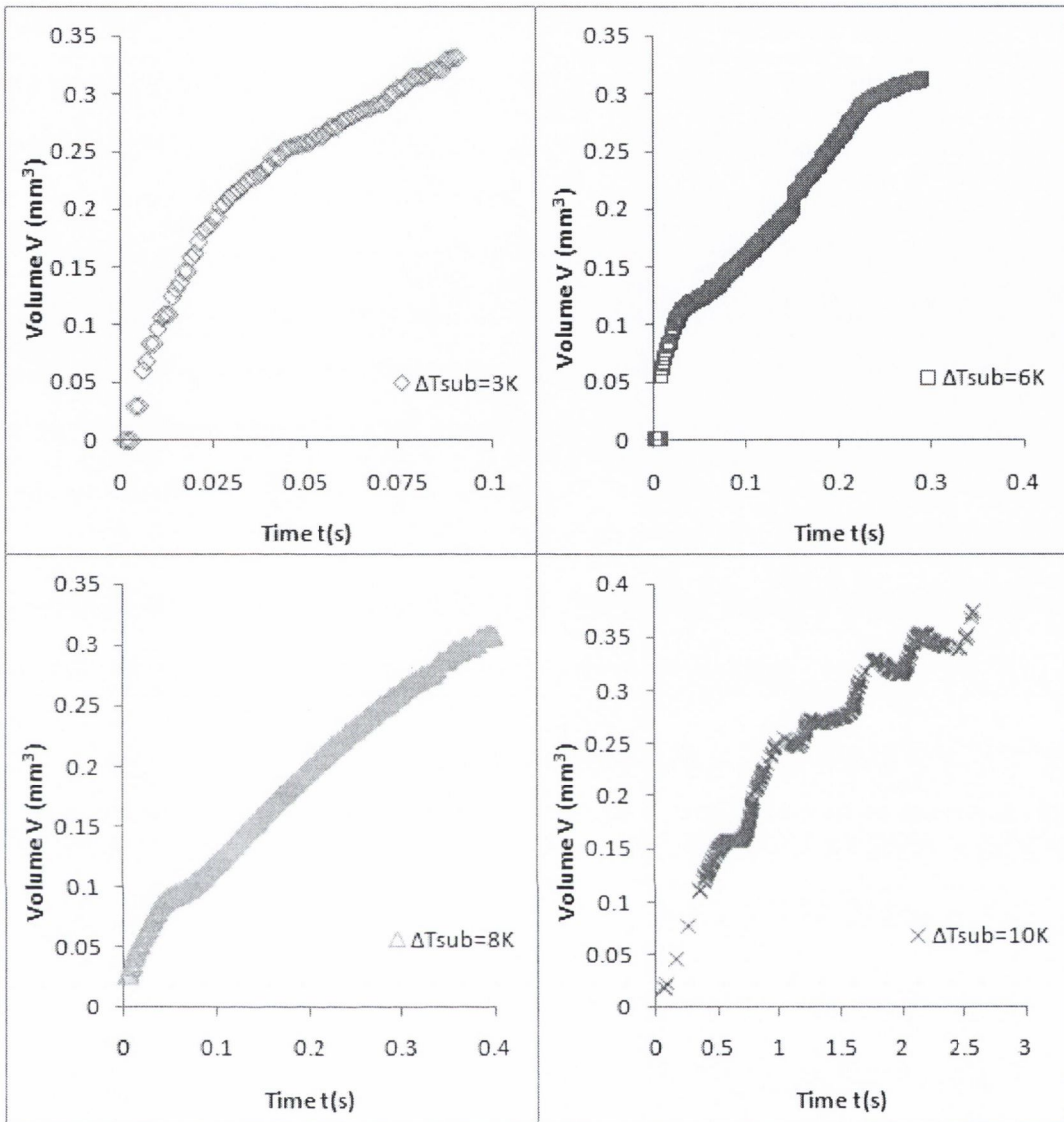
Figure 4.45: Bubble volumetric growths for various subcooling levels

Above, it has been stated that bubble growth is governed by the heat transfer at the vapour-liquid interface and the heat transfer governs the mass flow rate of vapour into the bubble, i.e., *dV/dt*. Figure 4.46 shows the rates of dimensional bubble volumetric growth rate (dV/dt) for the case of $\Delta T_{sub}$=3 K and $\Delta T_{sub}$=8 K. As mentioned previously, the $\Delta T_{sub}$=3 K is regarded as a condition near saturation and as such should be less influenced by condensation. The $\Delta T_{sub}$=8 K case, however, is expected to be strongly influenced by condensation. Therefore, the heat transfer at

the bubble interface must be significantly different between these two cases, and this is depicted in Figure 4.46. For the case of $\Delta T_{sub}$=3 K, dV/dt begins relatively high. Here the lower subcooling and the higher wall superheat (Table 2) result in a thicker thermal boundary layer and a higher superheat to drive vaporization. As the energy stored in the macrolayer is depleted the growth rate drops and plateaus somewhat before departure. The small hook feature near departure is due to the sensitivity of the first derivative on curve fitting function and not likely physical. For the case of $\Delta T_{sub}$=8 K in which the growth time is longer, *dV/dt* begins notably lower. Here the wall temperature and associated superheat (Table 2) is lower so that a smaller driving potential for heat transfer exists resulting in a lower growth rate. Once again the growth rate decreases as the energy stored in the macrolayer is depleted and the growth rate plateaus. The lower driving potential together with the fact that significant condensation is occurring over the bubble cap results in a much lower growth rate compared with the low subcooling case. Since the bubble must reach a critical size for it to depart, this growth rate is sustained over a considerable time period compared with the low subcooling case. It can be summarized that the growth rate curves will be different depending on the heat transfer conditions, in particular the levels of condensation.

For the comparative analysis of the net heat transfer at the bubble interface between the subcooled boiling and saturated boiling cases, the rate of non-dimensional bubble volume change (*dV\*/dt\**) for the case of $\Delta T_{sub}$=3 K and $\Delta T_{sub}$=8 K is presented in Figure 4.47. As discussed previously in Section 4.5 for the case of saturated boiling, bubble growth complies well with the growth laws $V^* = 2.5 \times t^*$ for early growth and $V^* = t^{*0.6}$ for late growth. For low subcooling ($\Delta T_{sub}$=3 K), the trend of *dV\*/dt\** is close to following the saturated growth laws, i.e., starts at ~2.5 and drops more or less asymptotically to close to the $0.6/t^{*0.4}$ curve (probably a bit lower due to some condensation). Again the upward sloping hook feature is due to the sensitivity of *dV/dt* on the curve fit and not likely realistic. However when the subcooling is larger, as is the case for $\Delta T_{sub}$=8 K, the *dV\*/dt\** trend does not

asymptotically approach the two growth laws. It drops at a considerable rate initially as the energy in the superheated layer is quickly depleted. The magnitude of $dV^*/dt^*$ is then notably below the other curves which must be due to relatively high rates of condensation occurring. Subsequent to a small recovery, possibly due to fluid motions partially re-establishing the macrolayer, there is a continual decline in $dV^*/dt^*$ opposed to an asymptotic plateau. Thus, condensation is becoming continually more important as the bubble approaches departure.
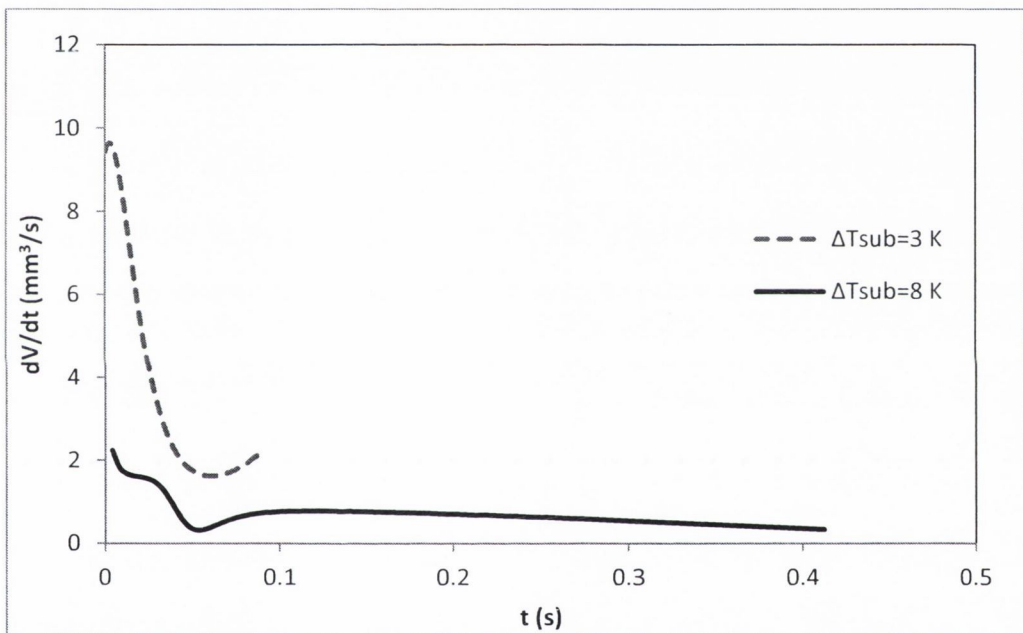


Figure 4.46: Rate of dimensional bubble volume change
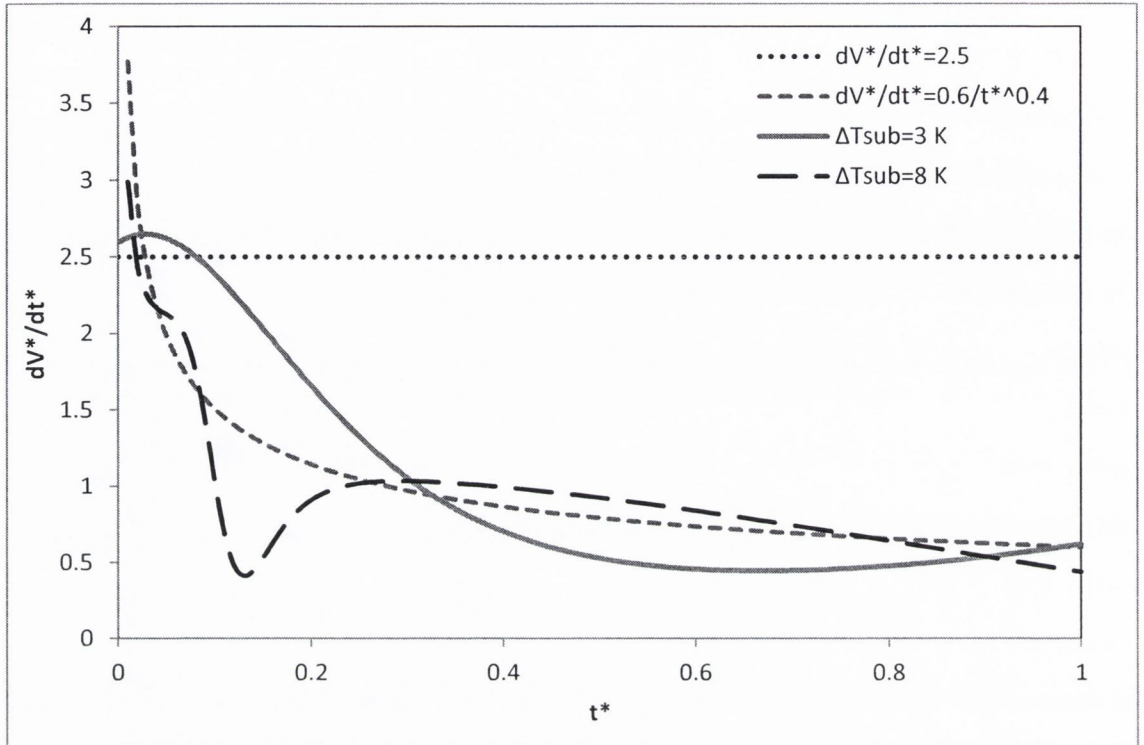
Figure 4.47: Rate of non dimensional bubble volume change

### 4.9.3 Contact angle development

As described in Section 4.8.1, the measurement of contact angles in the case of saturated boiling is not accurate due to mirage effects at the bubble foot. Thus, the contact angles in the case of subcooled boiling are determined by the same technique which was used in the case of saturated boiling (Section 4.8.1) since these are all quasi static bubbles. Figure 4.48 shows the comparison of corrected contact angle histories for various subcooling levels and saturated boiling. First, the corrected contact angles for all levels of subcooling tested are reasonably close to one another, indicating that the contact angle can be described independently from subcooling levels. Secondly, the histories of the contact angle for subcooled boiling show a fairly similar trend to that of the saturated boiling case for $t^* < 0.1$. However for the later stage ($t^* > 0.1$)

until departure it is found that the bubble in saturated boiling has a larger contact angle compared to the subcooled boiling indicating that the bubble in saturated boiling is more elongated. At the near departure stage, the percentage difference of contact angle for subcooled boiling and saturated boiling is about ~30%. According to Son et al. (1999), the increase in contact angle led to the departing bubbles being larger, consistent with the present data of subcooled boiling and saturated boiling.
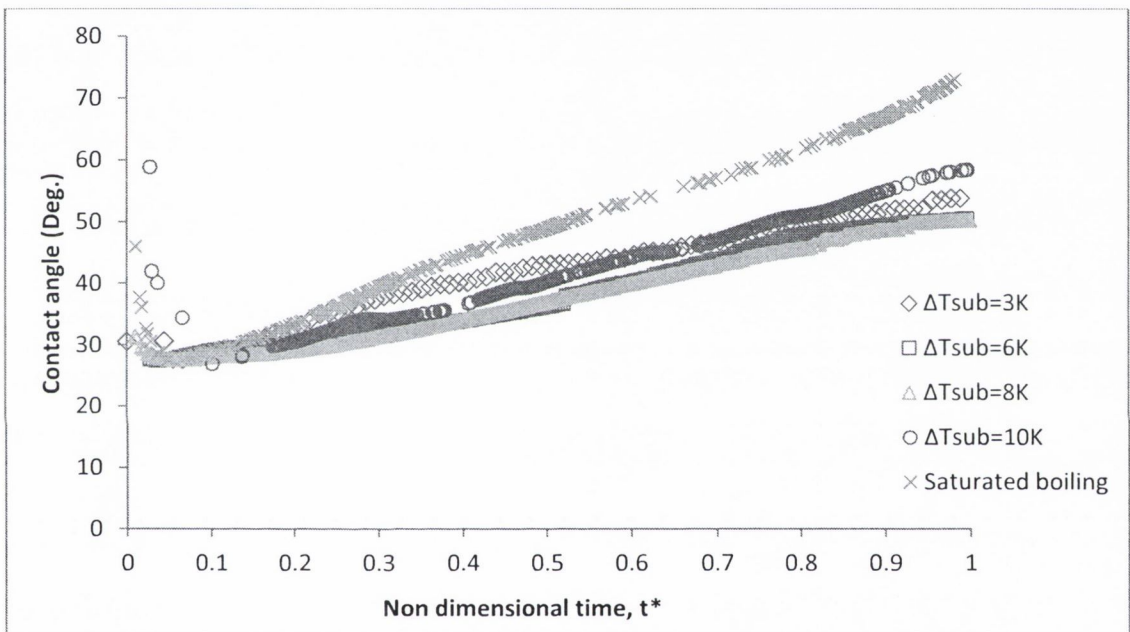


Figure 4.48: Comparison of contact angle (corrected) histories of subcooled boiling and saturated boiling

### 4.9.4  Forces acting on a growing bubble

Figure 4.49 and Figure 4.50 present the vertical forces acting on a growing bubble in subcooled boiling for $\Delta T_{sub} = 3$ K and $\Delta T_{sub} = 8$ K cases respectively. From the figures, it clearly shows that the upwardly directed force, i.e., buoyancy force, $F_{bouy,1}$ acting on the growing bubble can be considered as almost independent of the level of subcooling, which is expected for the quasi static bubbles with approximately the same shape. The buoyancy force increases steadily with the growth of the bubble since it is proportional to the bubble volume. The magnitude of this buoyancy force acting on the bubble at departure is approximately 4.2 µN. This magnitude is about $\sim$27% smaller than the magnitude of buoyancy force in the case of saturated boiling which has been presented in Section 4.8.2. This is expected due to the difference in bubble sizes between the two cases, as previously discussed in Section 4.9.2.

Another upwardly directed force is the so-called contact pressure force, $F_{bouy,3}$ which is largest at the beginning of the growth period since the bubble curvature is largest when the bubble is small. This force decreases sharply as the bubble expands, decreasing its curvature, up to $t^* \approx 0.1$ after which it decreased gradually until the bubble departs ($F_{bouy,3} \approx 1.48$ µN at departure). The magnitude of this force at departure is about $\sim$11% larger compared to the magnitude for the case of saturated boiling (Section 4.8.2). The only downwardly directed force is that of surface tension. This force decreases in magnitude as the contact angle initially decreases, reaches its lowest magnitude and subsequently begins to increase in magnitude as the contact angle increases. It reaches a value of $F_\sigma \approx$-5.4 µN at departure. This magnitude is approximately $\sim$19% smaller compared to the magnitude in the case of saturated boiling which is expected due to the difference of contact angles between these two cases as presented in the previous section.
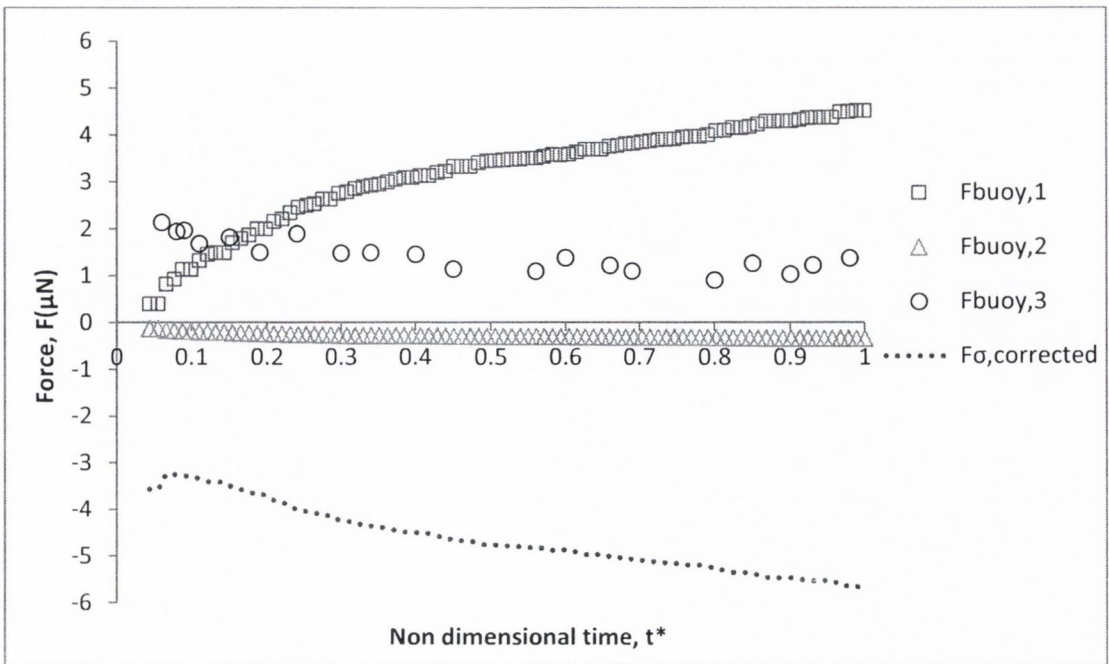
Figure 4.49: Vertical forces acting on a growing bubble in subcooled boiling for low subcooling ($\Delta T_{sub}$=3 K)
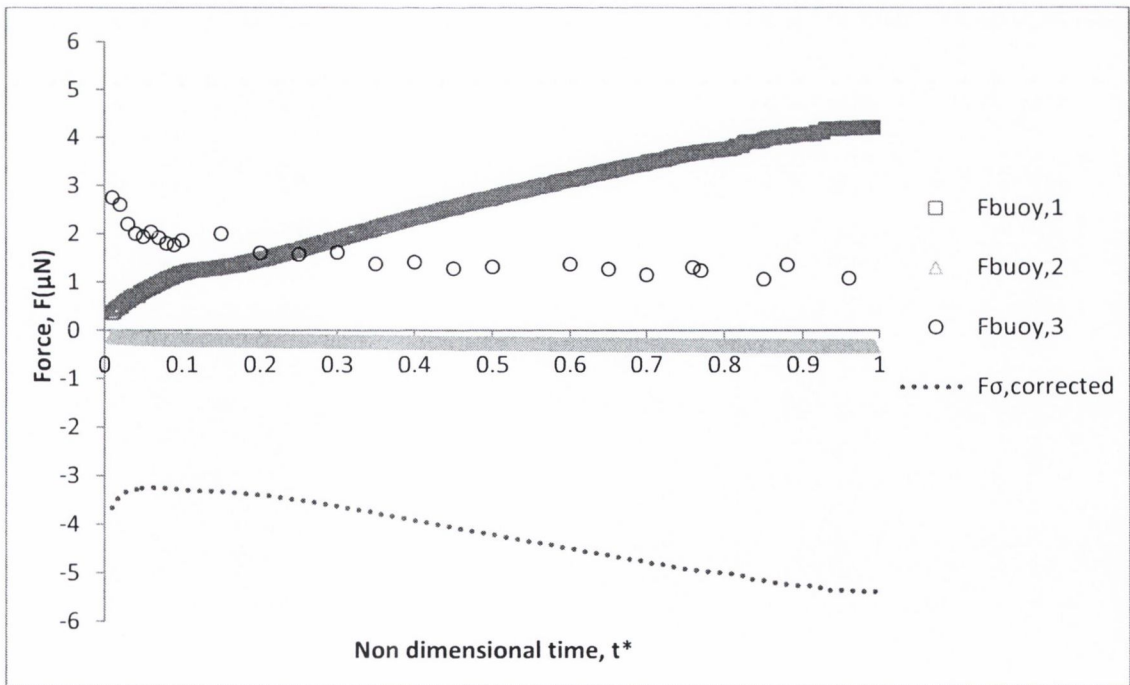


Figure 4.50: Vertical forces acting on a growing bubble in subcooled boiling for high subcooling ($\Delta T_{sub}$=8 K)

# CHAPTER 5

## CONCLUSION

Single isolated bubble growth dynamics from an artificial nucleation site in pool boiling has been investigated experimentally. An experimental facility has been developed to perform the study. The experiments have been conducted at atmospheric pressure with the environmentally friendly refrigerant HFE-7000 used as the working fluid. A high speed video camera with a combination of a powerful lens and a tube extension has been used to capture the bubble images during boiling. Image processing in Matlab has been used to process the images and determine relevant parameters which characterize growth and departure.

In the analysis of the bubble growth dynamics, it was found that the bubble waiting and growth times decrease as the wall superheat is increased resulting in a significant increase in the bubble frequency. However, bubble growth was determined to be quasi-static such that the bubble size at departure was independent of superheat resulting in an independence of bubble departure size with frequency, which contradicts early theories. The bubble growth curves are found to collapse very well onto a single curve which is independent of wall superheat and to comply with the empirical growth laws;

$$V^* = \begin{cases} 2.5 \times t^* & \text{for } t^* < 0.1 \\ t^{*0.6} & \text{for } t^* > 0.1 \end{cases}$$

The rapid volumetric growth ($V^*=2.5t^*$) at the initial stage ($t^*<0.1$) is due to the high level of sensible energy in the superheated thermal boundary layer causing a rapid volumetric growth rate. During this stage the volume growth is sustained when

there is abundant energy at a high superheat in the superheated layer. At the later stage ($t^*>0.1$), energy in the superheated liquid layer has largely been depleted causing a slower volumetric growth rate. During this stage, the volumetric growth decreases with time, indicating that even though the surface area is increasing, it is no longer increasing at a rate that can compensate for the decreasing rate of heat transfer. The empirical growth laws of the present study are notably different from the classical growth laws in analytical studies, including Plesset and Zwick (1954), Forster and Zuber (1954), Scriven (1959) and Cooper and Lloyd (1969) since these studies idealize the geometry and thermal fields.

From the analysis of the bubble aspect ratio, it is found that the bubbles for the case of high wall superheats, i.e., $\Delta T_w$=9.1 K and 11.8 K are seen to experience oscillations for the growth interval $0.05 < t^* \leq 1$. The oscillations of the bubble shape are due to the interaction of the growing bubble with the previous bubble since the waiting time decreases and growth rates increase with wall superheat and as a result less time is available for the previous bubble to rise before nucleation of the next bubble.

The measurement of the contact angle is considered to have a non-negligible error, and is likely over-estimated due to the mirage effect. The measured contact angles were corrected by calculating the value which would satisfy the vertical force balance. Since these are all quasi static bubbles, the method gives the same contact angle history for each superheat tested.

Analysis of vertical forces i.e. buoyancy, contact pressure and surface tension forces acting on a growing bubble can be considered as independent of the wall superheat, which is expected for quasi static bubbles with approximately the same shape. The buoyancy force increases steadily with the growth of the bubble since it is proportional to the bubble volume, with the magnitude at departure of approximately 5.8 μN. The contact pressure force begins high since the bubble curvature is high when the bubble is small and it decreases sharply as the bubble expands rapidly up to

$t^* \approx 0.1$. After that, it decreases gradually until the bubble departs ($F_{bouy,3} \approx 1.33$ μN at departure). For the surface tension force, it decreases in magnitude as the contact angle initially decreases, reaches a minimum and subsequently begins to increase in magnitude as the contact angle increases. It reaches a value of $F_\sigma \approx -6.7$ μN at departure. The liquid inertia force, $F_{li}$ appears significant at high wall superheats, i.e., $\Delta T_w = 9.1$ K with an undulating profile. This is believed to be due to force interactions with the wake and body of the previously departed bubble. It is concluded that the appearance of bubble shape oscillations indicates the transition from isolated bubble to bubble column growth regimes.

### *Effects of Liquid Subcooling*

In the subcooled boiling experiments the shapes of the bubbles are similar to the saturated boiling for the early growth stage $t^* \leq 0.1$. At the later stage ($t^* > 0.1$), the bubble for the case of subcooled boiling is less elongated compared to the case of saturated boiling. It is not immediately clear as to the precise mechanism for this shape change but it can be due to a net downward force, possibly by the fluid moving downward as a result of higher density difference, or due to surface tension variations with temperature. For the latter, the temperature coefficient of surface tension is not known so additional work is required to test this hypothesis.

The bubble departure frequency is relatively high for low subcooling ($\Delta T_{sub} = 3$ K) and decreases sharply as the subcooling is increased. This trend is consistent with Zhao and Tsuruta (2002) but contrary to the study of Demiray and Kim (2004). The lower energy in the boundary layer for subcooled conditions and the surface tension variations with temperature affect the growth rates of the bubble. The bubble size is about $\approx 29\%$ smaller compared to volume of bubble at departure for the case of saturated boiling which is due to the growing bubbles experiencing condensation at the bubble cap, possibly coupled with surface tension effects. The bubble growth times are found to increase with increasing subcooling and the increase of the bubble growth time between the mid subcooling and high subcooling cases is quite large. This

is because a bubble growing in highly subcooled bulk liquid has to grow over a longer period of time because of the lower amount of energy stored in the boundary layer combined with condensation occuring, meaning that more time is required for the bubble to grow to a size where it is sufficient for bouyancy to overcome the adhesive force enabling departure.

The bubble growth curves show notable differences between the three levels of subcooling, where there is an abrupt inflection for the higher subcooling levels not observed for the low subcooling and saturated cases. This trend is also true for the $\Delta T_{sub}$=10 K case, except that the bubble oscillates. The inflection is due to condensation changing the bubble growth dynamics as shown by comparing the bubble volumetric growth rate curves. Here the effects of subcooling and associated condensation altered the heat and mass transfer over the entire lifetime of the bubbles investigated.

Finally, evaluation of the contact angle history and associated forces showed an independence from subcooling levels. However, the size and shape of the bubbles with subcooling were notably different than those of saturated boiling. Although the results are preliminary, there is evidence to suggest that subcooling reduces the size of the bubbles and thus the magnitudes of the vertical forces acting upon them.

***Future works***

The research work carried out here is considered to be one of the few/early studies that investigate the dynamics of a single bubble growth in nucleate pool boiling by using modern technologies, i.e., high speed video camera with high magnification lens and powerful computer programming of image processing in Matlab. With current techniques and technologies, there are more studies that could be done in the future in order to lead towards a complete understanding of the fundamental physics of bubble dynamics, flow and heat transfer at small time and length scales. Some recommendations for the future works are as follows;

- By using the present experimental techniques, the analysis of bubble growth without the existence of microlayer (bubble pinned at the cavity mouth) could be extended to the bubble growth with microlayer evaporation which has significant influence on heat transfer in nucleate boiling.

- The present experiment of single bubble growth in subcooled boiling only considered relatively low subcooling levels. Further work could be extended to higher levels of subcooling in order to gain more comprehensive understanding of the influence of liquid subcooling on bubble growth.

- The present bubble images and research findings, including the heat transfer rate into the bubble and the criterion of bubble departure, could provide significant information to the development of bubble growth modelling in nucleate pool boiling.

- The measurement and analysis technique developed could be extended to investigating bubble dynamics on natural surfaces, where bubbles grow and depart from naturally occurring nucleation sites.

# REFERENCES

3M. 2014. *3M™ Novec™ Engineered Fluid 7000 Data Sheet* [Online]. Available: www.3M.com 2014].

ADELBERG, M. 1963. Gravitational effect upon nucleate boiling heat transfer. *Advances in the Astronautical Sciences,* 14, 196-223.

BODE, A. 2008. Single bubble dynamics and transient pressure during subcooled nucleate pool boiling. *Int. J. Heat Mass Transfer,* 51, 353-360.

CAREY, V. P. 2008. *Liquid-vapor phase-change phenomena,* New York, Taylor & Francis.

CHEN, W., MEI, R. & KLAUSNER, J. 1996. Vapour bubble growth in highly subcooled heterogeneous boiling. *Convective Flow Boiling.* Washington, DC: Taylor & Francis.

CHESTERS, A. 1977. Analytical solution for the profile and volume of a small drop or bubble symmetrical about a vertical axis. *Journal of Fluid Mechanics* 81, 609-624.

CLARK, J. A. & MERTE, H. 1963. Nucleate, transition and film boiling heat transfer at zero gravity. *Advances in the Astronautical Sciences,* 14, 177-196.

COLE, R. 1967. Bubble frequencies and departure volumes at subatmospheric pressures. *AIChE Journal,* 13, 779-783.

COLE, R. & SHULMAN, H. L. 1966. Bubble growth rates at high Jakob numbers. *Int. J. Heat Mass Transfer,* 9, 1377-1390.

COOPER, M. G. 1983. The 'mirage' in boiling. *Int. J. Heat Mass Transfer,* 26, 1088-1090.

COOPER, M. G. & LLOYD, A. J. P. 1969. The microlayer in nucleate pol boiling. *Int. J. Heat Mass Transfer,* 12, 895-913.

DEMIRAY, F. & KIM, J. 2004. Microscale heat transfer measurements during pool boiling of FC-72: effect of subcooling. *Int. J. Heat Mass Transfer,* 47, 3257-3268.

DI BARI, S. & ROBINSON, A. J. 2013. Experimental study of gas injected bubble growth from submerged orifices. *Experimental Thermal and Fluid Science,* 44, 124-137.

FAGHRI, A. & ZHANG, Y. 2006. *Transport phenomena in multiphase systems,* Elsevier.

FORSTER, H. K. & ZUBER, N. 1954. Growth of a vapor bubble in a superheated liquid. *J. Applied Physics,* 25, 474-478.

FRITZ, W. 1935. Maximum volume of vapour bubbles. *Phys Z.,* 36, 379-384.

HAN, C.-Y. & GRIFFITH, P. 1962. The mechanism of heat transfer in nucleate pool boiling. *Technical Report 19, Massachusetts Institute of Technology.*

HAN, C.-Y. & GRIFFITH, P. 1965. The mechanism of heat transfer in nucleate pool boiling-part I bubble initiation, growth and departure. *Int. J. Heat Mass Transfer,* 8, 887-904.

HSU, Y. 1962. On the size range of active nucleation cavities on a heated surface. *Journal of Heat Transfer,* 84, 207-216.

HSU, Y. & GRAHAM, R. W. 1986. Transport processes in boiling and two-phase systems, including near-critical fluids.

IBRAHIM, E. A. & JUDD, R. L. 1985. An experimental investigation of the effect of subcooling on bubble growth and waiting time in nucleate boiling. *Journal of Heat Transfer,* 107, 168-174.

JUDD, R. L. 1999. The role of bubble waiting time in steady nucleate boiling. *Journal of Heat Transfer,* 121, 852-855.

JUDD, R. L., MERTE, H. & ULUCAKLI, M. E. 1991. Variation of superheat with subcooling in nucleate pool boiling. *Journal of Heat Transfer,* 113, 201-208.

KANG, S., BARTSCH, G., JIA, D. & CHEN, X.-J. 1993. Investigation of bubble dynamics in pool boiling: Part I - A synthesis model for bubble growth in terms of liquid subcooling and surface conditions. *Presented at the National Heat Transfer Conference Atlanta, Georgia.*

KESHOCK, E. G. & SIEGEL, R. 1964. Forces acting on bubbles in nucleate boiling under normal and reduced gravity conditions. *NASA Tech. Note,* TN D-2299.

KIM, J. & KIM, M. H. 2006. On the departure behaviors of bubble at nucleate pool boiling. *Int. J. of Multiphase Flow,* 32, 1269-1286.

KIPER, A. M. 1971. Minimum bubble departure diameter in nucleate pool boiling. *Int. J. Heat Mass Transfer,* 14, 931-937.

KLAUSNER, J., MEI, R., BERNHARD, D. & ZENG, L. 1993. Vapor bubble departure in forced convection boiling. *Int. J. Heat Mass Transfer,* 36, 651-662.

KOBUS, C. J. & WEDEKIND, G. L. 2001. An experimental investigation into natural convection heat transfer from horizontal isothermal circular disks. *Int. J. Heat Mass Transfer,* 44, 3381-3384.

LEE, H. C., OH, B. D., BAE, S. W. & KIM, M. H. 2003. Single bubble growth in saturated pool boiling on a constant wall temperature surface. *Int. J. of Multiphase Flow,* 29, 1857-1874.

LEGENDRE, D., COLIN, C. & COQUARD, T. 2008. Lift, drag and added mass of a hemispherical bubble sliding and growing on a wall in a viscous linear shear flow. *Philos. Trans. R. Soc. London,* 366, 2233-2248.

LESAGE, F. J., COTTON, J. S. & ROBINSON, A. J. 2013. Analysis of quasi-static vapour bubble shape during growth and departure. *Physics of Fluids,* 25, 067103-1-21.

LIEN, Y. & GRIFFITH, P. 1969. Bubble growth in reduced pressure. *Ph.D. Thesis, Massachusetts Institute of Technology, Cambridge.*

MAGNAUDET, J., RIVERO, M. & FABRE, J. 1995. Accelerated flows past a rigid sphere or a spherical bubble. I. Steady straining flow. *Journal of Fluid Mechanics,* 284, 97-135.

MCFADDEN, P. W. & GRASSMANN, P. 1962. The relation between bubble frequency and diameter during nucleate pool boiling. *Int. J. Heat Mass Transfer,* 5, 169-173.

MEI, R., CHEN, W. & KLAUSNER, J. F. 1995. Vapor bubble growth in heterogeneous boiling. Part I: Formulation. *Int. J. Heat Mass Transfer,* 38, 909-919.

MIKIC, B. B. & ROHSENOW, W. M. 1969. Bubble growth rates in non-uniform temperature field. *Progress in Heat and Mass Transfer,* 2, 283-293.

MIKIC, B. B., ROHSENOW, W. M. & GRIFFITH, P. 1970. On bubble growth rates. *Int. J. Heat Mass Transfer,* 13, 657-666.

NIEMELA, J. J., SKRBEK, L., SREENIVASAN, K. R. & DONNELLY, R. J. 2000. Turbulent convection at very high Rayleigh numbers. *Macmillan Magazines Ltd,* 404.

NUKIYAMA, S. 1934. Maximum and minimum values of the heat q transmitted from metal to boiling water under atmospheric pressure. *J. Soc. Mech. Eng. Jpn,* 37, 367-374.

PLESSET, M. S. & ZWICK, S. A. 1954. The growth of vapor bubbles in superheated liquids. *Journal Applied Physics,* 25, 493-500.

PROSPERETTI, A. & PLESSET, M. S. 1978. Vapour bubble growth in a superheated liquid. *Journal Fluid Mechanics,* 85, 349-368.

RAYLEIGH, L. 1917. Pressure due to collapse of bubbles. *Phil. Mag.,* 94.

ROBINSON, A. J. 2002. Bubble growth dynamics in boiling. *Ph.D Thesis, McMaster University.*

ROBINSON, A. J. & JUDD, R. L. 2004. The dynamics of spherical bubble growth. *Int. J. Heat Mass Transfer,* 47, 5101-5113.

ROHSENOW, W. M. 1951. A method of correlating heat transfer data for surface boiling of liquids. *Tech. Report (Massachusetts Institute of Technology, Heat Transfer Laboratory),* No. 5.

SCRIVEN, L. E. 1959. On the dynamics of phase growth. *Chemical Engineering Science,* 50, 3907-3917.

SIEDEL, S. 2012. *Bubble dynamics and boiling heat transfer: a study in the absence and in the presence of electric fields.* Ph.D, Universite de Lyon.

SIEDEL, S., CIOULACHTJIAN, S. & BONJOUR, J. 2008. Experimental analysis of bubble growth, departure and interactions during pool boiling on artificial nucleation sites. *Exp. Thermal and Fluid Science,* 32, 1504-1511.

SIEDEL, S., CIOULACHTJIAN, S., DI BARI, S., ROBINSON, A. J. & BONJOUR, J. 2014. Analysis of the interface curvature evolution during bubble growth. *Heat Transfer Engineering,* 35, 528-536.

SIEDEL, S., CIOULACHTJIAN, S., ROBINSON, A. J. & BONJOUR, J. 2013. Integral momentum balance on a growing bubble. *Physics of Fluids,* 25.

SON, G., DHIR, V. K. & RAMANUJAPU, N. 1999. Dynamics and heat transfer associated with a single bubble during nucleate boiling on a horizontal surface. *Journal of Heat Transfer,* 121, 623-631.

STEPHAN, K. & ABDELSALAM, M. 1980. Heat transfer correlations for natural convection boiling. *Int. J. Heat Mass Transfer,* 23, 73-87.

STRALEN, S. J. D. V., SOHA, M. S., COLE, R. & SLUYTER, W. M. 1975. Bubble growth rates in pure and binary systems, combined effect of relaxation and evaporation microlayers. *Int. J. Heat Mass Transfer,* 18, 453-467.

TATE, T. 1864. On the magnitude of a drop of liquid formed under different circumstances. *Philosophical Magazine,* 27, 176-185.

YANG, C., WU, Y., YUAN, X. & MA, C. 2000. Study on bubble dynamics for pool nucleate boiling. *Int. J. Heat Mass Transfer,* 43, 203-208.

ZENG, L. Z., KLAUSNER, J. F. & MEI, R. 1993. A unified model for the prediction of bubble detachment diameters in boiling systems-I. Pool boiling. *Int. J. Heat Mass Transfer,* 36, 2261-2270.

ZHAO, Y. & TSURUTA, T. 2002. Prediction of bubble behavior in subcooled pool boiling based on microlayer model. *JSME International Journal,* 45, 346-354.

ZUBER, N. 1959. *Report-Nr. AECU-4439,* AEC Technical Information Service Extention.

ZUBER, N. 1961. The dynamics of vapor bubbles in nonuniform temperature fields. *Int. J. Heat Mass Transfer,* 2, 83-98.

# APPENDIX A

## Image Processing Code

```
%%%%%%%%%%%%%%%%%%%%%%%%%%%%%%%%%%%%%%%%%%%%%%%%%%%%%%%%%%%%%%%%%%%%%%%%

                        Image processing

%%%%%%%%%%%%%%%%%%%%%%%%%%%%%%%%%%%%%%%%%%%%%%%%%%%%%%%%%%%%%%%%%%%%%%%%


Clear all

%%% Parameters  %%% These are the parameters to set %%%%%%%%%%%

FirstImage = 1; % Index of the first image to be processed

Step = 1; % Step between two images to process

LastImage = 58; % Index of the last image to be processed

fileFolder = fullfile('C:','Users','Muhad','Copy','Sat. Boiling
5-2-14','009-11.81','b5'); % Location of the images on the hard
drive

pattern = 'im*.jpg'; % Pattern of the image files if applicable

Csize = 1.5; % Characteristic length (calibrated distance) in
[mm]

Cpix = 273; % Number of pixels of the characteristic length

frequency = 1000; % Image frequency [fps]

nomXls = strcat('essai21K-6','-',mat2str(FirstImage),'-
',mat2str(Step),'-',mat2str(LastImage),'.xls'); % Name of the
excel result file



%%%%%%%%%%%%%%%%%%%%%%%%%%%%%%%%%%%%%%%%%%%%%%%%%%%%%%%%%%%%%%%%%%%%%%%%


% file location

dirImages = dir(fullfile(fileFolder,pattern));

fileNames = {dirImages.name}';
```

145

```
numFrames = numel(fileNames);

dirProg = pwd; % Locating current folder

% In code parameters

pix = Csize/Cpix; % pixel size in [mm]

periode = 1/frequency; % time step in [s]

n=floor((LastImage+1-FirstImage)/Step); % number of images to
be processed

% Variables initialisation

compteur= zeros(n,1); % Index of the frame processed

cImage= zeros(n,1); % Number on the image file

nImage=cell(n,1); % Name of the image

volume = zeros(n,1); % Bubble volume

volumecp = zeros(n,1); % Contact pressure volume

volumeTps = zeros(n,1); % Time of the frame

cg=zeros(n,1); % Height of center of gravity

Req=zeros(n,1); % Equivalent radius

largeur=zeros(n,1); % Bubble width

hauteur=zeros(n,1); % Bubble height

%Contact_Angle=zeros(n,1);

c=0; % Counter of the images correctly processed

c2=0; % Counter of the images processed

c3=0;

forNumImage = FirstImage:Step:LastImage

    c2=c2+1;


%%%% Image treatment

cd(fileFolder); % Moves to images location
```

```matlab
ImageInit = imread(fileNames{NumImage}); % Reads the current
image

cd(dirProg); % Moves back to initial location

    I = ImageInit(:,:,1); % Takes only the red layer of the
color format image

mm=size(I,2); % Number of pixels in width

nn=size(I,1); % Number of pixels in height



    BW1 = edge(I,'sobel'); % Sobel method to detect the high
gradients of gray



%%%% Bubble base

x0 = fix(size(BW1,2)*0.5); % x-ordinate of the middle bottom of
the image

gp = 0; % Base left initialization

dp = 0; % Base right initialization

for j = x0:-1:3 % It looks for the last white pixel on the left
hand side of x0

if BW1(size(BW1,1),j)==1

gp = j; % Base left found!

end

end



for j = x0:1:size(BW1,2)-3 % It looks for the last white pixel
on the left hand side of x0

if BW1(size(BW1,1),j)==1

dp = j; % Base right found!

end

end
```

```
notgood = 0; % Initialization of the error parameter

%%% Test to check if both sides of bubble base are captured

ifdp==0 || dp==gp || gp==0

notgood = 1; % Error if either side of the base was not found

end

%%% Selection of bubble contour

ifnotgood==0

        BW2 = bwselect(BW1,gp,size(BW1,1),8); % The white
object including the left side of the base is selected


%%% Test to check if the whole bubble contour has been captured

if BW2(size(BW1,1),dp)==0

notgood=1; % Oups! The right side of the base is not part of
the selected object

end


%%% If there was no error, the image processing can go on

If notgood==0

            c=c+1; % The counter of the correctly processed
images is increased


%%% Storing the bubble contour coordinates

np = sum(sum(BW2)); % Number of points in the contour

coox=zeros(np,1); % x-ordinate initialization

cooy=zeros(np,1); % x-ordinate initialization


cp=0; % Counter for the loop

for i=1:size(BW2,1)
```

```matlab
for j=1:size(BW2,2)

if(BW2(i,j)==1)

cp = cp+1;

coox(cp)=j;

cooy(cp)=size(BW2,1)+1-i; % The y axis is reversed

end

end

end


% Computing bubble size

vol=zeros(n,1); % Used to measure the bubble volume

volcp=zeros(n,1); % Used to measure the bubble volume above the
nucleation site for contact pressure

wvol=zeros(n,1); % Weighted volume for the center of gravity
measurement

larg = 0; % Maximal width of the bubble

haut=0; % Initialisation of the indicator stating if the upper
line of bubble was found

for i = 1:nn % Scanning each line from the upper end of the
image

                g = find(BW2(i,:),1,'first'); % Find the first
left pixel of the bubble

                d = find(BW2(i,:),1,'last'); % Find the last
right pixel of the bubble

if(not(isempty(g))) % If some white pixels were found in this
line

if(haut==0)

haut=1; % Apex found!

hauteur(c) = (nn - i + 1)*pix; % The bubble height is stored

end
```

```matlab
vol(i) = (d-g)^2 * (pi/4)*pix^3; % The 1 pixel height cylinder
volume is added

wvol(i) = vol(i)*(nn-i+0.5)*pix;

volcp(i)= min((d-g)^2*(pi/4)*pix^3,pi*0.09^2*pix); % idem

if((d-g+1)>larg)

larg=(d-g+1);

end

end

end

volumeTps(c)=c2*periode*Step; % Time from first processed frame

volume(c)=sum(vol); % Bubble volume

volumecp(c)=sum(volcp); % Contact pressure volume

largeur(c)=larg*pix; % Bubble width

cg(c)=sum(wvol)/sum(vol); % Height of center of gravity

Req(c) = ((3*volume(c))/(4*pi))^(1/3); % Equivalent radius

compteur(c)=c2; % Index of image processed

cImage(c)=NumImage; % Number of the image file

nImage(c)=fileNames(NumImage); % Name of the image file


%%%% Added code adapted from Sergio's to catch the curvature

bound=zeros(np,2); % We want to create a matrix with the
coordinates of all points from the contour

        c3=0;

for i=1:mm

for j=1:nn

if(BW2(j,i)==1)

                    c3=c3+1;

bound(c3,1:2)=[nn+1-j i];
```

```
end

end

end

tang=zeros(n,1);

        bound(:,1)=1.1*max(bound(:,1))-bound(:,1);

%bound = bound*pix;

symm_bound = make_bubble_symmetric(bound);

symm_bound = sortrows(symm_bound);

symm_bound(:,1) = symm_bound(:,1)-symm_bound(1,1);

fa = 1;

fb = 0.3;

        bred7 = Sam_Smooth_bondaries_symm(symm_bound,fa,fb);

%iii=c; % Parameter used in sam_Finding_curvature

scale=pix; % Parameter used in sam_Finding_curvature

cstore =c;

%Finding_Curvature

sam_Finding_Curvature

Contact_Angle_Deg  =Find_the_contact_angle(bred7);

Contact_Angle = tang;

%Bubble3D

        c = cstore;


end

end

end


if(not(isempty(compteur)))
```

```matlab
% Taking only the non-zero part of each variable matrices

compteur= compteur(1:c); % Index of the frame processed

cImage= cImage(1:c); % Number on the image file

nImage=nImage(1:c); % Name of the image

volume = volume(1:c); % Bubble volume

volumecp = volumecp(1:c); % Contact pressure volume

volumeTps = volumeTps(1:c); % Time of the frame

cg=cg(1:c); % Height of center of gravity

Req=Req(1:c); % Equivalent radius

largeur=largeur(1:c); % Bubble width

hauteur=hauteur(1:c); % Bubble height

%Contact_Angle=Contact_Angle(:,1);

% Saving all data in an Excel file

classeur={};

warningoffMATLAB:xlswrite:AddSheet

nomFeuille = 'data';

classeur(1,1:14)={'count','numfile','namefile','time','volume',
'norm. time','norm. volume','heightCoG','eq.
radius','height','width','aspectratio','Contact pressure
volume','Contact angle'};

classeur(2,1:14)={' ',' ',' ','s','mm3',' ','
',' mm','mm','mm','mm',' ','mm3','degree'};

classeur((1:c)+2,1)=mat2cell(compteur,ones(1,c),1); %#ok<*MMTC>

classeur((1:c)+2,2)=mat2cell(cImage,ones(1,c),1);

classeur((1:c)+2,3)=nImage;

classeur((1:c)+2,4)=mat2cell(volumeTps,ones(1,c),1);

classeur((1:c)+2,5)=mat2cell(volume,ones(1,c),1);

classeur((1:c)+2,6)=mat2cell((volumeTps./((LastImage-FirstImage
+ 1)*periode)),ones(1,c),1);
```

```
classeur((1:c)+2,7)=mat2cell((volume./volume(end)),ones(1,c),1)
;
classeur((1:c)+2,8)=mat2cell(cg,ones(1,c),1);
classeur((1:c)+2,9)=mat2cell(Req,ones(1,c),1);
classeur((1:c)+2,10)=mat2cell(hauteur,ones(1,c),1);
classeur((1:c)+2,11)=mat2cell(largeur,ones(1,c),1);
classeur((1:c)+2,12)=mat2cell((hauteur./largeur),ones(1,c),1);
classeur((1:c)+2,13)=mat2cell(volumecp,ones(1,c),1);


xlswrite(nomXls,classeur,nomFeuille,'A1');
end


disp('Work done !');
```

# APPENDIX B

## Rate of Change of Bubble Volume
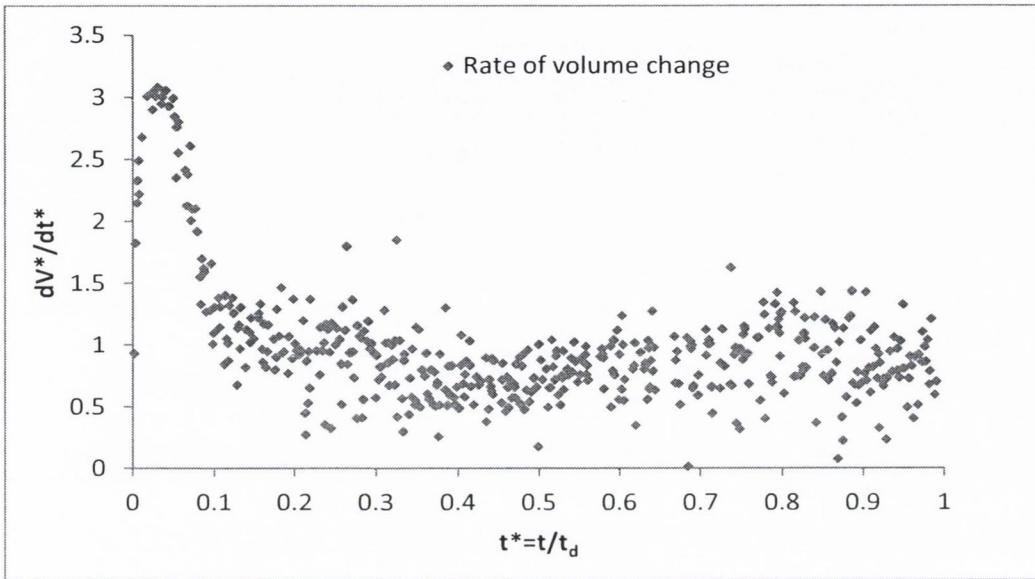


Figure B-1: Rate of change of bubble volume for wall superheat, $\Delta T_w$=2.2 K
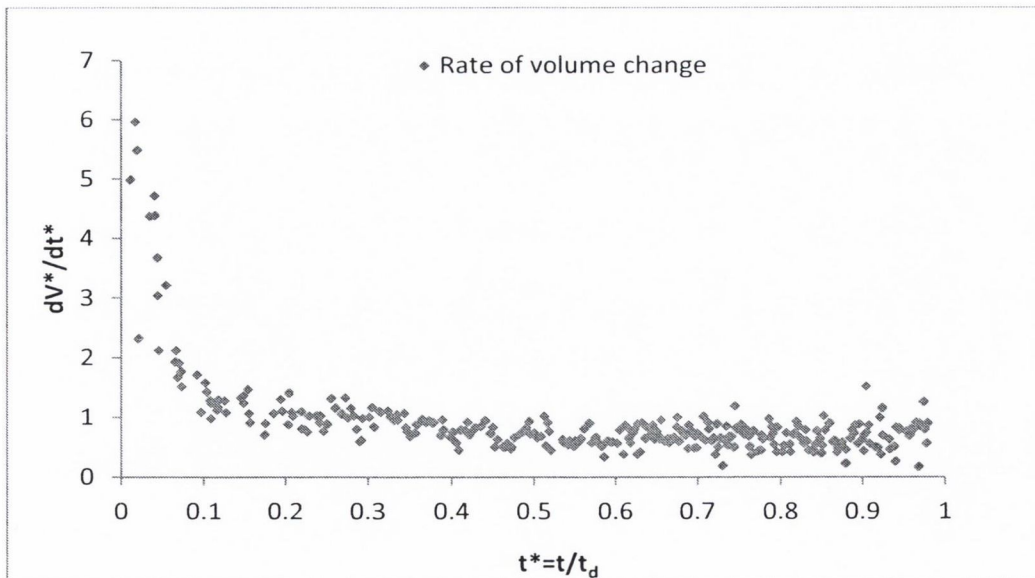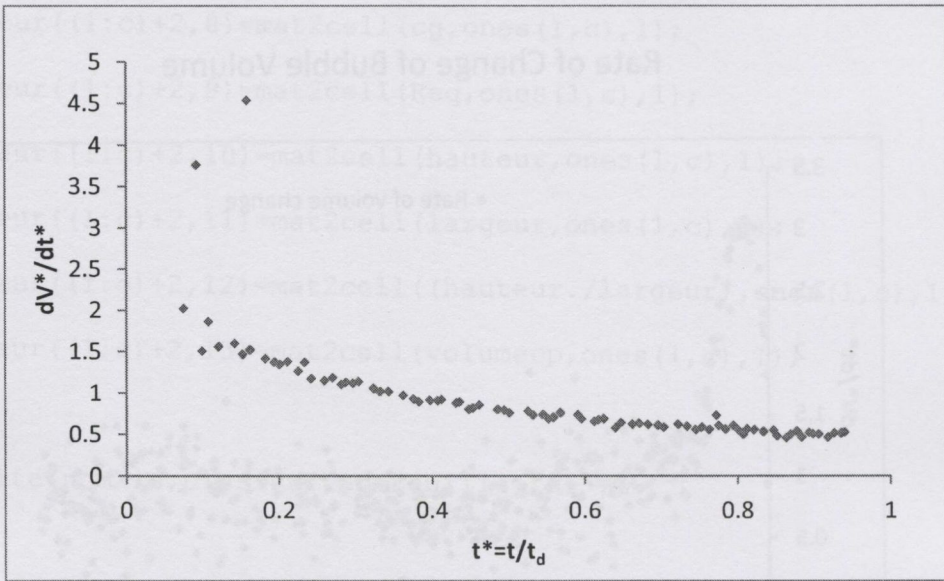


Figure B-2: Rate of change of bubble volume for wall superheat, $\Delta T_w$=6.1 K

Figure B-3: Rate of change of bubble volume for wall superheat, $\Delta T_w$=9.1 K
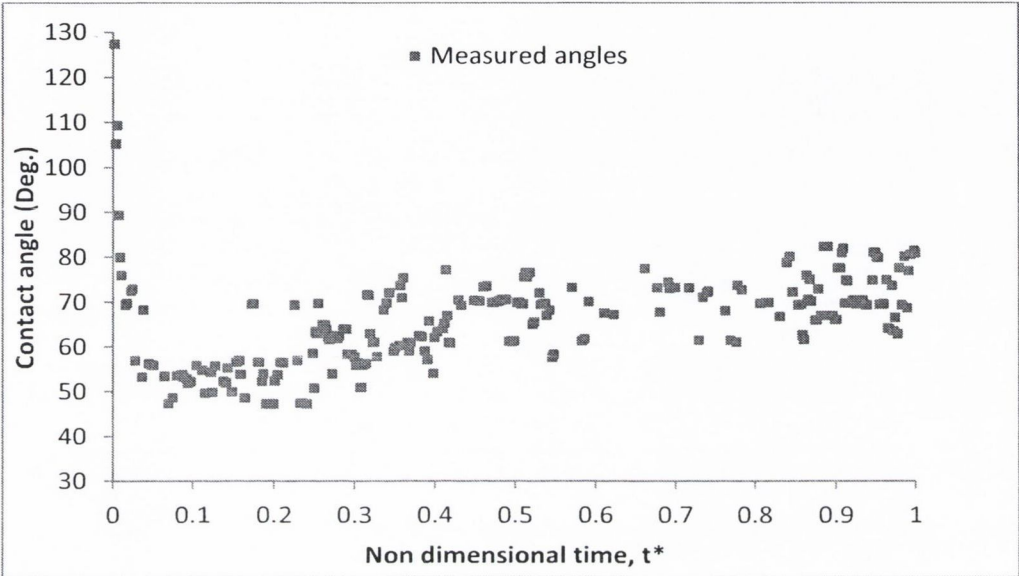
# APPENDIX C

## Contact Angle Histories



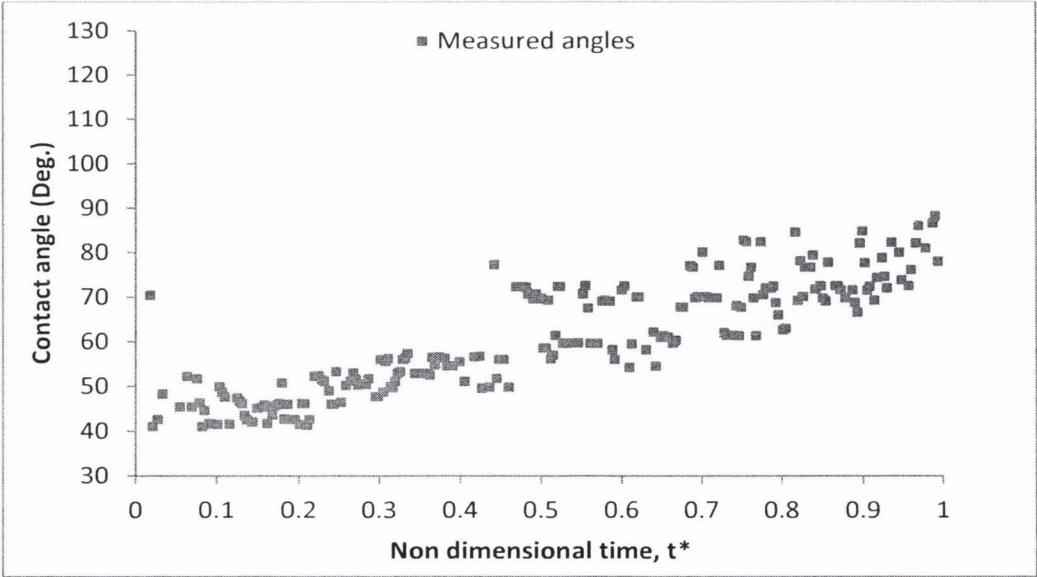Figure C-1: Contact angle evolution for wall superheat $\Delta T_w$=2.2 K



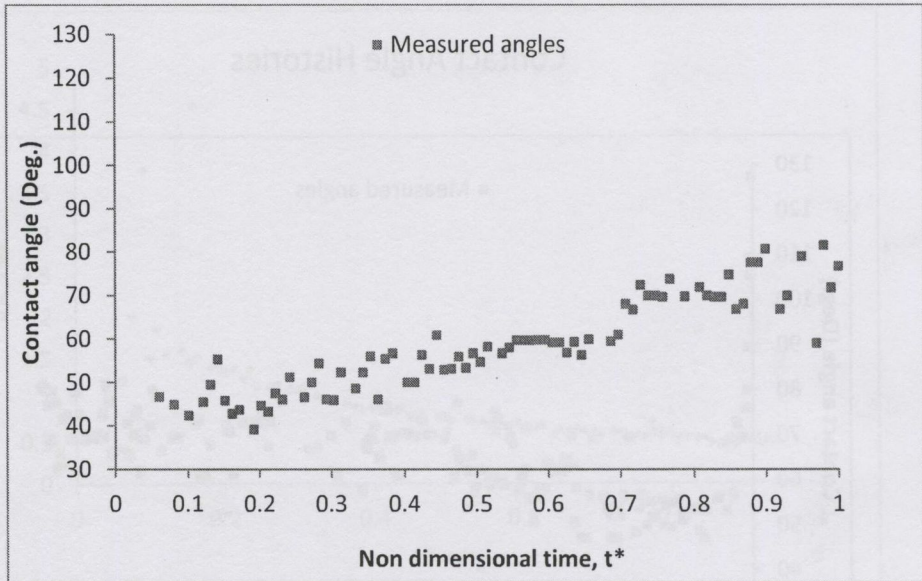Figure C-2: Contact angle evolution for wall superheat $\Delta T_w$=6.1 K

Figure C-3: Contact angle evolution for $\Delta T_w$=9.1 K

# Bubble Growth Dynamics in Nucleate Pool Boiling with Liquid Subcooling Effects

Muhad Rozi Mat Nawi

Department of Mechanical and Manufacturing Engineering

Parsons Building

Trinity College

Dublin 2

Ireland

November 2014

A thesis submitted to the University of Dublin in partial fulfilment of the requirements for the degree of Ph.D

# Bubble Growth Dynamics in Nucleate Pool Boiling with Liquid Subcooling Effects

Muhad Rozi Mat Nawi

## ABSTRACT

Heat transfer in nucleate pool boiling has been characterized by very high dissipated heat fluxes whilst requiring low driving temperature differences. The rate of bubble growth and the subsequent bubble motion has a tremendous influence on the heat transfer. In order to gain a deeper understanding of the mechanisms responsible for this, basic knowledge of bubble growth dynamics is required. To this end, single isolated bubble growth dynamics from an artificial nucleation site in pool boiling has been investigated experimentally in this study. An experimental facility has been developed to perform the study. The experiments have been conducted at atmospheric pressure with an environmental friendly refrigerant HFE-7000 as the working fluid. A high speed video camera with a combination of powerful lens and a tube extension has been used to capture the bubble images during boiling. Image processing in Matlab has been used to process the images and determine relevant parameters which characterize growth and departure.

In the analysis of the bubble growth dynamics, it was found that the bubble's waiting and growth times decrease when the wall superheat is increased, resulting in a significant increase in the bubble frequency. However, bubble growth was determined to be quasi-static such that the bubble size at departure was independent of superheat resulting in an independence of bubble departure size with frequency which contradicts earlier theories. The new growth law was determined which is notably different from the classical growth laws in early classical analytical studies. Bubbles were observed to oscillate at higher wall superheats due to the interaction of the growing bubble with the previous bubble since the waiting time is very short for the high superheats. The measurement of the contact angle is considered to have a

non-negligible error due to the mirage effects. A technique has been developed that corrects for the mirage by calculating the contact angle value which satisfies the vertical force balance for the quasi-static bubbles. For this special case, for a given bubble volume all the forces acting on a growing bubble can be considered as independent of wall superheat. The liquid inertia force appears significant at high wall superheats with an undulating profile due to interaction with the previously departed bubble and the momentum force becomes noticeable for the case of high superheat.

For the experiment with bulk liquid temperatures below the saturation temperature, i.e., subcooled boiling, the shapes of the bubbles at the early growth stage was found less elongated compared to the case of saturated boiling, possibly due to downward force by the fluid moving downward as a result of higher density difference. The bubble size is found to be approximately 29% smaller compared to the bubble volume at departure for the case of saturated boiling due to condensation at the bubble cap. The bubble growth curves show notable differences between the three levels of subcooling i.e. low, mid and high subcooling with a continuous growth curve closer to the saturated case for low subcooling and an abrupt change for mid and high subcooling. Oscillations were observed for the case of high subcooling due to changes in the net flow of heat and mass into/out-of the bubble. The bubble volumetric growth rate curves depend strongly on the level of subcooling, with them being closer to the saturated growth laws for the lower subcooling though notably different for the higher subcooling cases due to high rates of condensation. The contact angles are found to be independent of subcooling levels with smaller contact angles compared with the saturated case. All the vertical forces acting on a growing bubble can be considered as independent of levels of subcooling and lower magnitudes were measured compared to the saturated boiling measurements.